EXPERIMENTAL STUDY OF SUBMERGED SINGLE-PORT THERMAL DISCHARGES

by

GAROLD EUGENE KOESTER

AB, University of Idaho
(1968)

SB, University of Utah
(1972)

Submitted in partial fulfillment of the

Requirements for the Degree of

Master of Science in Civil Engineering

at the

Massachusetts Institute of Technology

May 1974

Signature of Author.....
Department of Civil Engineering, May 10, 1974

Certified by .....
Thesis Supervisor

Accepted by. .....
Chairman, Departmental Committee on Graduate Students
of the Department of Civil Engineering

ACKNOWLEDGEMENTS

To E. Eric Adams, Graduate Research Assistant, whose guidance and constructive counsel were of inestimable help, I owe and gratefully give my most sincere thanks. The assistance of Joseph Rosenson, undergraduate student, is acknowledged. Supervision was provided by Prof. D. R. F. Harleman, Professor of Civil Engineering, and the manuscript was typed by S. Demeris.

ABSTRACT

EXPERIMENTAL STUDY OF SUBMERGED SINGLE-PORT THERMAL DISCHARGES

by

GAROLD EUGENE KOESTER

Submitted to the Department of Civil Engineering on May 10, 1974 in partial fulfillment of the requirements for the degree of Master of Science in Civil Engineering

An experimental investigation of the temperature field induced by the heated effluent from a submerged single-port discharge is conducted. Primary emphasis is directed to the study of the interaction of a shallow water jet with the bottom and the free surface. The parametric Froude number $\mathbb{F}_o$ ranged between 4.9 and 15.7, the relative water depth H/D_o ranged between 1.9 and 6.3, the relative crossflow v/u_o ranged between 0.020 and 0.074, and the relative discharge submergence z/H ranged between near surface ($z/H \simeq 0$) and near bottom ($z/H \simeq 1$). Graphic dimensionless relationships among the pertinent parameters are presented to illustrate the jet's behavior and for use in the preliminary design of shallow water thermal outfalls.

Reasonable correlation has been found at large relative water depths with the analytical prediction of Stolzenbach et al (1972). The non-dimensional relative jet penetration depth parameter h_{max}/H is introduced to define a discharge configuration as a hydrodynamically deep water or shallow water situation.

Thesis Supervisor: Donald R. F. Harleman

Title: Professor of Civil Engineering

TABLE OF CONTENTS

I INTRODUCTION

The large quantities of waste-heat discharged from steam electric power plants is a consequence of the low efficiency at which they operate. Present levels of efficiency are about 40% for fossil fuel plants and about 33% for nuclear plants. Water, being the only economic cooling fluid for steam condensers, is the medium by which this heat is rejected to the environment. High concentrations of heat in natural bodies of water can be detrimental to the aquatic life and natural chemical processes. For this reason, governmental agencies have imposed criteria regulating thermal discharges. A usual criterion of temperature regulations is that large induced temperature rises are restricted to a mixing (dilution) zone, defined as the area in the immediate vicinity of the point of discharge where the heated effluent is diluted with the receiving water.

In this respect, the type of hydraulic structure used for the discharge of heated effluent has an important effect on the temperature distribution in the water environment; it determines the hydraulic characteristics of the discharge which govern the rate of dilution. In general, the rate of dilution is a function of the existing turbulence and velocity of the receiving water, the turbulence induced by the kinetic energy of the effluent, and the density difference between the effluent and receiving water. The areal extent of the temperature distribution is a function of the dilution rate plus the number and orientation of ports in the discharge structure.

Heated effluents are often discharged into water bodies which are shallow relative to the characteristic size of the discharge port. This occurs because the large quantities of heated effluent require discharge sources of large dimension. It is possible to construct hydraulic structures that induce surface spreading with minimal mixing. Consider a surface discharge characterized by surface spreading at low Froude numbers. The region of temperature increase tends to be localized because the rate of heat transfer to the atmosphere is great. By avoiding total mixing, the volume of water which has a higher than normal temperature is minimized.

On the other hand, hydraulic structures can be constructed to achieve complete mixing with possible storage of waste heat below thermoclines. In shallow water, surface and submerged discharges at high Froude number exhibit similar temperature distributions. The general feature is that the mixing zone extends from the water surface to the bottom of the receiving body over long distances. With the extensive mixing, the temperature rise above the ambient is minimized, although the volume of water affected by a temperature rise is greatly increased. Heat dissipation to the atmosphere is reduced by the lower surface temperature. When mixing devices are used to keep temperature rise within allowable limits, there is likely to be a corresponding reduction in the heat flux from the water to the atmosphere by all processes: radiation, evaporation and conduction. The alternatives elected should depend on the

predicted ecological effects of the heated effluent.

With this engineering decision in mind, this study is presented as part of the continuing research effort to understand and predict the behavior of thermal discharges at the Ralph M. Parsons Laboratory. Due to the complicated flow pattern which results from the interaction of a shallow water jet with the bottom and the free surface, a quantitative analysis of either surface or submerged bouyant jets in shallow water is beyond the scope of this study. The nature of this investigation is experimental and addresses the problem of predicting temperature concentrations in a large body of water induced by the heat flow from a single port discharge structure. The objective is to present graphic dimensionless relationships of the pertinent parameters describing the heat flow with emphasis on the near surface configuration in a shallow body of water. Application of this study is anticipated to aid in the preliminary design of shallow water thermal outfalls.

11 THEORETICAL BACKGROUND

2.1 General Characteristics

A single-port discharge is in essence a round-buoyant jet. The physical processes that dominate its hydrodynamic behavior under unconfined conditions are generally grouped into three separate regions, see Figure 2-1. The NEAR FIELD processes are governed by the dynamic and buoyant characteristics of the discharge and of the ambient water in the immediate vicinity. Very near the outfall the fluid motion is dominated by inertia forces arising from the initial flux of momentum and is characterized by shear-generated free turbulence which induces entrainment flow of the ambient water into the jet. The increasing flow of the jet is diffused with a simultaneous reduction of velocities and temperature. Entrainment continues until the jet velocity is reduced to a velocity comparable with that of the ambient water. The buoyancy forces tend to deflect the axis of the jet toward the free surface or, as in the case of a near-surface jet, resist its vertical penetration.

The second region is the TRANSITION between the near field and the far field. Further dilution of temperature due to entrainment effectively ceases at this point. A stable region is achieved that is characterized by vertical stability of the surface layer of mixed water. Buoyancy forces, generating density currents, and the ambient currents convect the mixed water away from the near field.

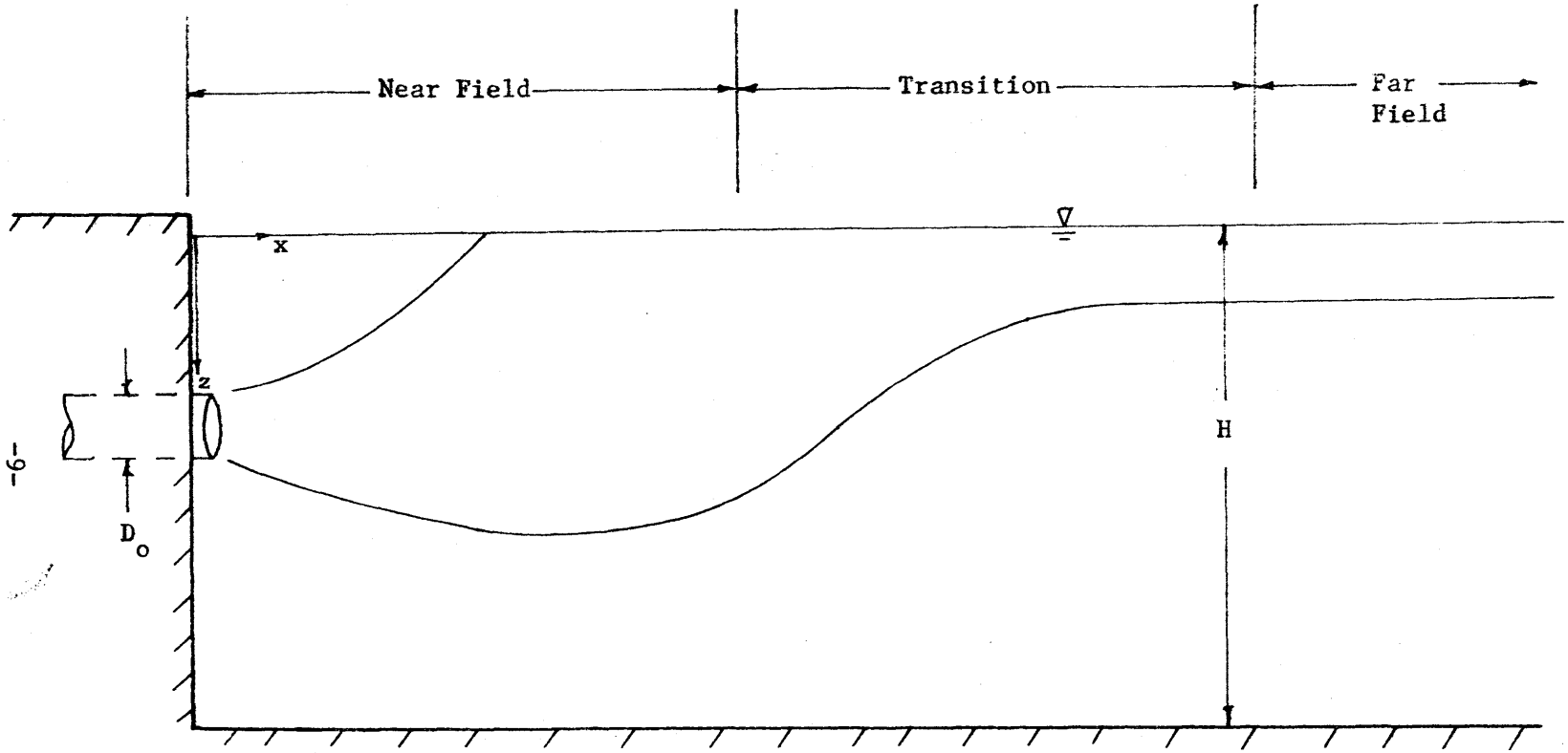

Figure 2-1: Region of Physical Processes that Govern a Single-port Thermal Discharge

In the FAR FIELD the convection of the mixed water continues to be dominated by the ambient currents. Additional temperature decrease occurs through diffusion which is generated by ambient turbulence and through surface heat loss to the atmosphere which is the ultimate heat sink. This study pertains primarily to the near field phenomena.

2.2 Mathematical Analysis

The mathematical analysis of a buoyant jet aims at a description of the jet flow field, temperature field and trajectory as a function of ambient flow parameters, initial jet parameters, and experimentally determined coefficients, see Figure 2-2.

2.2.1 Round Buoyant Jet

For a round buoyant jet the governing equations of fluid motion and heat conservation are formulated under the following assumptions:

a) The flow is steady: $\partial/\partial t = 0$.

b) Fluctuating turbulent quantities are small compared to the mean.

c) Turbulent eddy velocities are the dominant transport mechanism.

d) Viscous effects are neglected: Large Reynolds number.

e) The Baussinesq approximation is applied: $\frac{\Delta\rho}{\rho} << 1$

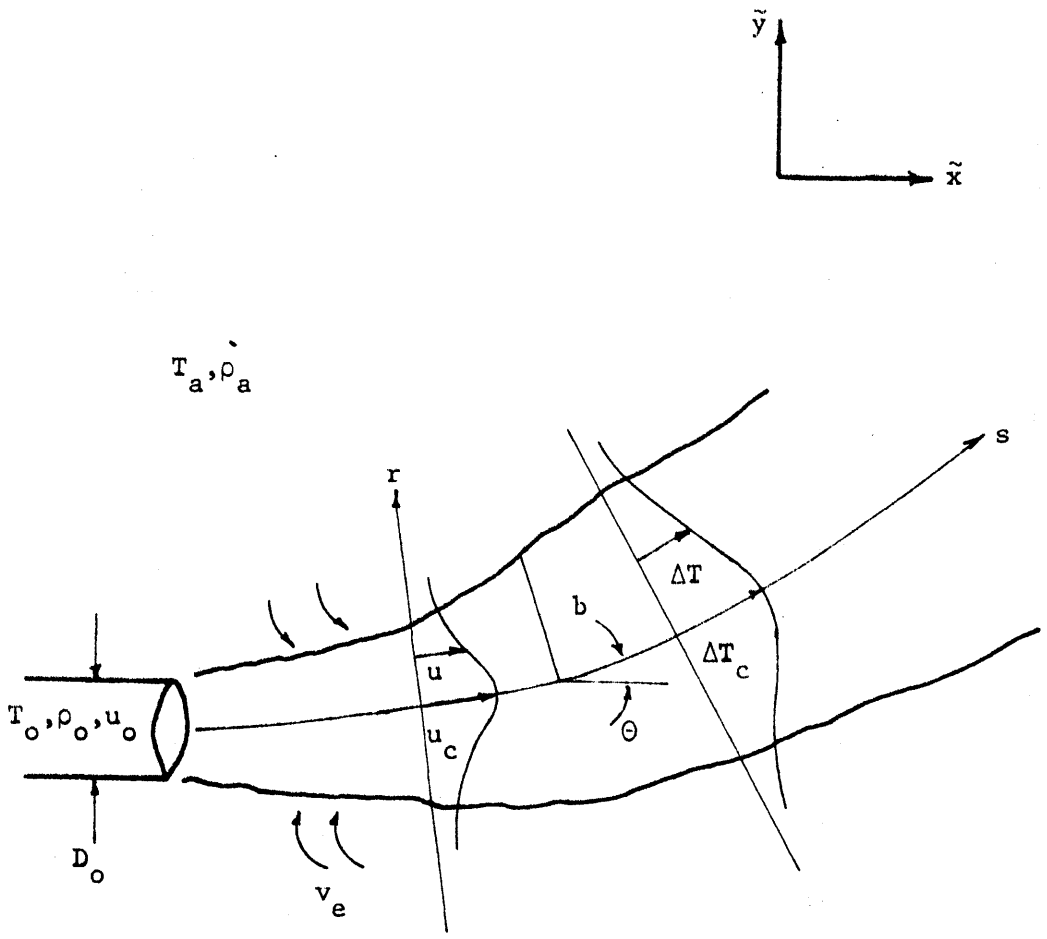

Figure 2-2: Definition Diagram for Round Buoyant Jet

The time-average equations of motion are:

Continuity

$$\frac{1}{r}\frac{\partial}{\partial r}(rv) + \frac{\partial u}{\partial s} = 0 \qquad (2\text{-}1)$$

Axial Momentum:

$$\rho_a \frac{u\partial u}{\partial s} + \rho_a \frac{v\partial u}{\partial r} = -\frac{\partial P}{\partial s} + \rho g \sin\theta - \frac{\rho_a}{r}\frac{\partial}{\partial r}(r\overline{u'v'}) - \rho_a \frac{\partial \overline{v'^2}}{\partial s} \qquad (2\text{-}2)$$

Radial Momentum:

$$\rho_a \frac{u\partial v}{\partial s} + \rho_a \frac{v\partial v}{\partial r} = -\frac{\partial P}{\partial r} + \rho g \cos\theta - \frac{\rho_a}{r}\frac{\partial}{\partial r}(r\overline{v'^2}) - \rho_a \frac{\partial \overline{u'v'}}{\partial s} \qquad (2\text{-}3)$$

Heat Conservation

$$u\frac{\partial T}{\partial s} + v\frac{\partial T}{\partial r} = -\frac{\partial \overline{u'T'}}{\partial s} - \frac{1\partial}{r\partial r}(r\overline{T'v'}) \qquad (2\text{-}4)$$

in which

s,r = cylindrical coordinates, $\partial/\partial\phi = \nu$

u,v = mean velocities in s,r directions

u',v' = velocity fluctuations in s, r directions

ρ = mean local density

ρ_a = constant ambient density

T = mean temperature

T' = temperature fluctuations

θ = angle between x axis and s axis

The main properties of the jet flow field make simplification of the governing equations possible. They are:

a) The pressure around the jet is hydrostatic.

b) The increase of mass flow rate is equal to the entrainment of ambient fluid per unit length of jet.

c) The boundary layer approximation is utilized. Convection by transverse velocities are small compared to convection by axial velocities. Diffusion in the axial direction is small compared to diffusion in the transverse direction.

d) A consequence of the first assumption is that horizontal momentum of the jet is conserved.

e) There is a similarity of flow. Velocities, temperature and density can be described very closely by Gaussian distributions, i.e., by equations of the form

$$u(r,s) = u_c(s)\exp[-K(r/s)^2] \qquad (2\text{-}5)$$

$$\Delta T(r,s) = \Delta T_c(s)\exp[-K\lambda(r/s)^2] \qquad (2\text{-}6)$$

$$\Delta\rho(r,s) = \Delta\rho_c(s)\exp[-K\lambda(r/s)^2] \qquad (2\text{-}7)$$

where

$u(r,s)$ = the local velocity

$u_c(s)$ = the velocity at the centerline

$\Delta T(r,s)$ = the local temperature rise; $\Delta T = (T-T_a)$

$\Delta T_c(s)$ = temperature rise at the centerline; $\Delta T_c=(T_o-T_a)$

$\Delta\rho(r,s)$ = the local density deficit; $\Delta\rho = (\rho_a - \rho)$

$\Delta\rho_c(s)$ = density deficit at the centerline; $\Delta\rho_c=(\rho_c-\rho_o)$

K and λ = experimentally determined dimensionless coefficients describing the gross effects of the turbulent mixing process.

f) The density of the water is assumed to vary linearly with temperature

$$\rho(T) = \rho_a[1 - \beta(T-T_a)] \tag{2-8}$$

where β is the coefficient of thermal expansion. The concentration of the heat, c_h, in the jet water is formulated in terms of density as

$$c_h = \frac{\rho_a - \rho}{\rho_a - \rho_o} \tag{2-9}$$

Due to the entrainment of ambient water, the degree of dilution, D, is commonly defined as

$$D = \frac{1}{c_h} = \frac{\rho_a - \rho_o}{\rho_a - \rho} \tag{2-10}$$

where

ρ = the local density

ρ_a = the density of the ambient fluid

ρ_o = the density of the jet fluid

Substituting Equation (2-8) into Equation (2-10) the temperature dilution is obtained

$$D = \frac{T_o - T_a}{T - T_a} \tag{2-11}$$

where

T = the local temperature

T_a = the ambient temperature

T_o = the jet temperature at the jet exit

The simplified governing equations become:

Continuity:

$$\frac{1}{r}\frac{\partial}{\partial r}(rv) + \frac{\partial u}{\partial s} = 0 \tag{2-12}$$

Momentum:

$$\frac{u\partial u}{\partial s} + \frac{v\partial u}{\partial r} = \rho g \sin\theta - \frac{1}{r}\frac{\partial}{\partial r}(r\overline{u'v'}) \tag{2-13}$$

$$0 = \rho g \cos\theta - \frac{1}{r}\frac{\partial}{\partial r}(r\overline{v'^2}) \tag{2-14}$$

Conservation of Heat:

$$u\frac{\partial T}{\partial s} + v\frac{\partial T}{\partial r} = -\frac{1}{r}\frac{\partial}{\partial r}(r\overline{T'v'}) \tag{2-15}$$

With the boundary conditions:

$$v = 0$$

$$\overline{u'v'} = 0$$

$$\Delta T = 0 \qquad \text{as } r \to \infty$$

$$T'v' = 0$$

The continuity equation, assuming small variation in density, can be expressed as

$$\frac{d}{ds}\int_0^\infty 2\pi u(s,r)\,r\,dr = Q' \tag{2-16}$$

where Q' is the rate of entrainment of the ambient water per unit length of the jet. The equation for the conservation of heat is

$$\frac{d}{ds}\int_0^\infty 2\pi u(s,r)T(s,r)\,r\,dr = 0 \tag{2-17}$$

The conservation of momentum equation in the horizontal direction is

$$\cos\theta \int_0^\infty 2\pi\rho u^2(s,r)rdr = \frac{\pi D_o^2}{4} u_o^2 \qquad (2\text{-}18)$$

The conservation in the vertical direction is expressed by the equation

$$\sin\theta \int_0^\infty 2\pi\rho u^2(s,r)rdr = g \int_0^\infty ds \int_0^\infty 2\pi[\rho_o - \rho(s,r)\ rdr \qquad (2\text{-}19)$$

where

$$\rho(T) = \rho_a[1-\beta(T-T_a)] \qquad (2\text{-}8)$$

Temperature, density and velocity along the trajectory of the jet are usually obtained as follows:

1) The assumed profiles, Equations (2-5) to (2-7), are substituted into the conservation equations.

2) Q' in the conservation of mass equation is approximated by

$$Q' = -2\pi b v_e \qquad (2\text{-}20)$$

where

$$v_e = -\alpha u_c \qquad (2\text{-}21)$$

and hence

$$Q' = 2\pi b\alpha u_c \qquad (2\text{-}22)$$

where α is an experimentally determined entrainment coefficient and b is a local width of the jet, usually taken as

$$b = \sqrt{\frac{8}{K}}\, s \qquad (2\text{-}23)$$

3) The resulting ordinary differential equations are then solved for ΔT_c, $\Delta \rho_c$, and u_c using the initial discharge conditions ΔT_o, $\Delta \rho_o$, and u_o.

2.2.2 Buoyant Near Surface Discharge

The engineering importance of the submerged jet as a means of dilution and disposal of heated water in large bodies of water has motivated numerous analytical and experimental studies. Of particular interest is a numerical model for determining jet properties at various distances from a buoyant near surface discharge in unconfined and unstratified water by Stolzenbach et al (1972). Their model considers a discharge Q_o of heated water at temperature T_o and density ρ_o from a rectangular open channel of depth h_o, width $2b_o$, and initial horizontal angle Θ_o at the surface of a receiving body of water at temperature T_a, density ρ_a and of large extent. A non-uniform current V may be present and it is assumed that the bottom of the receiving water does not interfere with the vertical development of the surface jet. With the assumptions presented in Section 2.2.1 the basic equations of mass, momentum and heat conservation may be simplified in rectangular coordinates:

Continuity:

$$\frac{\partial u}{\partial x} + \frac{\partial v}{\partial y} + \frac{\partial w}{\partial z} = 0 \qquad (2\text{-}24)$$

x-Momentum:

$$\frac{\partial u^2}{\partial x} + \frac{\partial uv}{\partial y} + \frac{\partial uw}{\partial z} = \beta g \int_z^{-\infty} \frac{\partial T}{\partial x}\, dz - \frac{\partial u'v'}{\partial y} - \frac{\partial u'w'}{\partial z} \qquad (2\text{-}25)$$

y-Momentum:

$$\frac{\partial uv}{\partial x} + \frac{\partial v^2}{\partial y} + \frac{\partial wv}{\partial z} = \beta g \int_z^\infty \frac{\partial T}{} dz + u^2 \frac{\partial \theta}{x} \qquad (2\text{-}26)$$

Heat Conservation:

$$\frac{\partial uT}{\partial x} + \frac{\partial vT}{\partial y} + \frac{\partial wT}{\partial z} = - \frac{\partial v'T'}{\partial y} - \frac{\partial w'T'}{\partial z} \qquad (2\text{-}27)$$

The technique used to develop the solution of these equations is to assume a structure for the velocity and temperature within the discharge and boundary conditions at the outer edges. The structure of the discharge is shown in Figures 2-3 and 2-4. The longitudinal velocity and temperature distributions are taken to be as follows, where η is the water surface elevation:

$$\begin{aligned} u &= u_c + V\cos\theta \\ \Delta T &= \Delta T_c \end{aligned} \qquad 0<|y|<s \qquad -r<z<\eta$$

$$\begin{aligned} u &= u_c f(\zeta_z) + V\cos\theta \\ \Delta T &= \Delta T_c t(\zeta_z) \end{aligned} \qquad 0<|y|<s \qquad -(r+h)<z<-r \qquad (2\text{-}28)$$

$$\begin{aligned} u &= u_c f(\zeta_y) + V\cos\theta \\ \Delta T &= \Delta T_c t(\zeta_y) \end{aligned} \qquad s<|y|<s+b \qquad -r<z<\eta$$

$$\begin{aligned} u &= u_c f(\zeta_y) f(\zeta_z) + V\cos\theta \\ \Delta T &= \Delta T_c t(\zeta_y) t(\zeta_z) \end{aligned} \qquad s<|y|<s+b \qquad -(r+h)<z<-r$$

where

$$\zeta_y = \frac{|y|-s}{b} \quad \text{and} \quad \zeta_z = \frac{-z-r}{h}$$

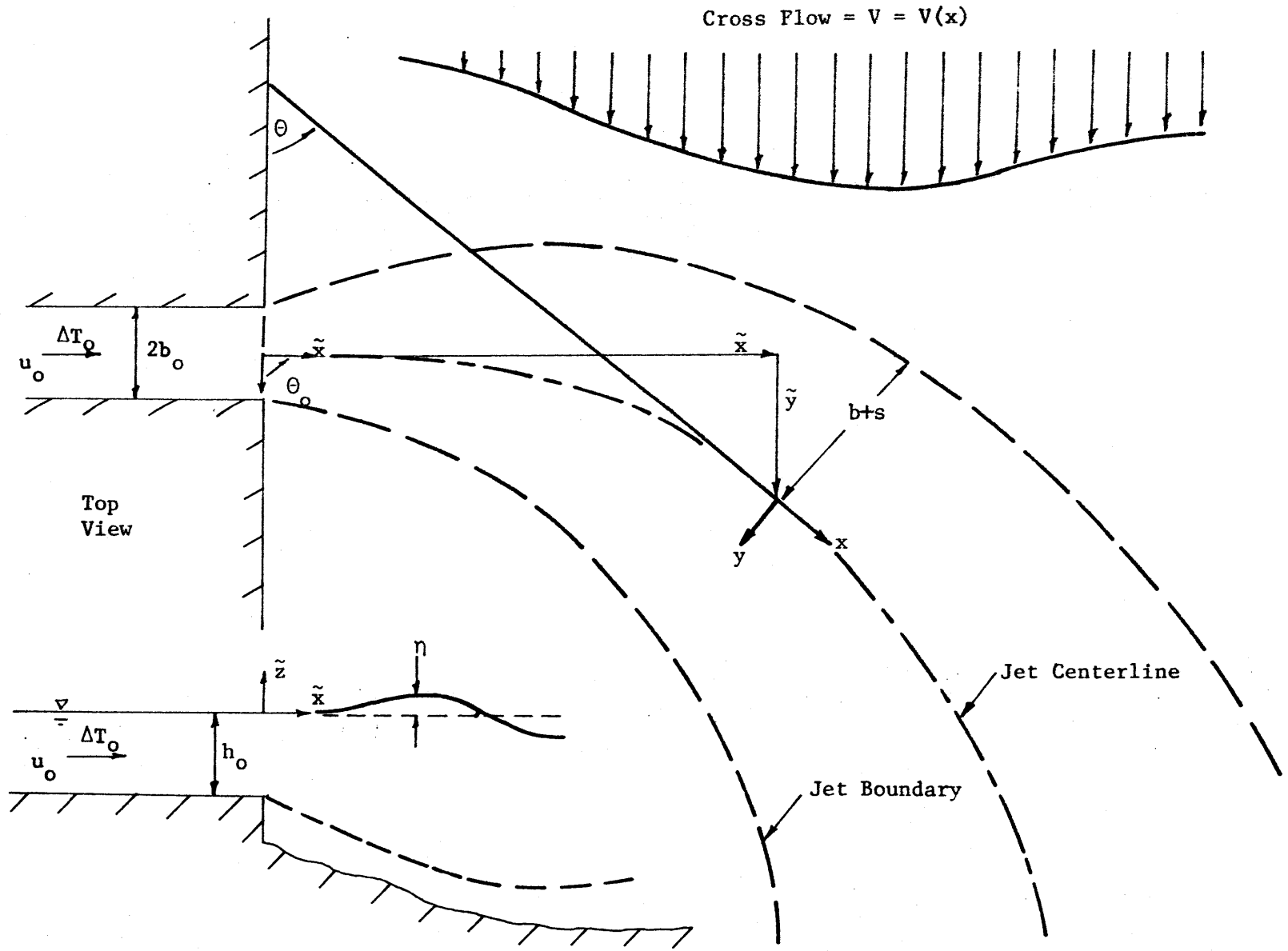

Figure 2-3: Coordinate Definitions

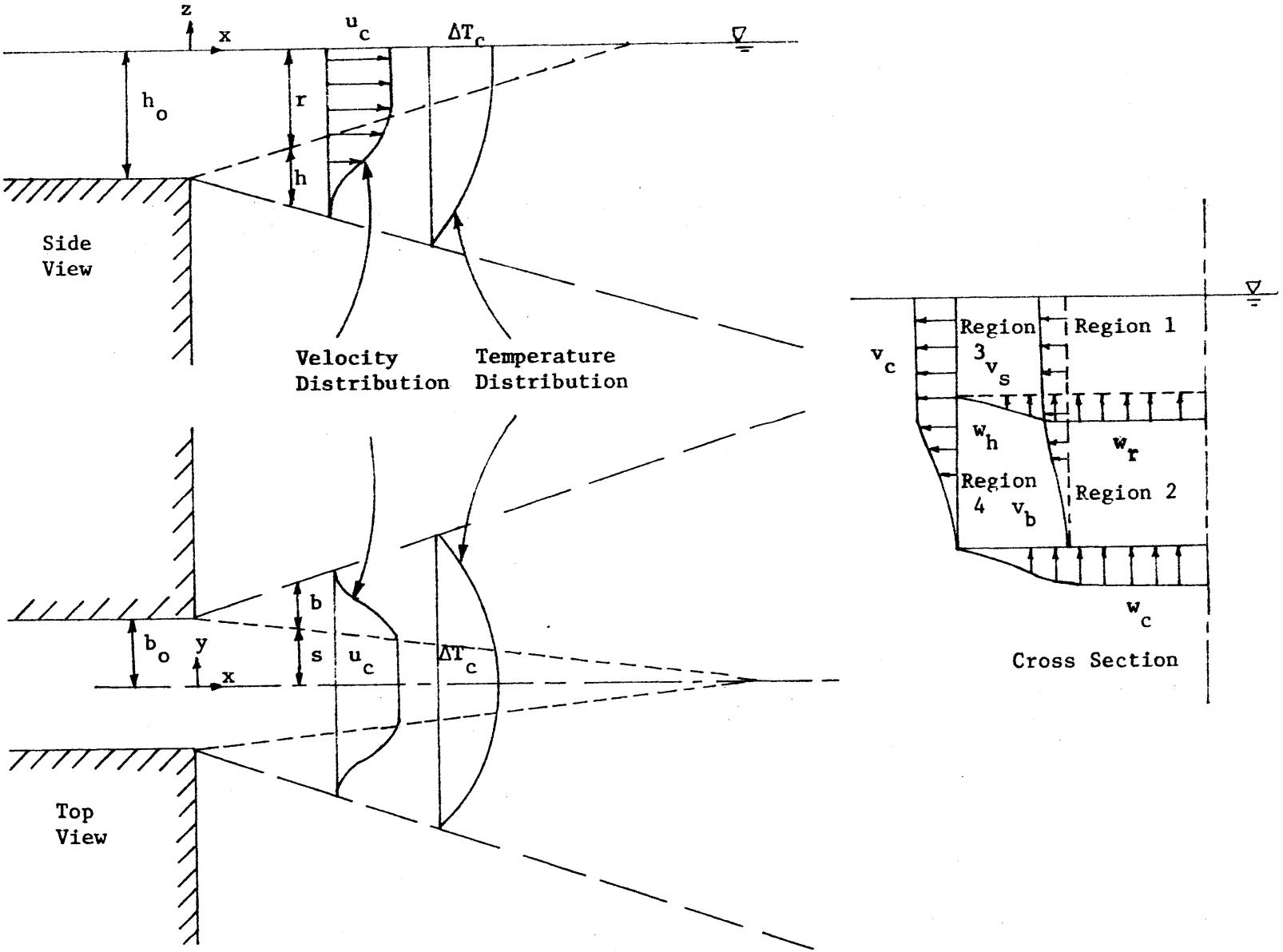

Figure 2-4: Discharge Structure

The lengths r and s pertain to the initial core region and h and b to the turbulent region of the jet (see Figure 2-4). The particular forms of the similarity functions are assumed to be as follows:

$$f(\zeta) = (1-\zeta^{3/2})^2$$
$$t(\zeta) = 1-\zeta^{3/2} \qquad (2\text{-}29)$$

The lateral velocity is geometrically related to the longitudinal velocity by:

$$\frac{v}{u} = \tan \phi \qquad (2\text{-}30)$$

where ϕ is the lateral jet stream line angle from the centerline in excess of the non-buoyant value. Then

$$v = \pm \left(\frac{db}{dx} - \varepsilon\right) u \, \zeta_y^{1/2} \qquad s<|y|<s+b$$
$$v = 0 \qquad \text{elsewhere} \qquad (2\text{-}31)$$

where the following conditions are satisfied:

1) $\tan \phi = 0$ at $y = 0$

2) $\tan \phi = \left(\frac{db}{dx} - \varepsilon\right)$ at $y = b+s$, where ε is the lateral spreading rate of a non-buoyant jet under the same conditions. Since the gravitational spread is induced by the lateral temperature gradient, the y dependence of $\frac{\partial T}{\partial y}$ is used to distribute $\tan \phi$ between $y = 0$ and $y = b+s$.

The boundary conditions are then given to be

$$v = u'v' = v'T' = 0 \qquad y = 0 \tag{2-32}$$

$$u'w' = 0$$

$$\begin{aligned} w &= w_r && 0<|y|<s \\ w &= w_h f(\zeta_y) && s<|y|<s+b \\ w &= 0 && s+b<|y| \end{aligned} \qquad z = -r \tag{2-33}$$

$$u'v' = 0$$

$$\begin{aligned} v &= \pm v_s && -r<z<\eta \\ v &= \pm v_b f(\zeta_z) && -(r+h)<z<-r \\ v &= 0 && z<-(r+h) \end{aligned} \qquad |y|=s \tag{2-34}$$

$$u \frac{\partial \eta}{\partial x} + v \frac{\partial \eta}{\partial y} = w$$

$$u'w' = 0 \qquad z = \eta \tag{2-35}$$

$$w'T' = k(T - T_a) \qquad z = \eta \tag{2-36}$$

The outer boundaries of the jet occur at the entrainment surface where no heat is transferred. The boundary conditions are:

$$u'w' = w'T' = 0$$

$$\begin{aligned} w &= w_e - V\cos\theta \frac{dh}{dx} && 0<|y|<s \\ w &= w_e f(\zeta_y) - V\cos\theta \frac{dh}{dx} && s<|y|<s+b \end{aligned} \qquad z = -(r+h) \tag{2-37}$$

$$u'v' = v'T' = 0$$

$$v = \pm v_e + V\cos\theta \frac{db}{dx} \qquad -r<z<\eta$$

$$v = \pm v_e f(\zeta_z) + V\cos\theta \frac{db}{dx} \qquad -(r+h)<z<-r \qquad y = s+b \qquad (2\text{-}38)$$

where w_e and v_e are the entrainment velocities. The entrainment velocities are assumed to be given by

$$\frac{v_e}{u_c} = \alpha_y$$

$$\frac{w_e}{u_c} = \alpha_z \exp\left[-C \frac{\beta g \Delta T_c h}{u_c^2}\right] \qquad (2\text{-}39)$$

where the exponent is in the form of a Richardson number. The entrainment coefficients, α_y and α_z, are determined such that the solution for the non-buoyant case ($T_o = T_a$) agrees with the experimental observations that the growth of a non-buoyant turbulent region is symmetrical:

$$\frac{db}{dx} = \frac{dh}{dy} = \varepsilon$$

$$\frac{ds}{dx} = \frac{dr}{dx} \qquad (2\text{-}40)$$

For non-buoyant jets discharging into a quiescent receiving water the spread rate, ε_o, is constant. In these cases $\varepsilon_o = 0.22$ for the similarity functions, f and k, used here. The boundary conditions at x = 0 are related to the discharge channel geometry, the flow rate Q_o, and the initial discharge temperature T_o.

$$r = h_o$$

$$s = b_o$$

$$h = b = 0$$

$$u = u_o = \frac{Q_o}{2h_o b_o} + V\cos_o \qquad x = 0 \qquad (2\text{-}41)$$

$$\Delta T_c = \Delta T_o$$

$$\theta = \theta_o$$

$$\tilde{x} = \tilde{y} = 0$$

Using their numerical model, Stolzenbach et al found the following trends in the stable region of the surface jet, for $F_o' > 3$:

$$D = \frac{\Delta T_o}{\Delta T_s} = 1.4\ F_o' \qquad (2\text{-}42)$$

$$\frac{\Delta T_o}{(\Delta T_{sc})_s} \simeq F_o' \qquad (2\text{-}43)$$

and

$$\frac{h_{max}}{\sqrt{h_o b_o}} \simeq 0.42\ F_o' \qquad (2\text{-}44)$$

where

$\Delta T_o = T_o - T_a$

$(\Delta T)_s$ = average fractional stable excess surface temperature rise in the jet

$(\Delta T_{sc})_s$ = stable surface centerline temperature rise

F_o = densimetric Froude number = $u_o/\sqrt{g'h_o}$

A = aspect ratio = h_o/b_o

$F_o' = u_o/\sqrt{g'(h_o b_o)^{1/2}} = F_o A^{1/4}$

u_o = discharge velocity = $Q_o/2h_o b_o$

$g' = \Delta\rho_o/\rho_o g$

h_{max} = maximum vertical penetration of the jet.

The circular discharge (Single-port) structure can be schematized so as to be used in their predictive model. The geometric form of the discharge is described by an aspect ratio

$$A = \frac{h_o}{b_o} \tag{2-45}$$

where

a) h_o is the actual maximum discharge channel depth;

$h_o = D_o$

b) b_o is such that the correct discharge channel area is preserved:

$$b_o = \frac{\text{channel area}}{2h_o} \tag{2-46}$$

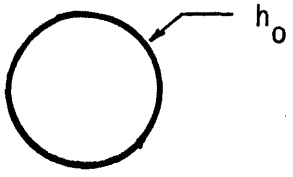

Hence

$$A = \frac{2h_o^2}{\text{channel area}}$$

The aspect ratio of a circle is A = 2.55. See Figure 2-5.

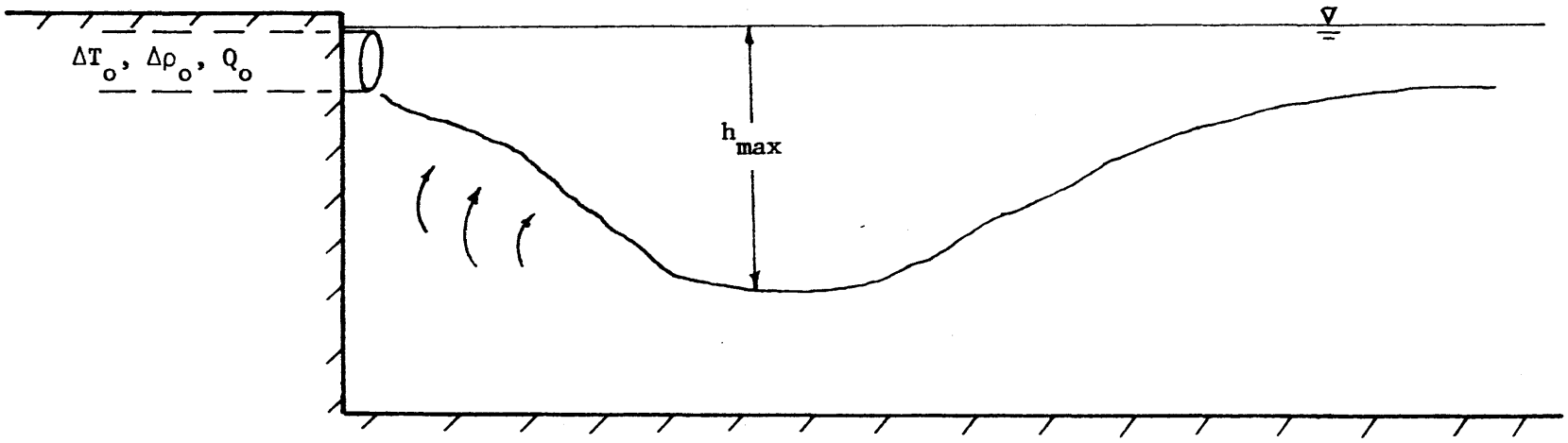

Figure 2-5: Schematic of the Single-port Heated Discharge

III EXPERIMENTAL EQUIPMENT AND PROCEDURES

3.1 Experimental Program

The experimental program considers a discharge Q_o of heated water at temperature T_o and density ρ_o from a circular pipe of diameter D_o at the edge of a receiving body of water of large extent, whose temperature T_a, density ρ_a and depth H are uniform. A uniform current v may be present in the receiving water and is parallel to the shoreline. See Figure 3-1.

For the results of the experiments to be relevant to field conditions, the correct scaling laws were observed. Dimensional analysis and a study of the equations governing turbulent jet behavior provide the dimensionless parameters which must be modeled.

In this study the scaling length is the diameter of the outfall, D_o. Stolzenbach has shown that the basic scaling length should be proportional to the square root of the discharge flow area $2h_o b_o$. In his study this length is taken as the square root of one half of the discharge flow area, $\sqrt{h_o b_o}$. From Equations (2-45) to (2-47)

$$\sqrt{h_o b_o} = 0.63\ D_o \tag{3-1}$$

Since entrainment increases with increasing jet momentum and decreases with increasing jet buoyancy, the densimetric Froude number $\mathbf{F}_o$ is used as a parameter for jet induced mixing. The densimetric Froude number is defined by

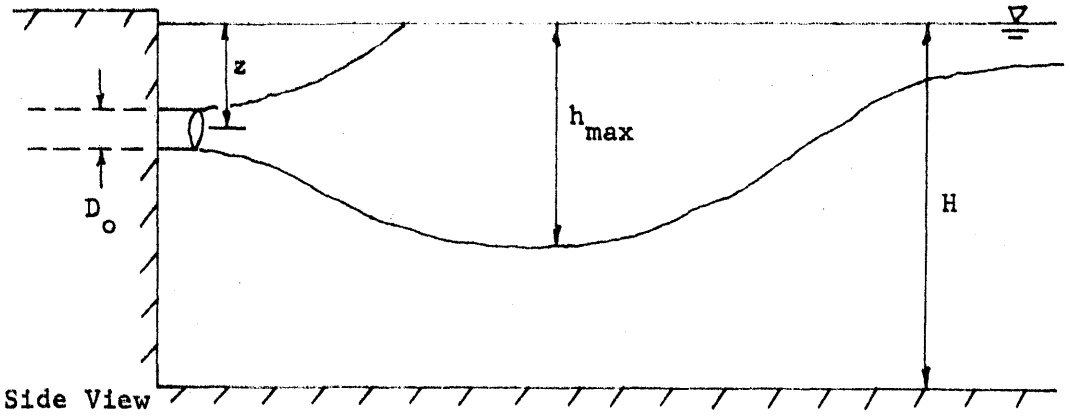

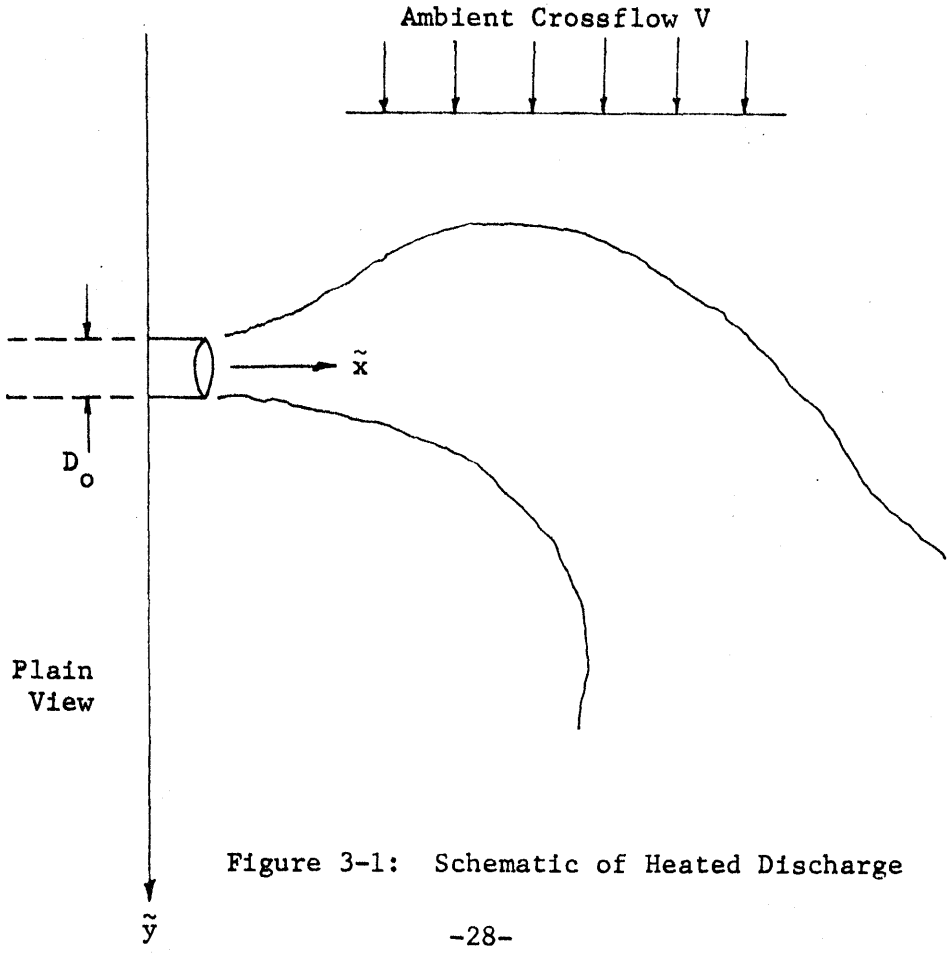

Figure 3-1: Schematic of Heated Discharge

$$\mathbb{F}_o = \frac{u_o}{\sqrt{g' D_o}} \tag{3-2}$$

where $g' = (\rho_o - \rho_a/\rho_a)g$ is the reduced acceleration of gravity at the discharge port.

A more general Froude number is the Aspect Densimetric Froude number which has been defined as

$$F_o' = \mathbb{F}_o A^{1/4} = \frac{u_o}{\sqrt{g'}\sqrt{h_o b_o}} \tag{3-3}$$

It incorporates the geometric as well as the dynamic characteristics of the discharge into one parameter and is useful when applying the results of this study to other discharge configurations.

The dimensionless water depth parameter is H/D_o, the relative discharge submergence is z/H and the crossflow parameter is v/u_o. The remaining dimensionless parameter characterizing the discharge is the Reynolds number, $\mathbb{R}_e$, defined as:

$$\mathbb{R}_e = \frac{u_o D_o}{\nu} \tag{3-4}$$

in which ν is the kinematic viscosity of water. In many free shear flows the gross characteristics of the flow fields are independent of Reynolds number provided that the Reynolds number is great enough for the flow to be turbulent throughout.

3.2 Experimental Limitations

The steady-state temperature concentrations induced by a single-port thermal discharge in a shallow body of water of large extent is desired. This relatively unconfined prototype situation, out of laboratory necessity, is confined in a basin model of finite extent. As a consequence, correct steady state results can never be achieved for long periods of time. The size of the model within the basin determines the duration that the model is allowed to run before significant boundary distortion comes into play. The scale size should be chosen small enough so that the near field mixing occurs in a small portion of the model and boundaries have small effect on the induced flow pattern and yet the scale size must be large enough to provide resolution in measurement and avoid scale effects.

A comparative study of the performance of different discharge configurations on a relative basis is easily achieved. But the results of the laboratory experiments as applied to prototype design problems are subject to a variety of interpretations.

3.3 Experimental Set-Up

Figure 3-2 shows the model set-up. The basin is 60' x 40' x 1 1/2' and is located on the first floor of the R. M. Parsons Laboratory. Being situated in an enclosed area, the model is free from undesirable disturbances due to weather. The shoreline is in effect a vertical breakwater constructed of 8" cinderblocks and the floor is covered with a 30 gauge vinyl liner. A recirculating crossflow is achieved using five (5) hp pumps drawing from five equal length manifolds on the suction side and supplying water to a mixing manifold which feeds five equal length manifolds on the pressure side. The purpose of the mixing manifold is to provide water of uniform temperature across the basin. A uniform flow distribution is maintained by using vertical slot weirs and a 4" thick section of rubberized horsehair matting on both upstream and downstream sections of the basin.

Discharge flow is warmed by passage through a steam heat exchanger and is mixed in a constant heat tank above the basin. The discharge structure is a section of PVC 80 pipe. The depth of the discharge can be adjusted from near surface to near bottom. Dye may be injected into the discharge to visualize the flow development and a small pump at the end of the basin removes water at the same rate as the discharge flow.

Temperatures are measured using an array of 100 Yellow Springs Instrument thermistors (Series 700, time constant = 9

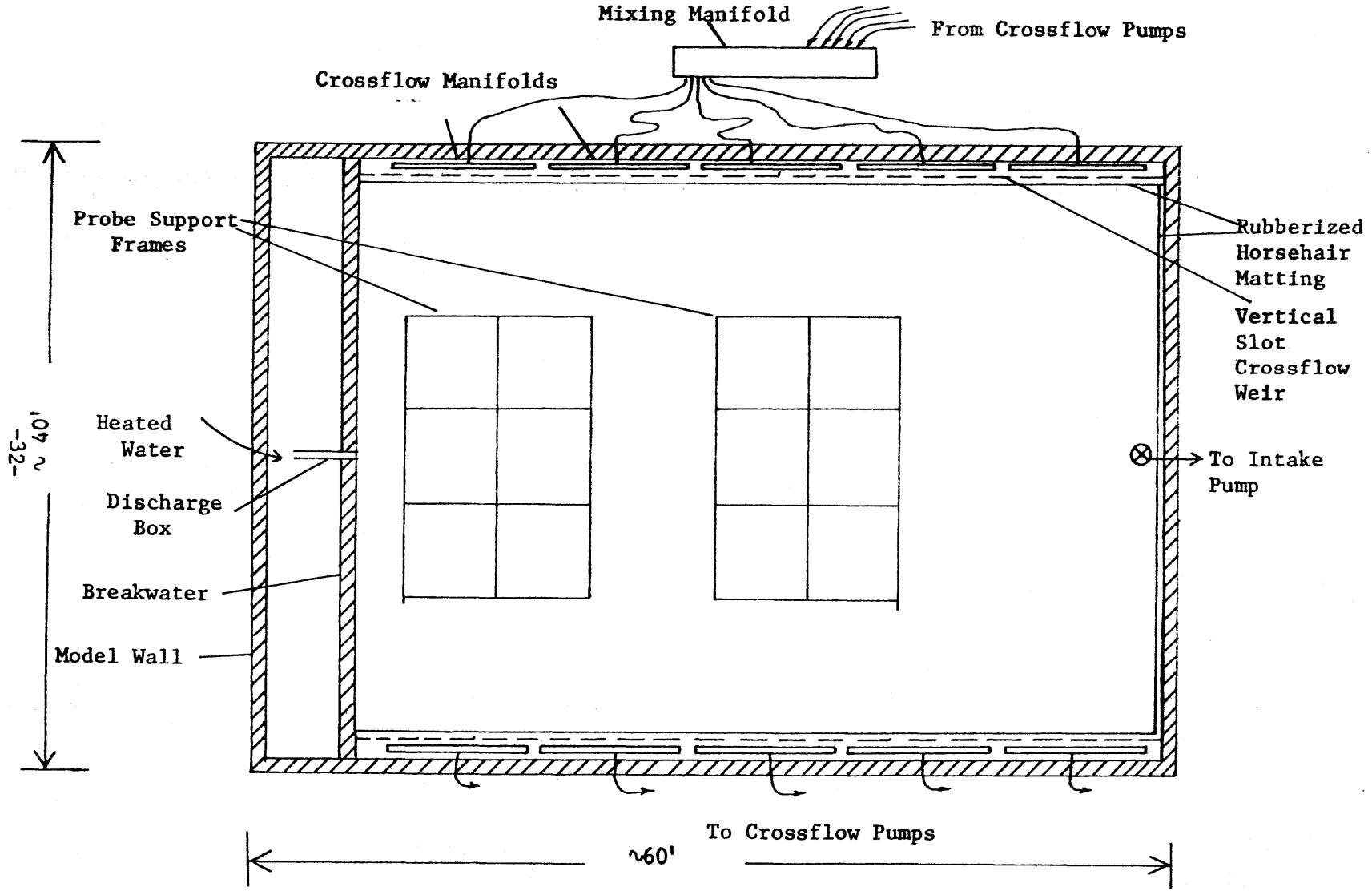

Figure 3-2: Experimental Setup

seconds). 98 probes are mounted on two wooden probe platforms using aluminum Dexion and two additional probes monitor hot water in the head tank and in the discharge box. Probe elevation may be adjusted during run operation by turning light hand-operated screw jacks located in the corners of the platforms.

A computer data acquisition system consisting of a digital thermometer and an electronic scanner manufactured by Digitec and a Hewlett Packard 2114B computer are used to record temperatures on a digitized tape. The tape is then converted to cards and data is run through a Fortran program which reduces it to dimensionless temperature rises. The results are printed in a format corresponding to the probe arrangement in the basin.

3.4 Procedure and Data Acquisition

A typical run takes about 60 minutes and starts when the basin is quiet and well-mixed. Initial scans on the surface and the bottom are taken to determine if any initial stratification exists and to reference subsequent temperature differences. Discharge and intake waters are turned on, a small quantity of dye is injected into the discharge and the plume is allowed to develop. After about 10 minutes scans are begun starting with the near surface and continuing to the near bottom, followed by a final scan on the surface. Each scan requires approximately 3 1/2 minutes: 2 minutes for scanning and 1 1/2 minutes for recording on digitized tape, during which time the platform is

cranked into position for the next scan. From 7 to 9 scans (including the initial two scans) were performed for each of the runs, depending on the water depth. Each run thus consists of 700 to 900 temperatures which are read into the computer. Output is in the form of a dimensionless temperature rise for each probe at each scan.

IV EXPERIMENTAL RESULTS

4.1 Introduction

The parametric study consisted of 49 laboratory experiments. The relevant physical variables and non-dimensional parameters are tabulated in Table 4.1. The densimetric Froude number $\mathbb{F}_o$ ranged between 4.9 and 15.7, the relative water depth H/D_o ranged between 1.9 and 6.3, the relative crossflow v/u_o ranged between 0.020 and 0.074, and the relative discharge submergence z/H ranged between near surface ($z/H \sim 0$) and near bottom ($z/H \sim 1$). The jet Reynolds number $\mathbb{R}_e$ varied between 7,900 and 12,000 indicative of turbulent flow.

The test results were analyzed with respect to induced surface temperature rise. The non-dimensional temperature rise $\Delta T_s/\Delta T_o$ at the surface is defined as

$$\frac{\Delta T_s}{\Delta T_o} = \frac{T_{surface} - T_a}{T_o - T_a} \tag{4-1}$$

The particular case of the non-dimensional surface centerline temperature at the surface $\frac{\Delta T_{sc}}{\Delta T_o}$ is defined as

$$\frac{\Delta T_{sc}}{\Delta T_o} = \frac{T_{surface\ centerline} - T_a}{T_o - T_a} \tag{4-2}$$

TABLE 4-1

EXPERIMENTAL DATA OF PARAMETRIC STUDY

Physical Parameters							Non-Dimensional Parameters								Experimental Results
Run No.	H (ft)	v (fps)	u_o (fps)	$\sqrt{h_o b_o}$ (ft)	D_o (ft)	ΔT_o (°F)	F_o'	F_o	z/H	v/u_o	R_e	$\frac{h_{max}}{H}$	H/D_o	$H/\sqrt{h_o b_o}$	$\frac{\Delta T_{max}}{\Delta T_o}$
1	0.67	0.0	1.13	0.07	.106	16.7	17.9	14.2	0	0.0	12017	0.75	6.3	10	0.46
2	0.67	0.0	1.13	0.07	.106	16.8	17.5	13.9	.33	0.0	12017	--	6.3	10	0.37
3	0.67	0.0	1.13	0.07	.106	18.4	16.7	13.2	.67	0.0	12017	--	6.3	10	0.26
4	0.67	0.0	1.13	0.07	.106	17.0	17.8	14.1	1.0	0.0	12017	--	6.3	10	0.18
5	0.48	0.0	1.13	0.07	.106	17.6	17.3	13.7	0	0.0	12017	1.00	5.0	7.2	0.50
6	0.48	0.0	1.13	0.07	.106	15.6	19.8	15.7	.33	0.0	12017	--	5.0	7.2	0.37
7	0.48	0.0	1.13	0.07	.106	16.5	17.5	13.8	.67	0.0	12017	--	5.0	7.2	0.26
8	0.48	0.0	1.13	0.07	.106	16.9	17.0	13.5	1.0	0.0	12017	--	5.0	7.2	0.19
9	0.40	0.0	1.13	0.07	.106	16.6	19.1	15.1	0	0.0	12017	1.34	3.8	6	0.37
10	0.40	0.0	1.13	0.07	.106	—	--	--	.33	0.0	12017	--	3.8	6	--
11	0.40	0.0	1.13	0.07	.106	17.9	18.4	14.5	.67	0.0	12017	--	3.8	6	0.33
12	0.40	0.0	1.13	0.07	.106	16.7	19.0	15.0	1.0	0.0	12017	--	3.8	6	0.20
13	0.20	0.0	1.13	0.07	.106	16.4	18.2	14.4	0	0.0	12017	2.55	1.9	3	0.41
14	0.20	0.0	1.13	0.07	.106	17.3	17.2	13.6	0.5	0.0	12017	--	1.9	3	0.44
15	0.20	0.0	1.13	0.07	.106	16.4	18.3	14.5	1.0	0.0	12017	--	1.9	3	0.35
16	0.79	0.0	0.82	0.08	.125	16.1	11.5	9.1	0	0.0	10191	0.42	6.3	10	0.37

TABLE 4-1 (CONTINUED)

EXPERIMENTAL DATA OF PARAMETRIC STUDY

Physical Parameters							Non-Dimensional Parameters								Experimental Results
Run No.	H (ft)	v (fps)	u_o (fps)	$\sqrt{h_o b_o}$ (ft)	D_o (ft)	ΔT_o (°F)	F_o'	F_o	z/H	v/u_o	R_e	$\frac{h_{max}}{H}$	H/D_o	$H/\sqrt{h_o b_o}$	$\frac{\Delta T_{max}}{\Delta T_o}$
17	0.79	0.0	0.82	0.08	.125	16.1	11.7	9.3	.33	0.0	10191	--	6.3	10	0.50
18	0.79	0.0	0.82	0.08	.125	16.3	11.1	8.8	.67	0.0	10191	--	6.3	10	0.20
19	0.79	0.0	0.82	0.08	.125	15.7	11.4	9.0	1.0	0.0	10191	--	6.3	10	0.16
20	0.47	0.0	0.82	0.08	.125	17.4	11.0	8.7	0	0.0	10191	0.78	3.8	6	0.46
21	0.47	0.0	0.82	0.08	.125	17.7	10.9	8.7	.33	0.0	10191	--	3.8	6	0.43
22	0.47	0.0	0.82	0.08	.125	16.3	11.5	9.1	.67	0.0	10191	--	3.8	6	0.25
23	0.47	0.0	0.82	0.08	.125	17.1	11.0	8.7	1.0	0.0	10191	--	3.8	6	0.25
24	0.24	0.0	0.82	0.08	.125	16.6	11.0	8.7	0	0.0	10191	1.54	1.9	3	0.44
25	0.24	0.0	0.82	0.08	.125	16.6	11.0	8.7	0.5	0.0	10191	--	1.9	3	0.41
26	0.24	0.0	0.82	0.08	.125	16.4	11.1	8.8	1.0	0.0	10191	--	1.9	3	0.31
27	0.82	0.0	0.49	0.10	.161	16.1	6.2	4.9	0	0.0	7912	0.33	4.5	8	0.53
28	0.82	0.0	0.49	0.10	.161	16.5	5.9	4.6	.33	0.0	7912	--	4.5	8	0.32
29	0.82	0.0	0.49	0.10	.161	16.1	6.3	5.0	.67	0.0	7912	--	4.5	8	0.32
30	0.82	0.0	0.49	0.10	.161	16.6	6.2	4.9	1.0	0.0	7912	--	4.5	8	0.21
31	0.61	0.0	0.49	0.10	.161	15.7	6.4	5.1	0	0.0	7912	0.45	3.8	6	0.59
32	0.61	0.0	0.49	0.10	.161	15.2	6.4	5.1	.33	0.0	7912	--	3.8	6	0.41

TABLE 4-1 (CONTINUED)
EXPERIMENTAL DATA OF PARAMETRIC STUDY

Physical Parameters							Non-Dimensional Parameters								Experimental Results
Run No.	H (ft)	v (fps)	u_o (fps)	$\sqrt{h_o b_o}$ (ft)	D_o (ft)	ΔT_o (°F)	F_o'	F_o	z/H	v/u_o	R_e	$\frac{h_{max}}{H}$	H/D_o	$H/\sqrt{h_o b_o}$	$\frac{\Delta T_{max}}{\Delta T_o}$
33	0.61	0.0	.49	0.10	.161	14.9	6.5	5.2	.67	0.0	7912	—	3.8	6	.41
34	0.61	0.0	.49	0.10	.161	15.7	6.4	5.1	1.0	0.0	7912	—	3.8	6	.32
35															
36	0.31	0.0	.49	0.10	.161	16.8	6.3	5.1	0	0.0	7912	0.88	1.9	3	.57
37	0.31	0.0	.49	0.10	.161	17.8	6.0	4.8	.5	0.0	7912	—	1.9	3	.57
38	0.31	0.0	.49	0.10	.161	15.2	6.7	5.3	1.0	0.0	7912	—	1.9	3	.42
50	0.40	0.060	1.13	0.07	.106	17.8	16.3	12.9	0	.049	12017	1.25	3.8	6	.22
51	0.40	0.060	1.13	0.07	.106	16.9	17.1	13.6	1.0	.049	12017	--	3.8	6	.14
54	0.47	0.047	0.82	0.08	.125	—	--	--	0	.058	10191	0.78	3.8	6	.25
55	0.47	0.047	0.82	0.08	.125	16.7	11.2	8.9	1.0	.058	10191	—	3.8	6	.19
56	0.61	0.036	0.49	0.10	.161	17.0	6.0	4.8	0	.074	7912	0.45	3.8	6	.48
57	0.61	0.036	0.49	0.10	.161	16.8	6.0	4.8	1.0	.074	7912	—	3.8	6	--
60	0.40	0.060	1.13	0.07	.106	17.4	16.5	13.0	0	.020	12017	1.25	3.8	6	.34
61	0.40	0.060	1.13	0.07	.106	16.3	17.4	13.7	1.0	.020	12017	--	3.8	6	.22
64	0.47	0.047	0.82	0.08	.125	16.7	11.2	8.9	0	.023	10191	0.78	3.8	6	.28
65	0.47	0.047	0.82	0.08	.125	16.4	11.3	9.0	1.0	.023	10191	—	3.8	6	.20
66	0.61	0.036	0.49	0.10	.161	16.4	6.1	4.8	0	.030	7912	0.45	3.8	6	.48
67	0.61	0.036	0.49	0.10	.161	16.2	6.1	4.8	1.0	.030	7912	—	3.8	6	.32

4.2 Single-port Discharge Without Crossflow

4.2.1 Near-Surface Discharge

Preliminary Observations

In the absence of ambient currents the most critical parameters governing the near-surface discharge behavior are the Froude number F_o and the relative water depth H/D_o. At Froude numbers between 1 and 2, the jet mixing is observed to be restricted to the lateral surface and the heated discharge is essentially "floated" on to the receiving water. At higher Froude numbers, increased mixing results in a greater volume of entrained water causing the jet to penetrate deeper and become attached to the bottom. The jet remains attached until buoyant forces overcome the effects of the entrainment. In relatively shallow depths, the results indicate substantial deviation of temperature distributions from those corresponding to the ideal conditions of unrestricted water depth characterizing Stolzenbach's (1971) predictive model for surface discharges.

Centerline and Areal Dilutions

Figures 4-1 to 4-4 are plots of centerline temperature rise versus longitudinal distance. Figures 4-5 to 4-7 are plots of excess temperature contours versus enclosed surface area.

These figures illustrate that in shallow water the temperature dilution is dependent upon the interrelationship between the relative water depth and the Froude number. The shape of the curves has important physical meaning. Note that with increasing

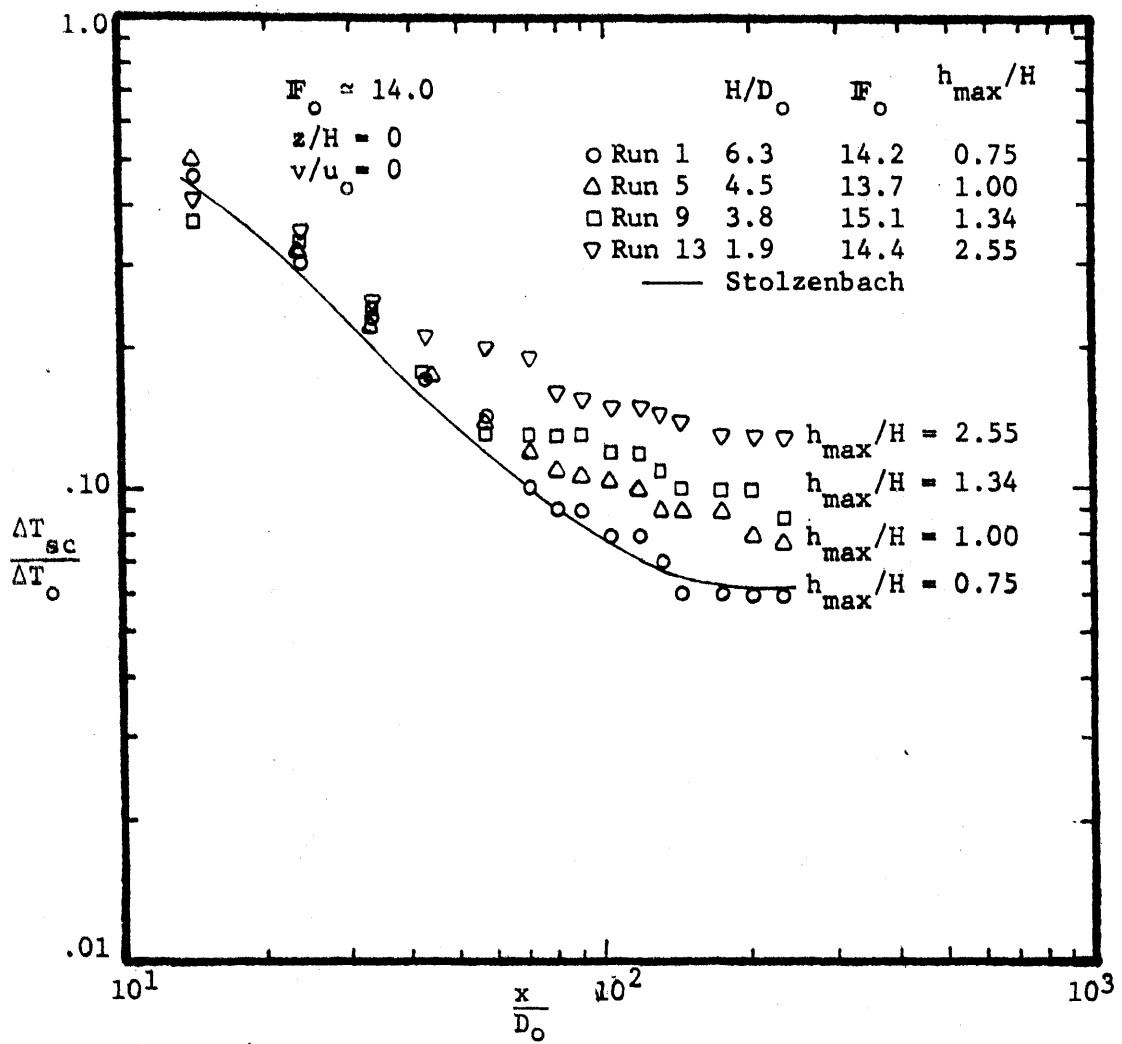

Figure 4-1: Surface Centerline Temperature Rise vs. Longitudinal Distance with Constant $F_o \simeq 14.0$

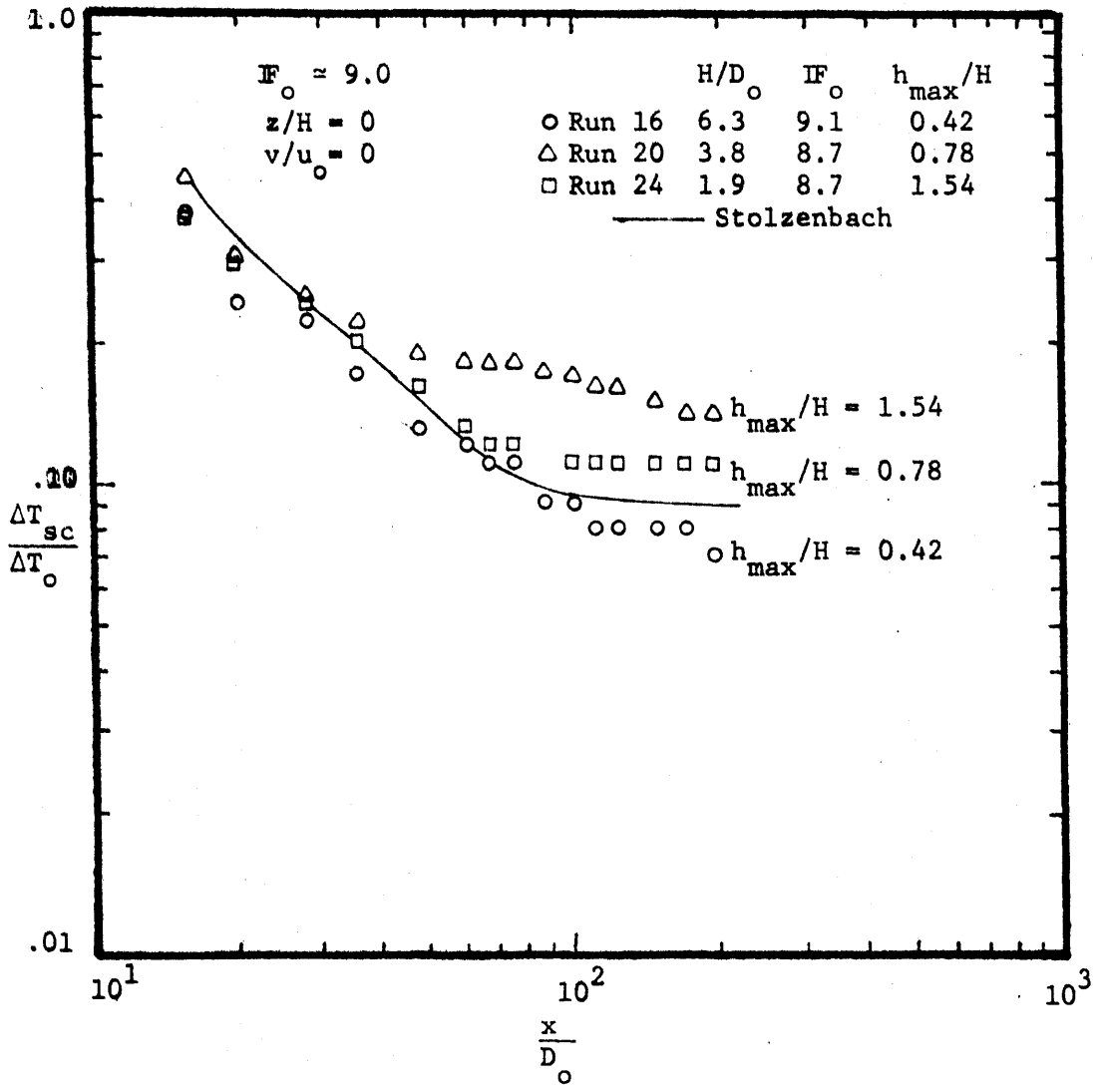

Figure 4-2: Surface Centerline Temperature Rise vs. Longitudinal Distance with Constant $\mathbb{F}_o \simeq 9.0$

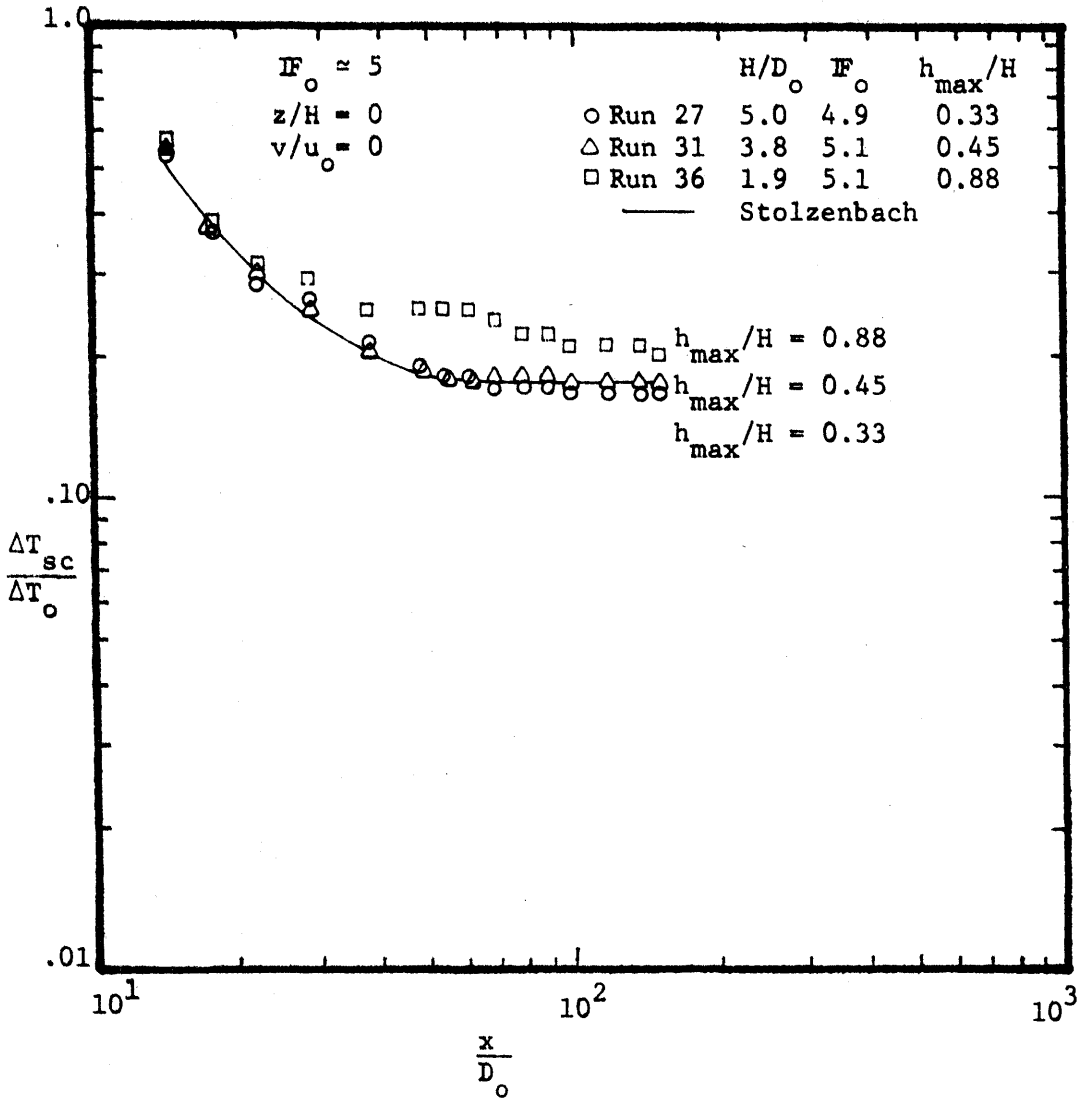

Figure 4-3: Surface Centerline Temperature Rise vs. Longitudinal Distance with Constant $\mathbb{F}_o \simeq 5.0$

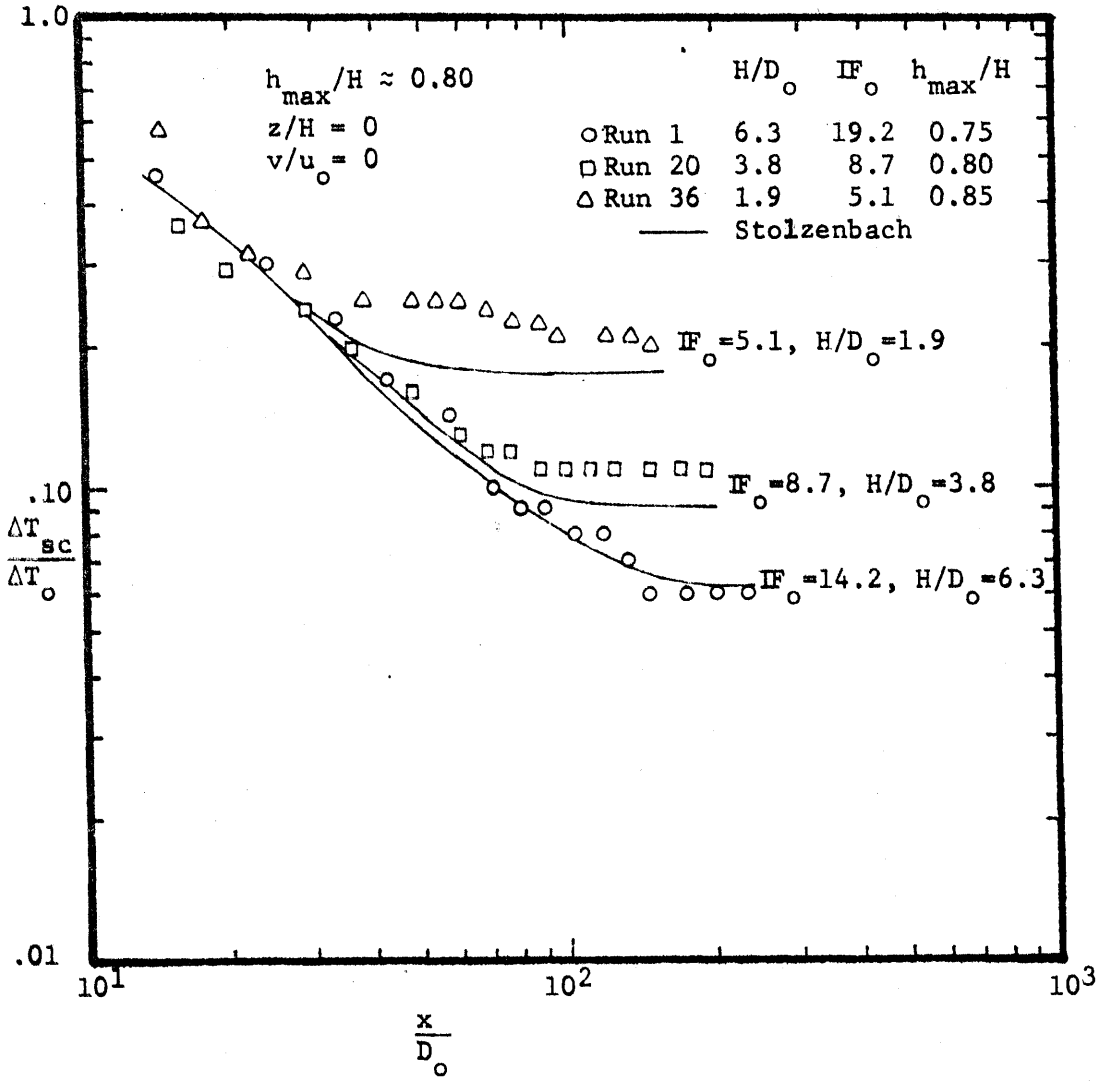

Figure 4-4: Surface Centerline Temperature Rise vs. Longitudinal Distance with Constant $h_{max}/H \sim 0.80$

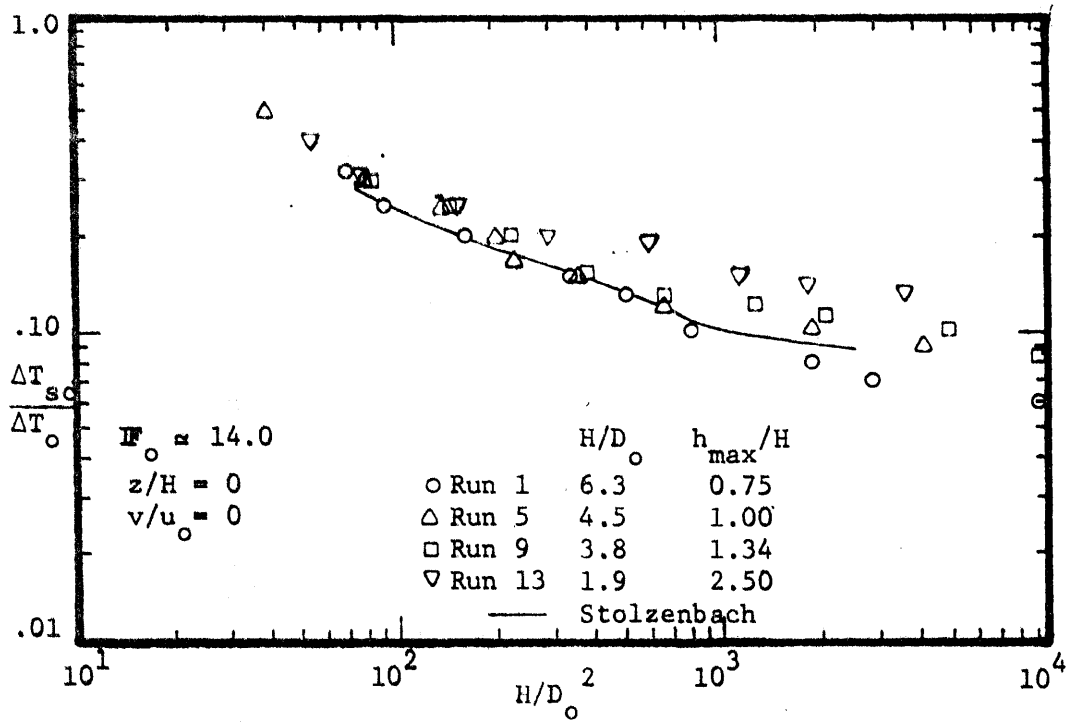

Figure 4-5: Excess Temperature Contours vs. Enclosed Surface Area with Constant $IF \simeq 14.0$

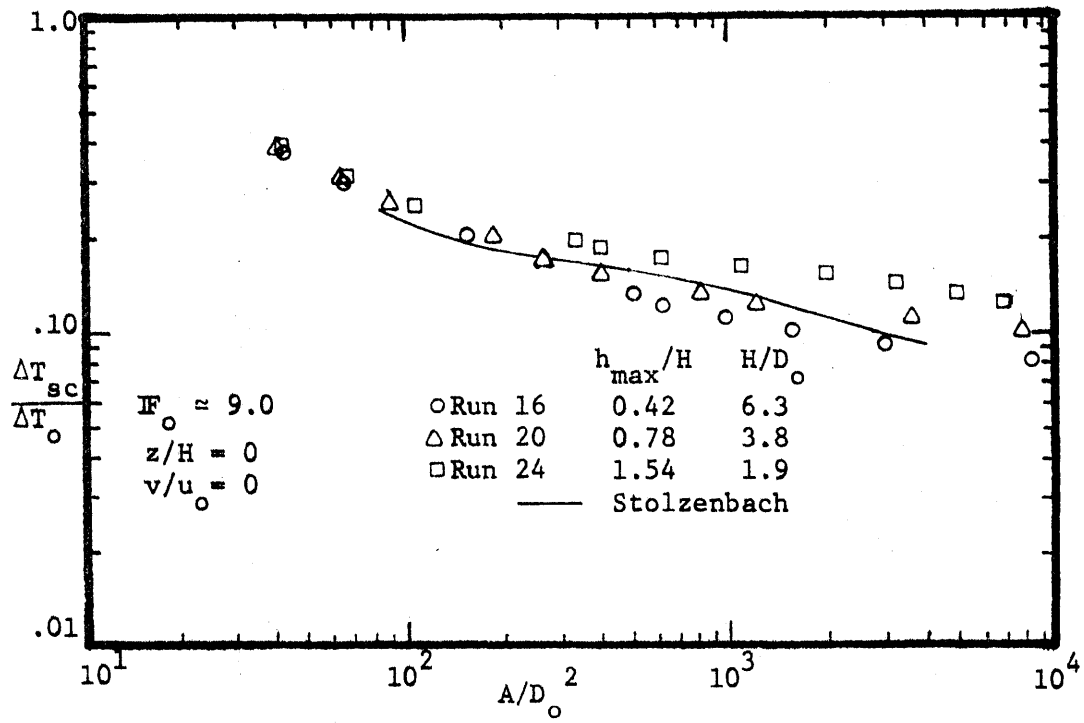

Figure 4-6: Excess Temperature Contours vs. Enclosed Surface Area with Constant $IF_o \simeq 9.0$

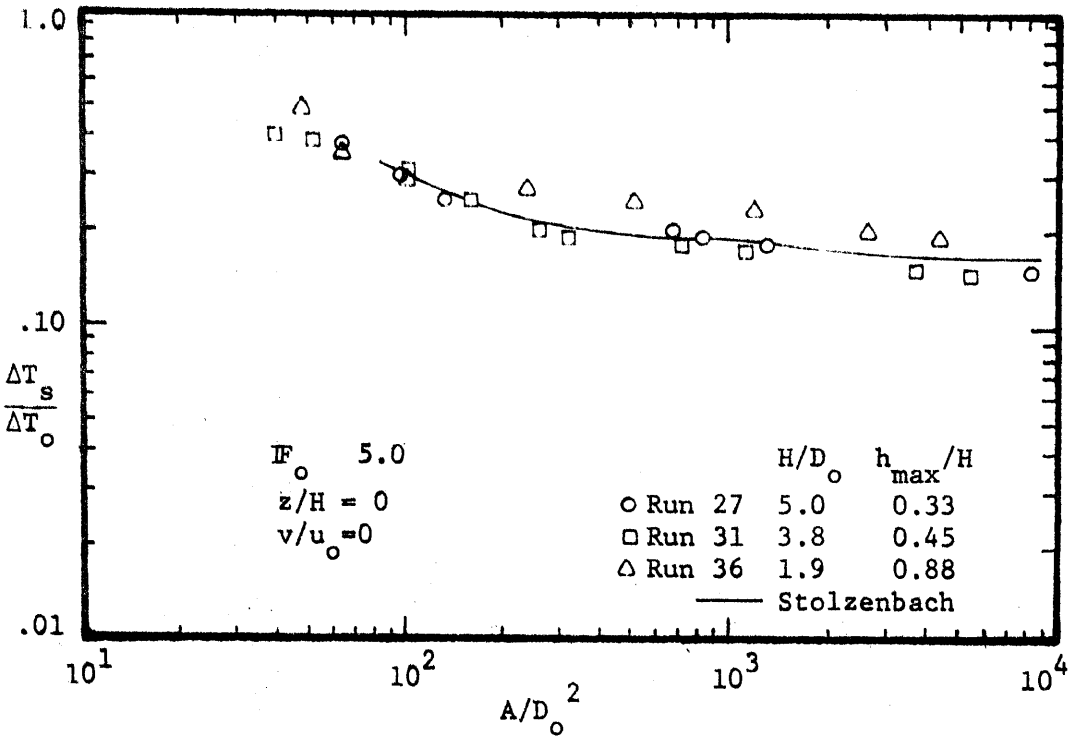

Figure 4-7: Excess Temperature Contours vs. Enclosed Surface Area with Constant $F_o \approx 5.0$

distance from the discharge the curves become flat. Hence, a large increase in distance or surface area results in a small incremental decrease in the temperature rise, $\Delta T_s/\Delta T_o$.

The results show that where horizontal inertial forces dominate, temperature dilutions increase with increasing Froude number or increasing water depth. The centerline temperature rises show increasing agreement and the areal temperature rises show fair agreement with Stolzenbach's model as H/D_o increases. Obviously, the theoretical results give unrealiztically low temperature concentrations at low water depths with the discrepancy increasing with decreasing relative water depth, (see Figures 4-1 to 4-3).

What "deep water" is depends on the relative magnitude of the Froude number. This can be reflected in the relative jet penetration parameter, $\frac{h_{max}}{H}$, which is defined in Chapter II

$$h_{max} = 0.42 \; F_o' \sqrt{h_o b_o} \qquad (2\text{-}41)$$

Note the magnitude of h_{max}/H in Figures 4-1 to 4-4, for those discharge configurations that show good agreement with Stolzenbach's prediction, i.e., "deep water" situations. The results suggest that for a given Froude number, there is a critical depth of water, beyond which the bottom does not significantly restrict jet entrainment. For the circular outfall, this critical configuration can be parameterized as

$$\left(\frac{h_{max}}{H}\right)_{crit} = f(IF_o, H/D_o) \qquad (4\text{-}3)$$

The importance of h_{max}/H with respect to temperature dilutions will be investigated further in the next section.

The fact that there is good agreement between the experimental results and Stolzenbach's prediction in "deep water" suggests that the hydraulic model was capable of simulating a semi-steady state condition before basin boundary effects dominated the flow pattern. Such a state is of short duration however.

Figure 4-8 is a plot of the relative maximum jet penetration depth, h_{max}/H. Both experimental results and theoretical prediction are presented. Figure 4-9 shows a typical vertical section of a surface jet. The isotherm $\Delta T/\Delta T_o = 0.0$ is used to define the boundary of the jet's penetration in the experimental results. These results show good agreement with Stolzenbach's et al (1972) prediction of the jet's maximum penetration

$$\frac{h_{max}}{H} = \frac{0.42\ IF_o'\ \sqrt{h_o b_o}}{H} \qquad (4\text{-}4)$$

and the maximum penetration of a round near-surface jet is accurately predicted by Equation (4-4) when

$$IF_o(D_o/H) \leq 3.1 \qquad (4\text{-}5)$$

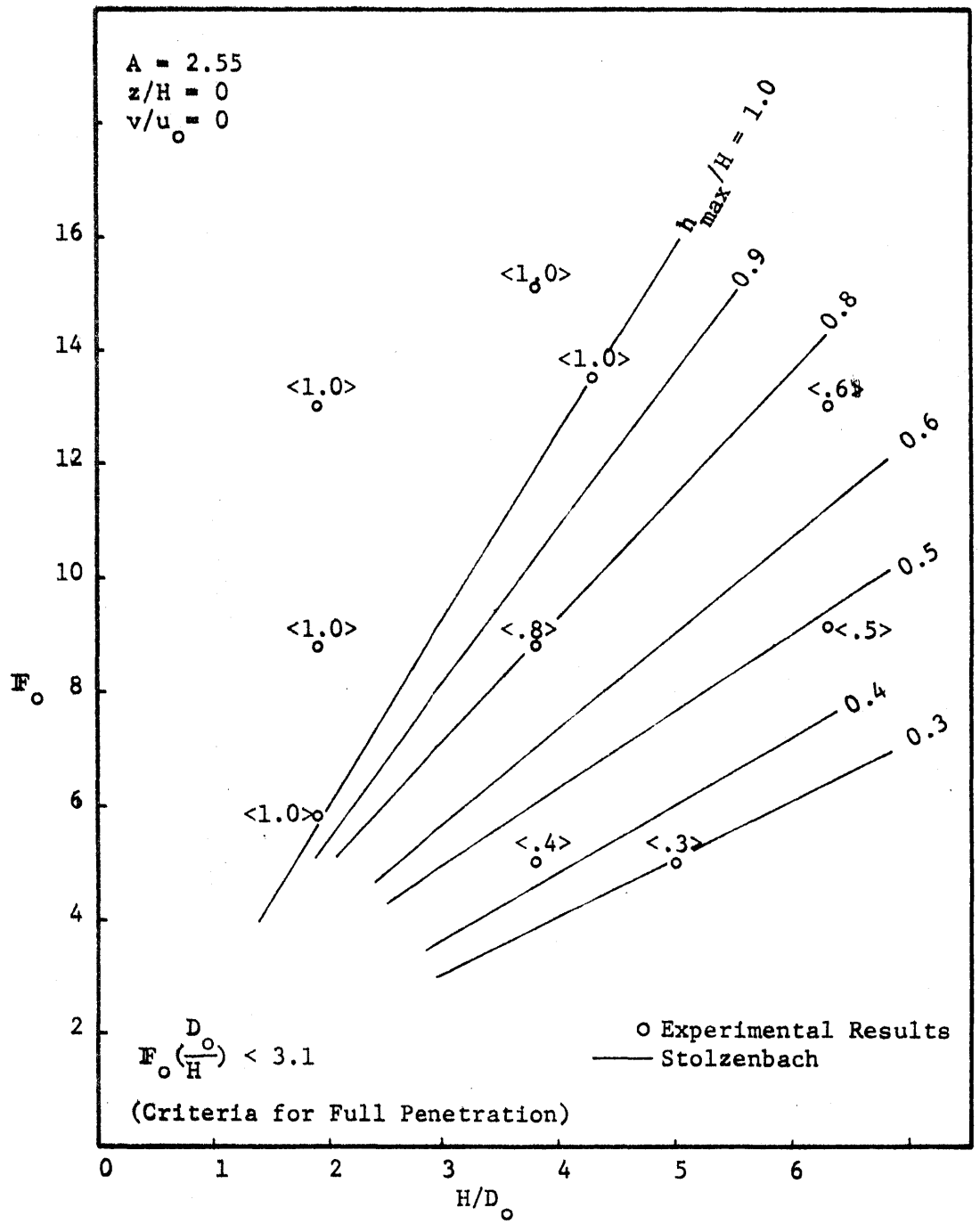

Figure 4-8: Maximum Jet Penetration Depth of Surface Discharge

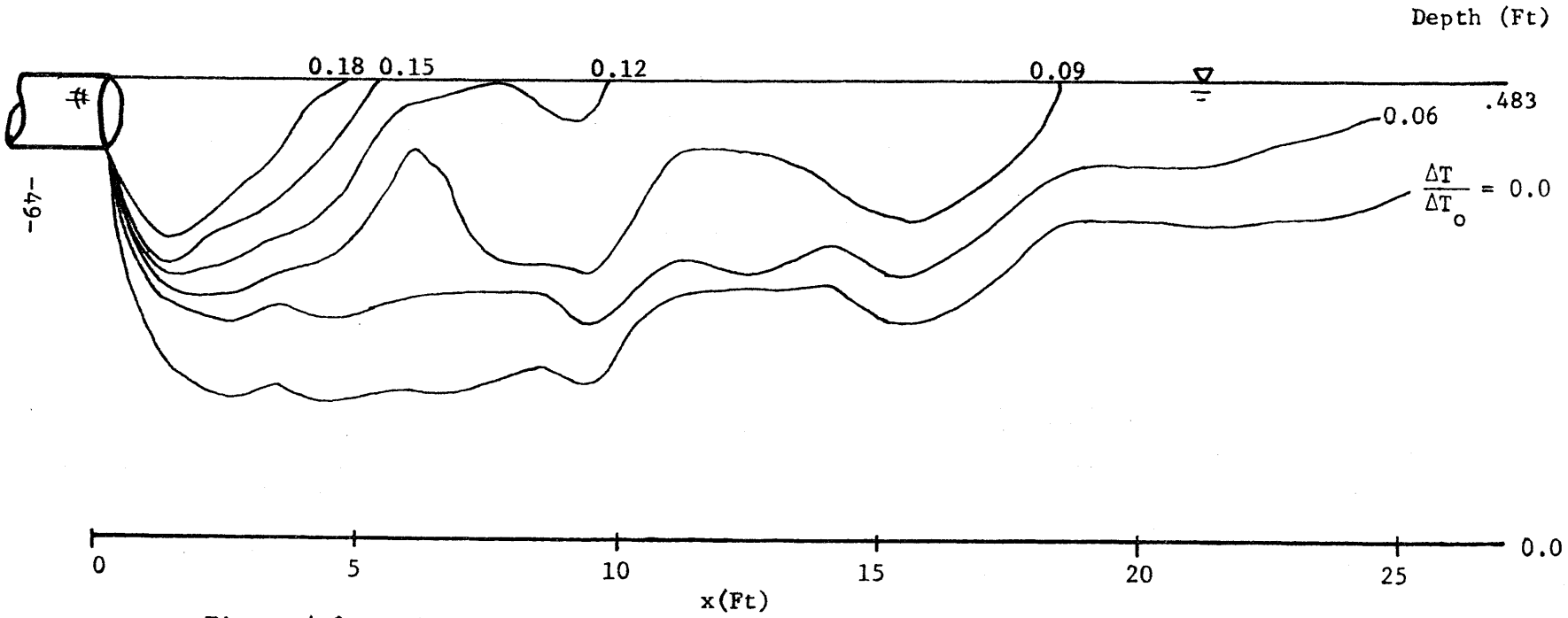

Figure 4-9: Schematic of Isotherms $\Delta T/\Delta T_o$ in the Vertical Plant, y = 0. Run No. 5

Stable Region Dilutions

Figure 4-10 characterizes the performance of a given discharge configuration ($I\!F_o$, H/D_o) in terms of the stable centerline temperature rise $(\frac{\Delta T_{sc}}{\Delta T_o})_s$. The stable centerline temperature is in principle the asymptotic limit of the $\Delta T_{sc}/\Delta T_o$ vs x/D_o curve; see Figures 4-1 to 4-3. The asymptotic values of $(\Delta T_{sc}/\Delta T_o)$ as $H/D_o \to \infty$ are obtained from Stolzenbach's model which is applicable in deep water. This is given by the inverse of Equation (2-40)

$$(\frac{\Delta T_{sc}}{\Delta T_o})_s \simeq 1/I\!F_o' \qquad (4\text{-}6)$$

These values are indicated on the right-hand side of the plots. The lines $(\Delta T_{sc}/\Delta T_o)_s$ = constant can be obtained by interpolating between the experimental values and then connecting the asymptotic points. Three separate regions can be distinguished.

Region I: The flow pattern resembles that of the unrestricted water depth condition. Consider a fixed value of $I\!F_o$ representing a given discharge condition. For increasing values of H/D_o, the stable centerline temperature rise $(\Delta T_{sc}/\Delta T_o)_s$ decreases down to a maximum value of $(H/D_o)_{crit}$. This indicates the dividing line between Regions I and II, and represents the point at which the assumption of an infinite extent of the ambient water becomes valid. The equation of the line in terms of h_{max} is:

$$(\frac{H}{D_o})_{crit} \simeq 3.3\ \ell n(\frac{h_{max}}{.45D_o}) \qquad (4\text{-}7)$$

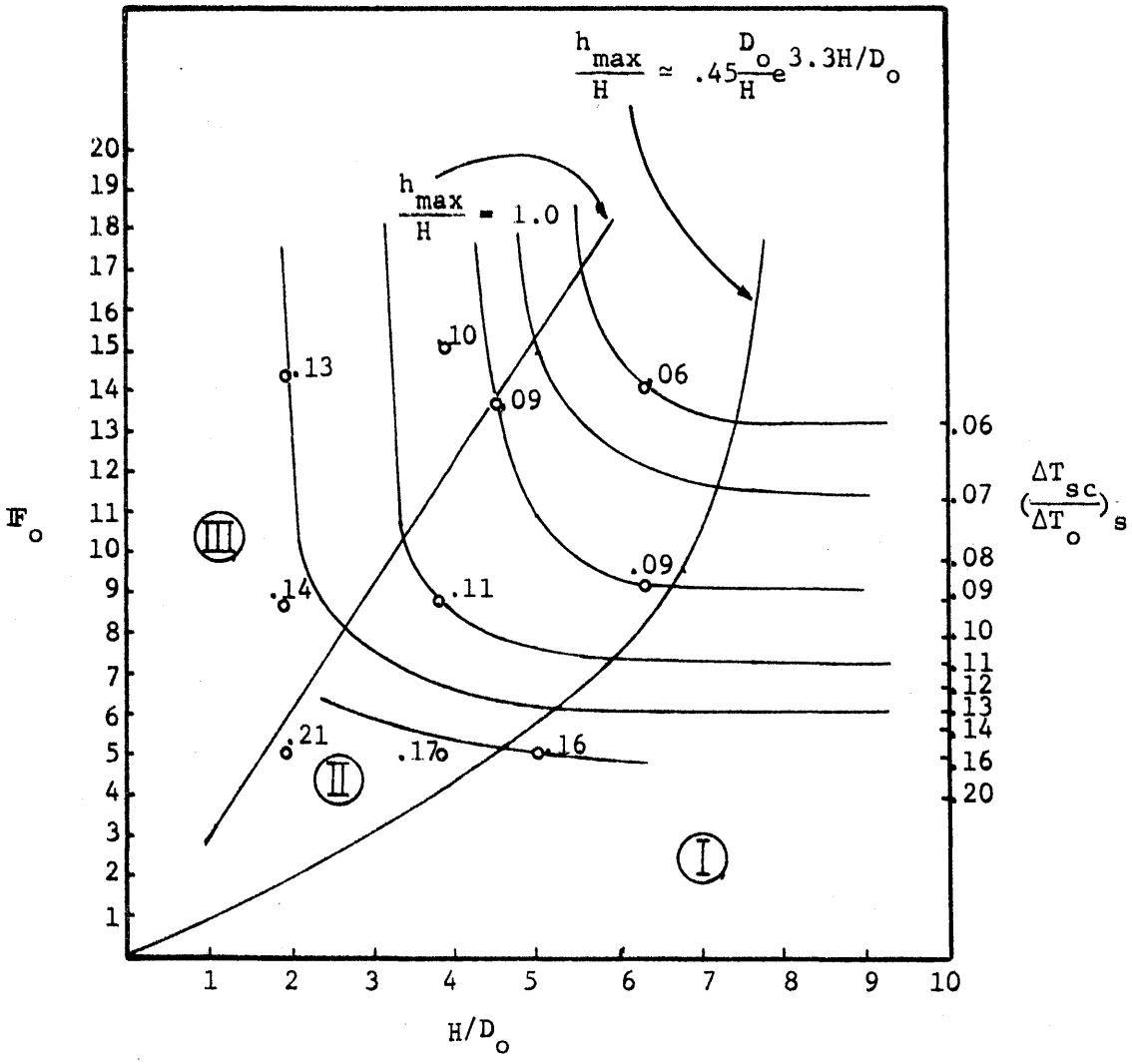

Figure 4-10: Stable Region Temperature Rise Near Surface Discharge

and

$$\text{If } \frac{H}{D} \geq 3.3 \ln\left(\frac{h_{max}}{.45D}\right) \qquad D_s = f(IF_o) \tag{4-8}$$

$$\text{If } \frac{H}{D_o} < 3.3 \ln\left(\frac{h_{max}}{.45D_o}\right) \qquad D_s = f(IF_o, H/D) \tag{4-9}$$

for Froude numbers 5 to 15. D_s is surface temperature dilution, $D_s = \left(\frac{\Delta T_{sc}}{\Delta T_o}\right)$.

Region II: The effect of decreasing relative water depth is to decrease temperature dilution and increase the areal distribution of the induced temperature rise. The ambient water does not remain stagnant since measureable currents are generated to replace the entrained water. From dye studies conducted in the model, large symmetrical opposing eddies are observed in the area of $x/D_o \sim 120$ from the discharge; see Figures 4-11 and 4-12. The jet is observed to be two dimensional in character as greater lateral entrainment combined with buoyant surface spread leads to re-entrainment of the heat. This phenomena results in a limited recirculation thus decreasing the validity of the equation of heat conservation (2-15). Note the position of the line $\frac{h_{max}}{H} = 1$. It is significant since it shows that for a fixed value of IF_o the bottom boundary affects jet behavior at depths of water greater than the depth of the jet's penetration.

Region III: In this region there is little dependence of $(\Delta T_{SC}/\Delta T_o)_s$ on IF_o when H/D_o is small. The water along the longitudinal axis of the discharge approaches fully mixed condition.

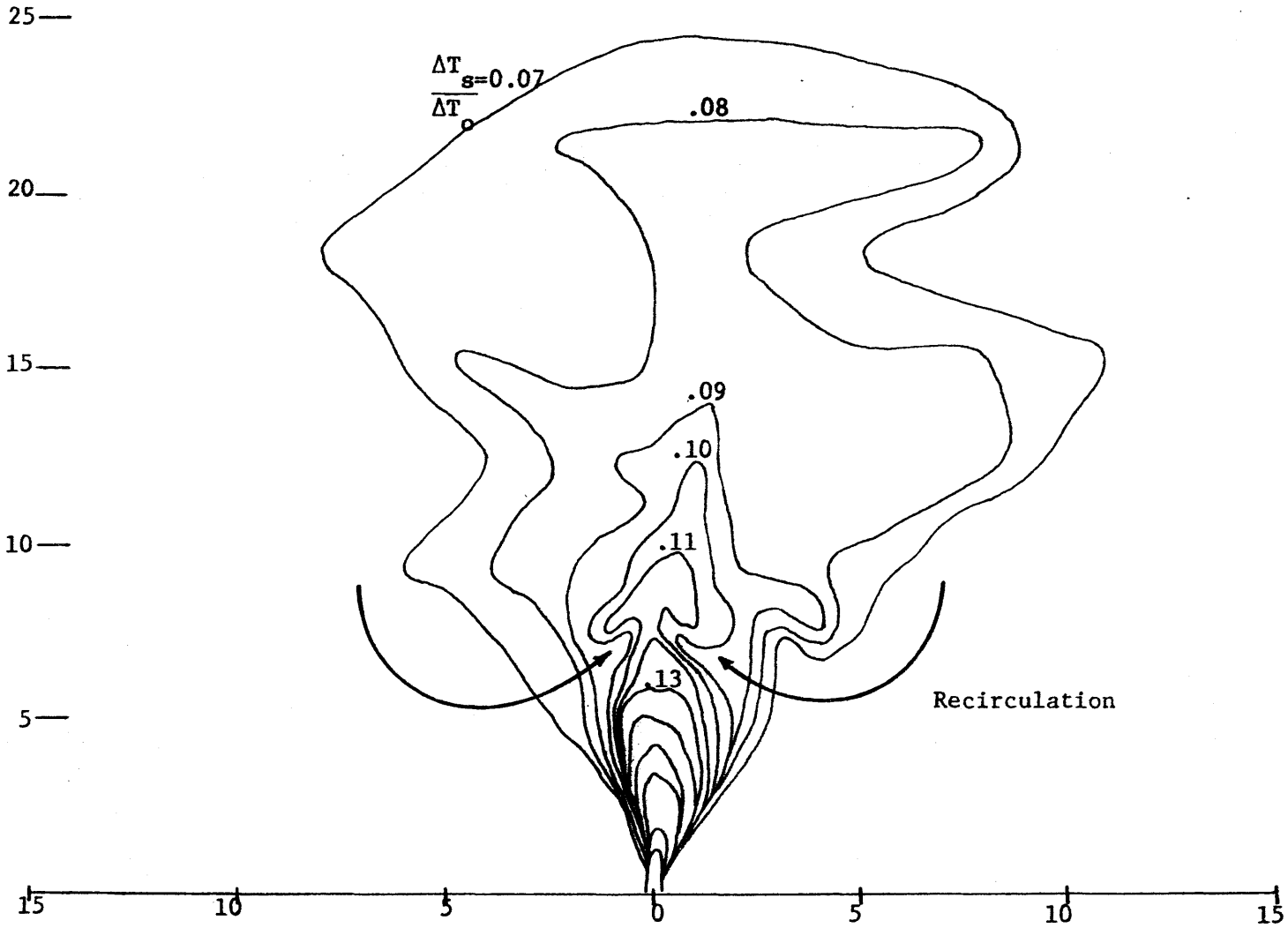

Figure 4-11: Surface Horizontal Temperature Distribution. Run No. 16, $z/H \simeq 0$

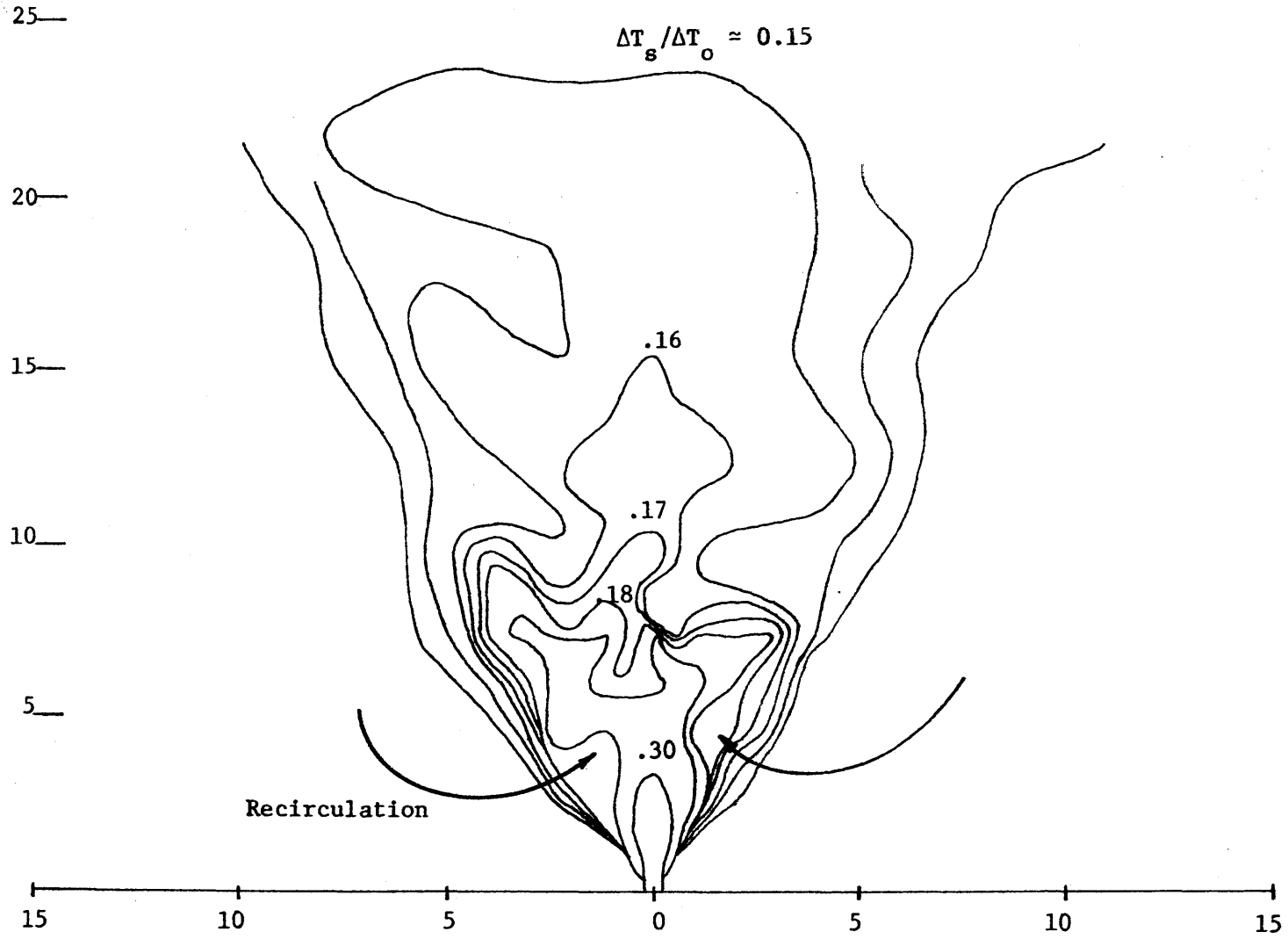

Figure 4-12: Surface Horizontal Temperature Distribution. Run No. 31, z/H ≃ 0

In this region

$$D_s = f(H/D_o) \qquad (4\text{-}10)$$

4.2.2 Discharges with Variable Submergence

Preliminary Observations

With increasing submergence, the observed effect of buoyancy is to deflect the jet trajectory toward the free surface and the greater the Froude number, the longer the trajectory. Due to the relatively low water depths, $H/D_o < 6.3$, the jet intersects the water surface at an angle ranging from 0° for near surface discharge to less than 90° as the discharge submergence approaches near bottom. Thus, the jet generally has a substantial horizontal velocity component at the surface which, for constant submergence, increases with increasing F_o.

Surface Centerline Dilutions

Figures 4-13 to 4-22 are plots of centerline temperature rise versus longitudinal distance. They show the effect of relative submergence z/H on temperature dilution with constant F_o and H/D_o. Figures 4-13 to 4-16 can be grouped with constant $F_o \sim 14.0$ and H/D_o ranging from 6.3 to 1.9. Similar groupings are possible for Figures 4-17 to 4-19 and for Figures 4-20 to 4-22 with $F_o \sim 9.0$ and 5.0, respectively.

The following phenomena are noted:

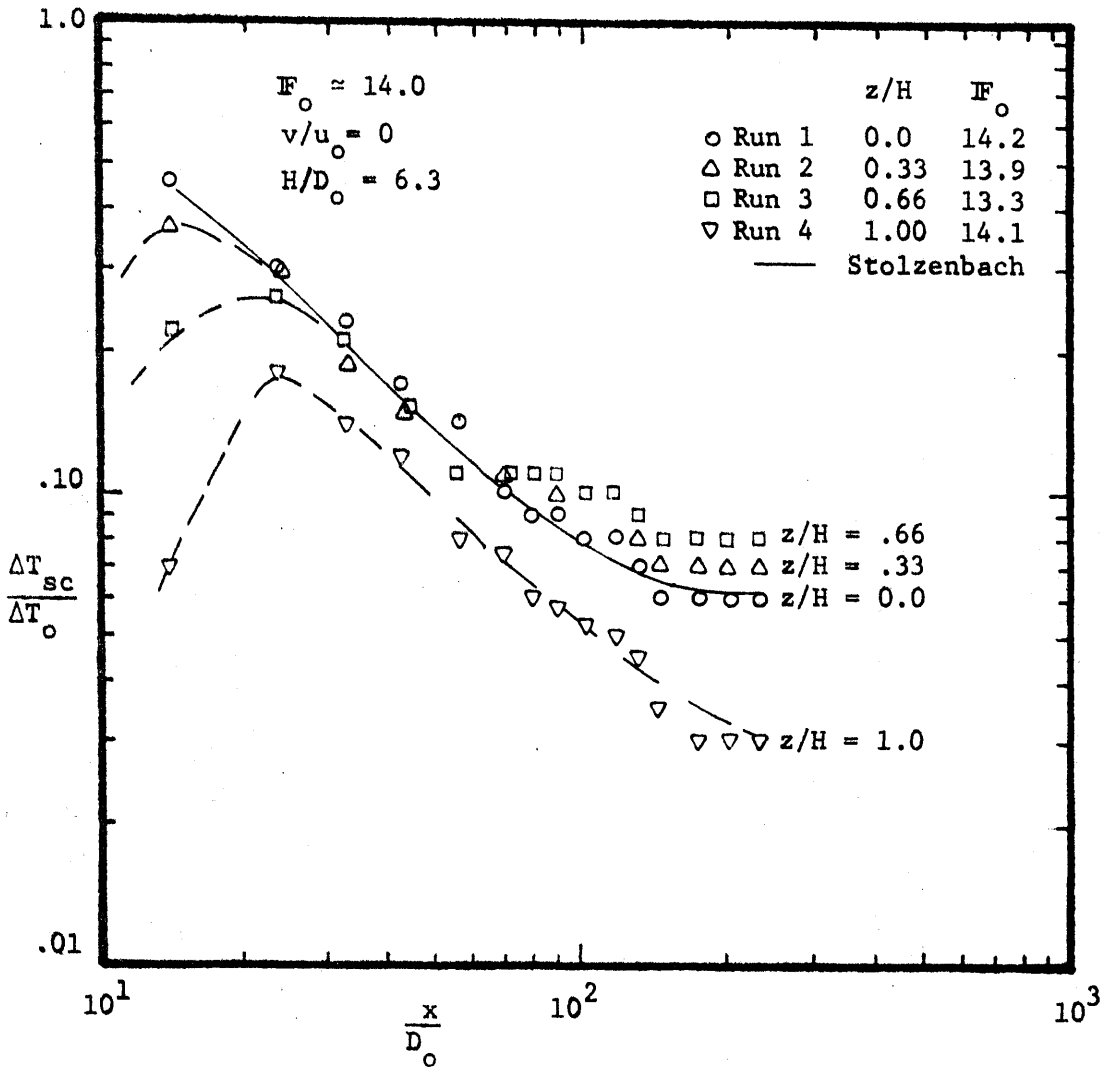

Figure 4-13: Surface Centerline Temperature Rise vs. Longitudinal Distance with Constant $F_o \simeq 14.0$, $H/D_o = 6.3$

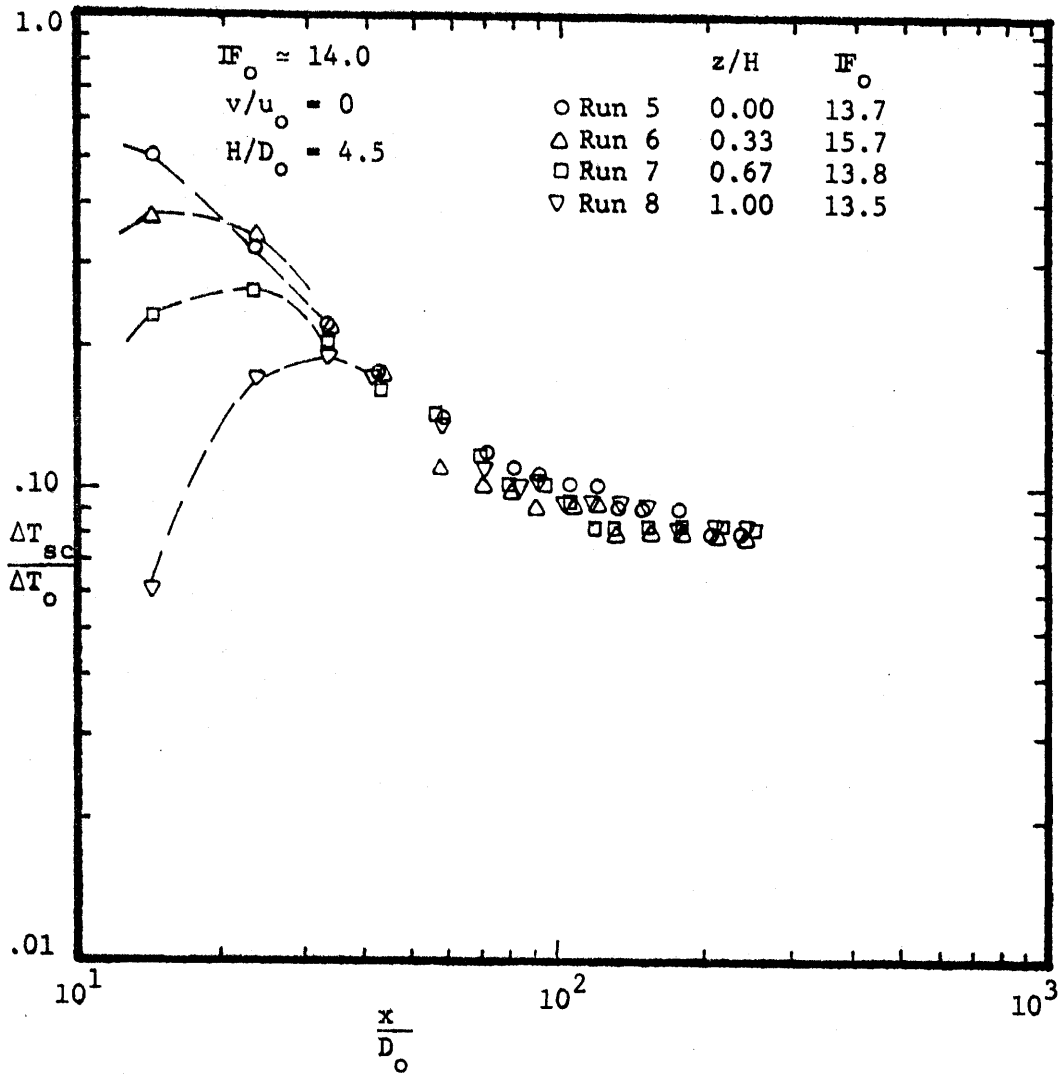

Figure 4-14: Surface Centerline Temperature Rise vs. Longitudinal Distance with Constant $\mathbb{F}_o \simeq 14.0$, $H/D_o = 4.5$

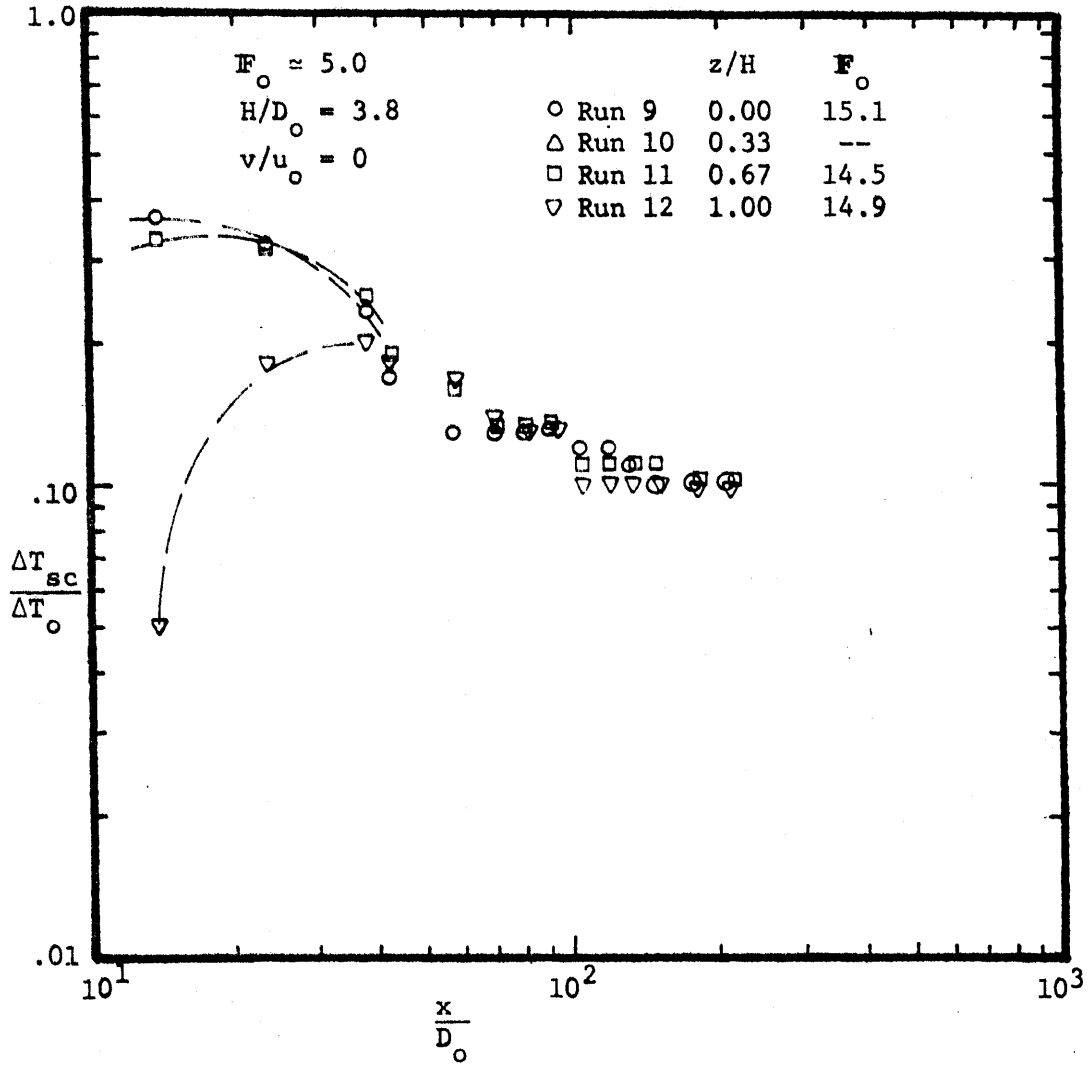

Figure 4-15: Surface Centerline Temperature Rise vs. Longitudinal Distance with Constant $F_o \simeq 15.0$, $H/D_o = 3.8$

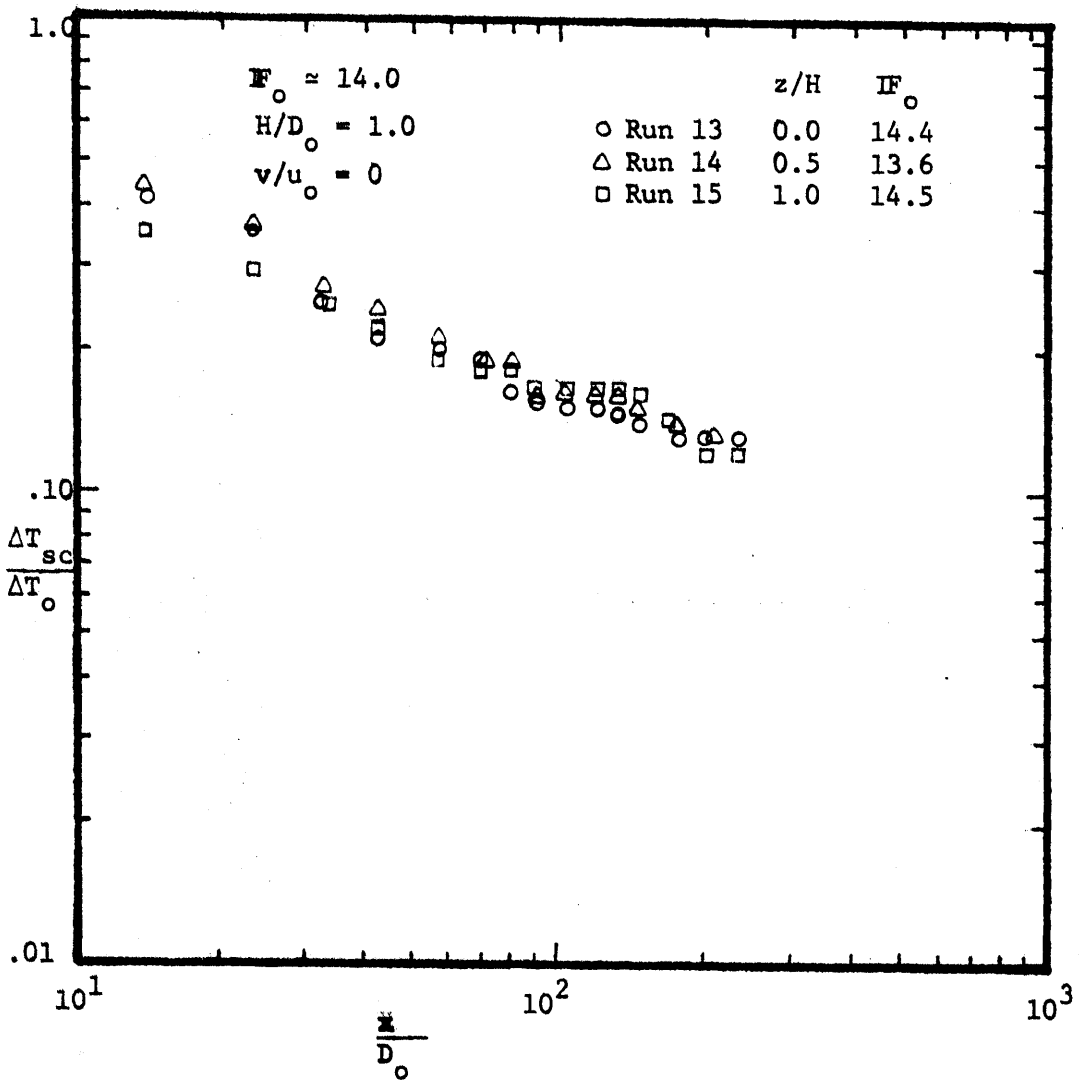

Figure 4-16: Surface Centerline Temperature Rise vs. Longitudinal Distance with Constant $IF_o \simeq 14.0$

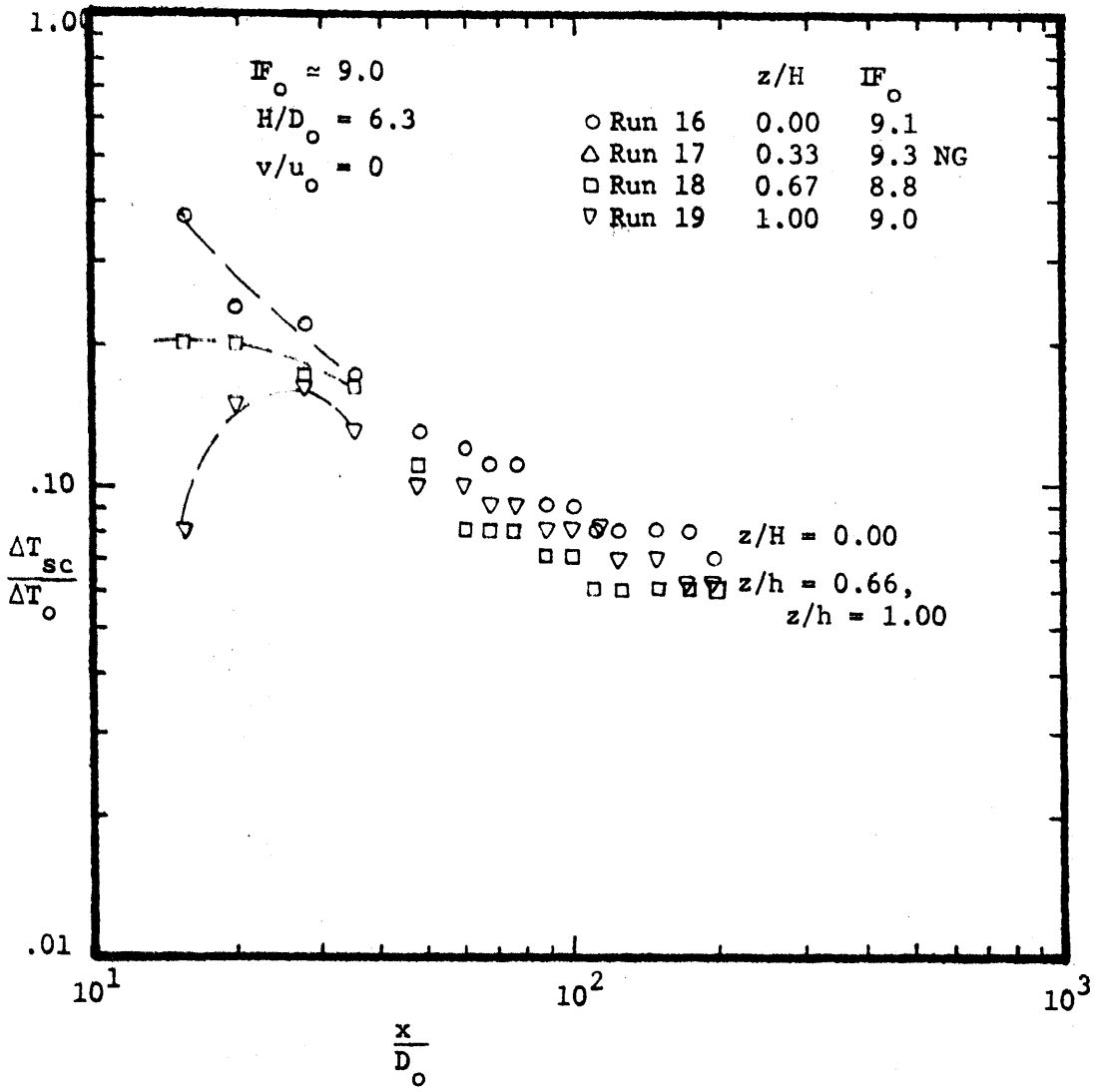

Figure 4-17: Surface Centerline Temperature Rise vs. Longitudinal Distance with Constant $IF_o \simeq 9.0$, $H/D_o = 6.3$

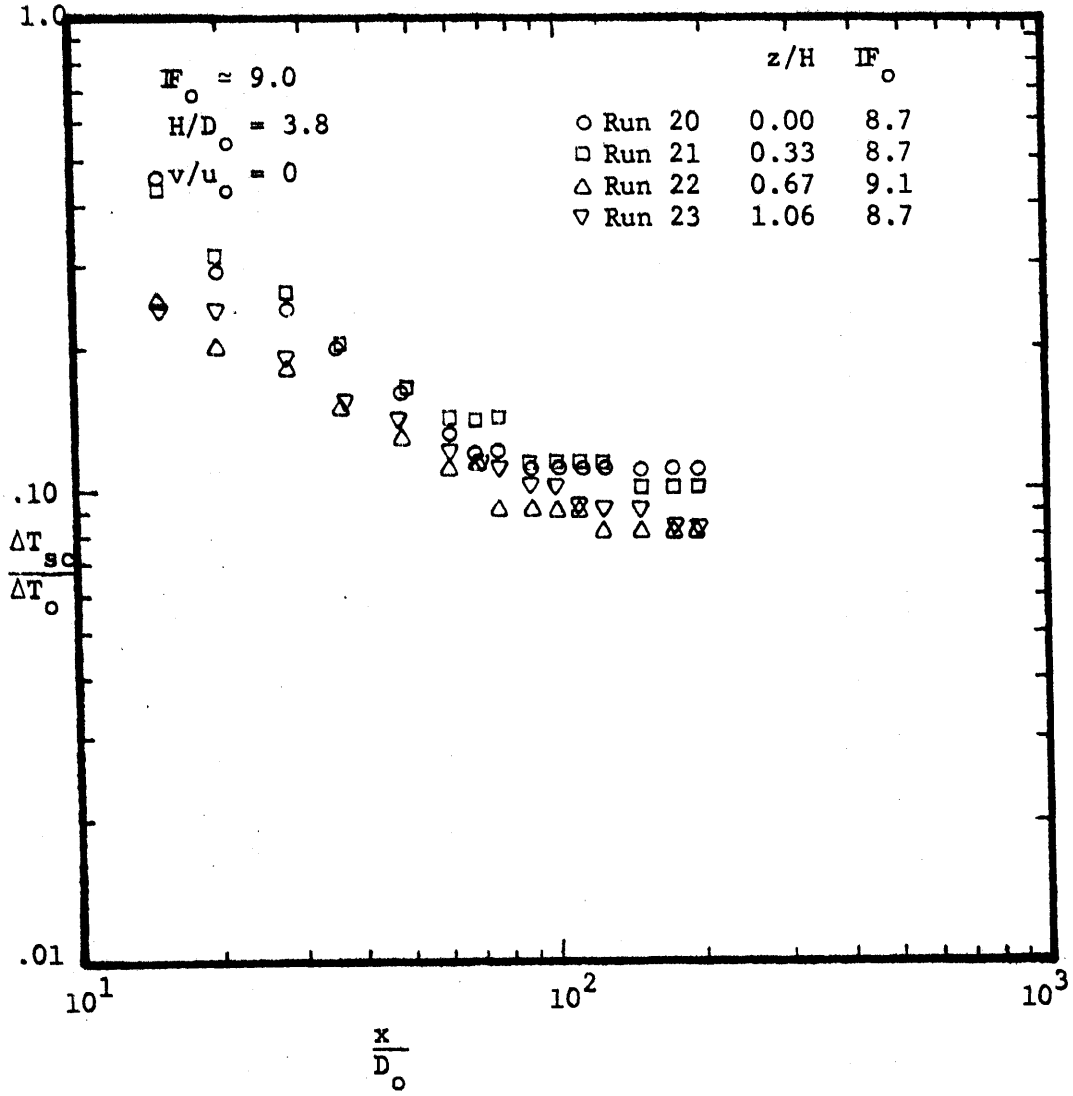

Figure 4-18: Surface Centerline Temperature Rise vs. Longitudinal Distance with Constant $F_o \simeq 9.0$, $H/D_o = 3.8$

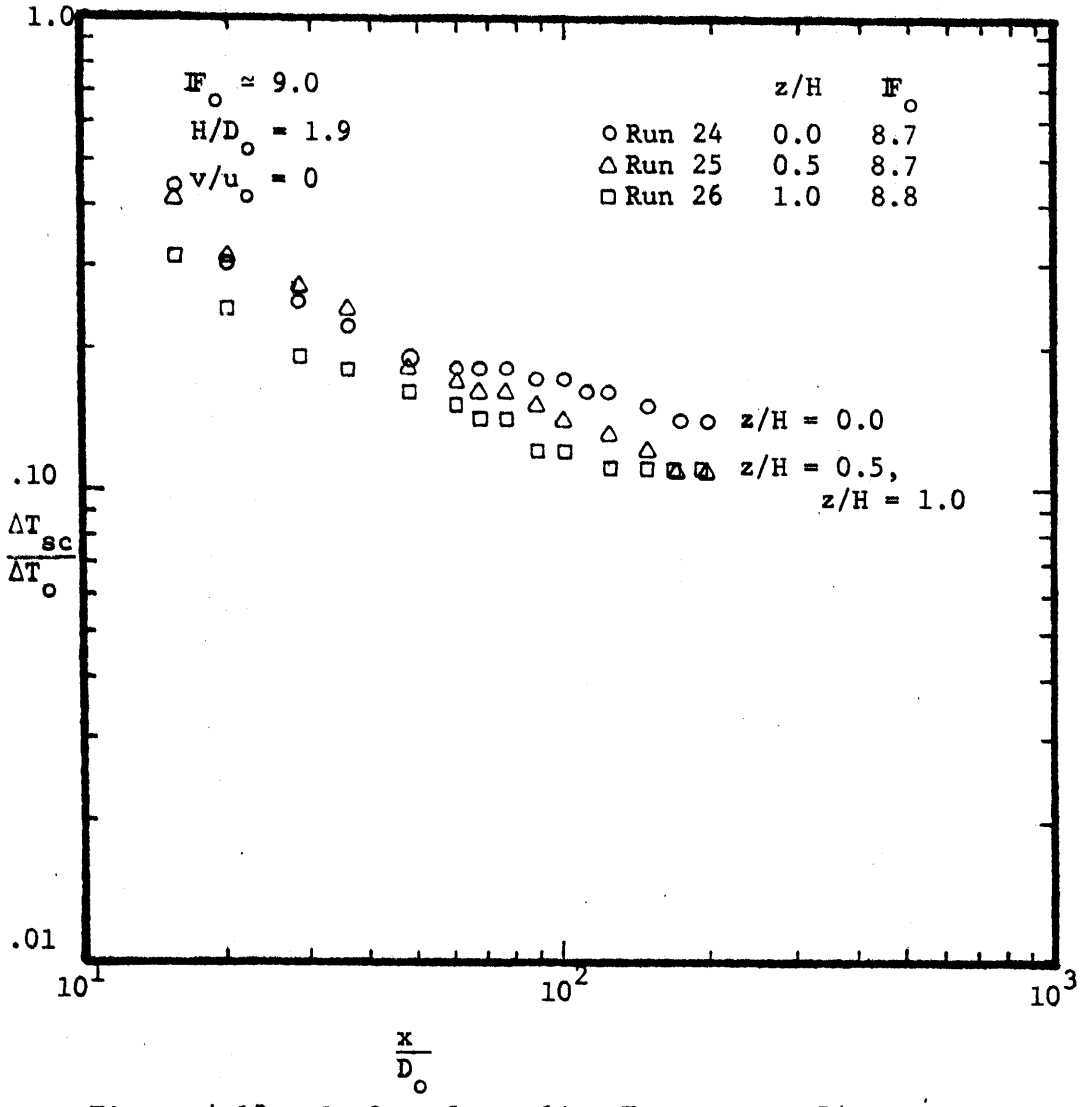

Figure 4-19: Surface Centerline Temperature Rise vs. Longitudinal Distance with Constant $F_o \simeq 9.0$, $H/D_o = 1.9$

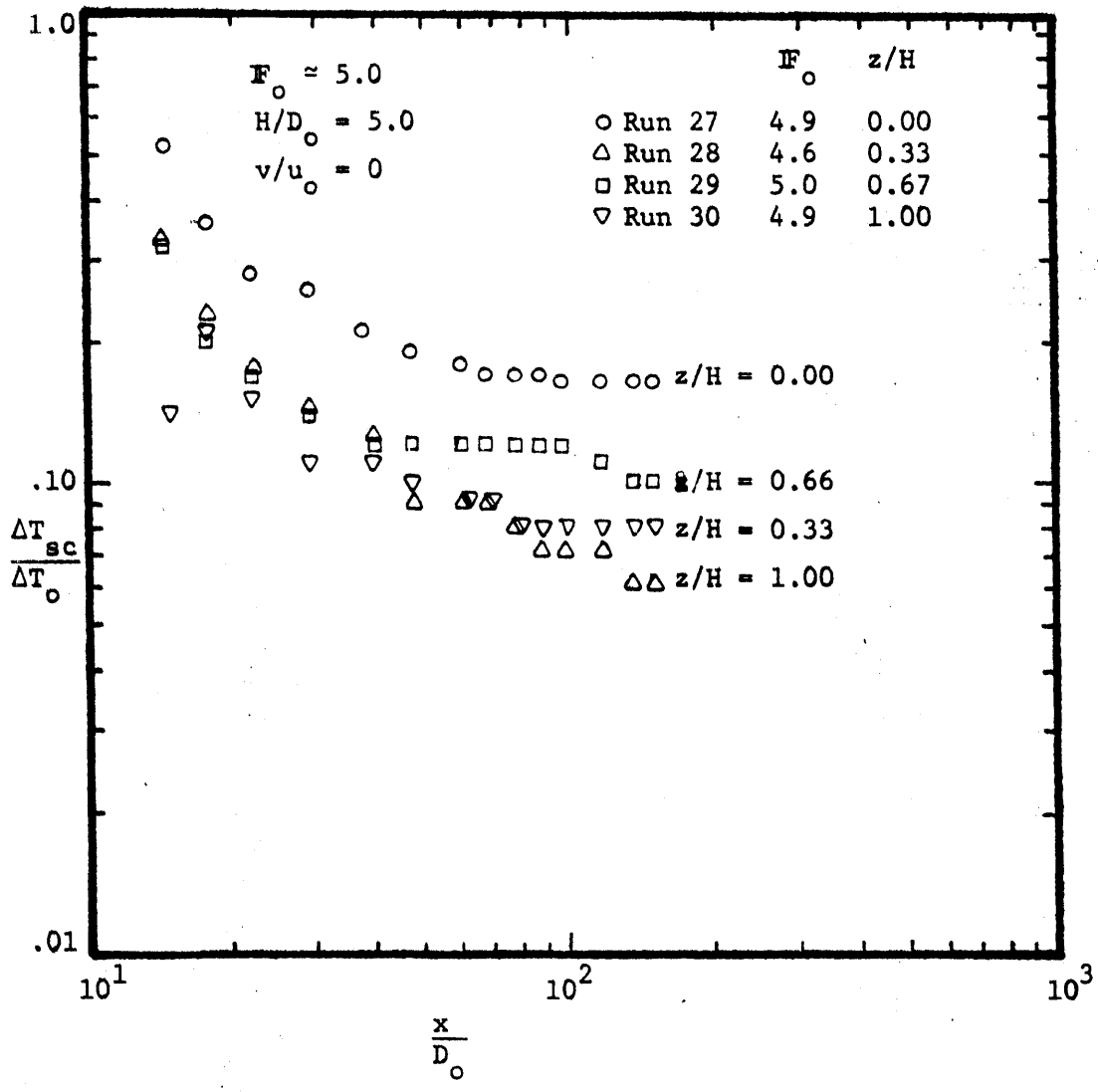

Figure 4-20: Surface Centerline Temperature Rise vs. Longitudinal Distance with Constant $F_o \simeq 5.0$, $H/D_o = 5.0$

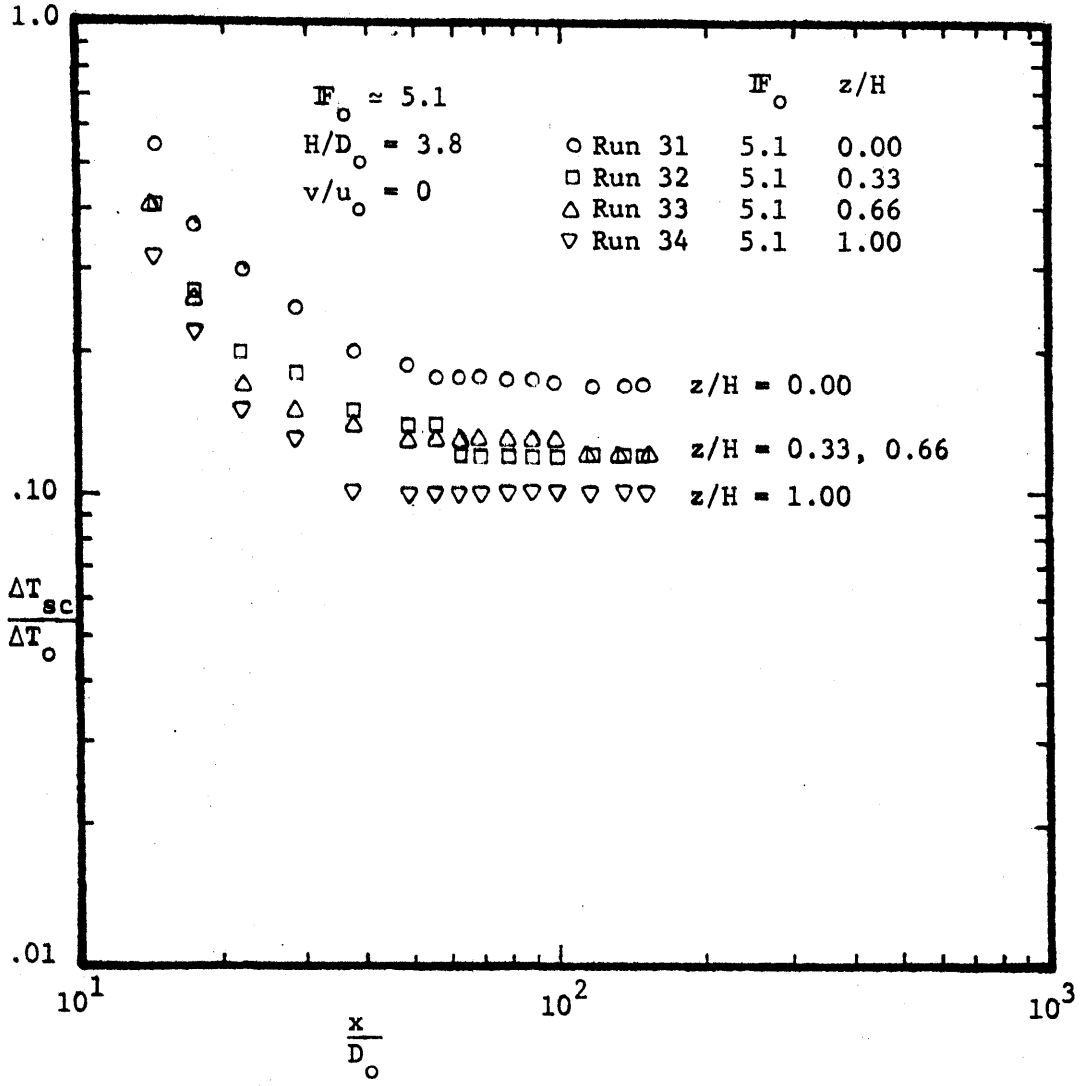

Figure 4-21: Surface Centerline Temperature Rise vs. Longitudinal Distance with Constant $IF_o \simeq 5.1$, $H/D_o = 3.8$

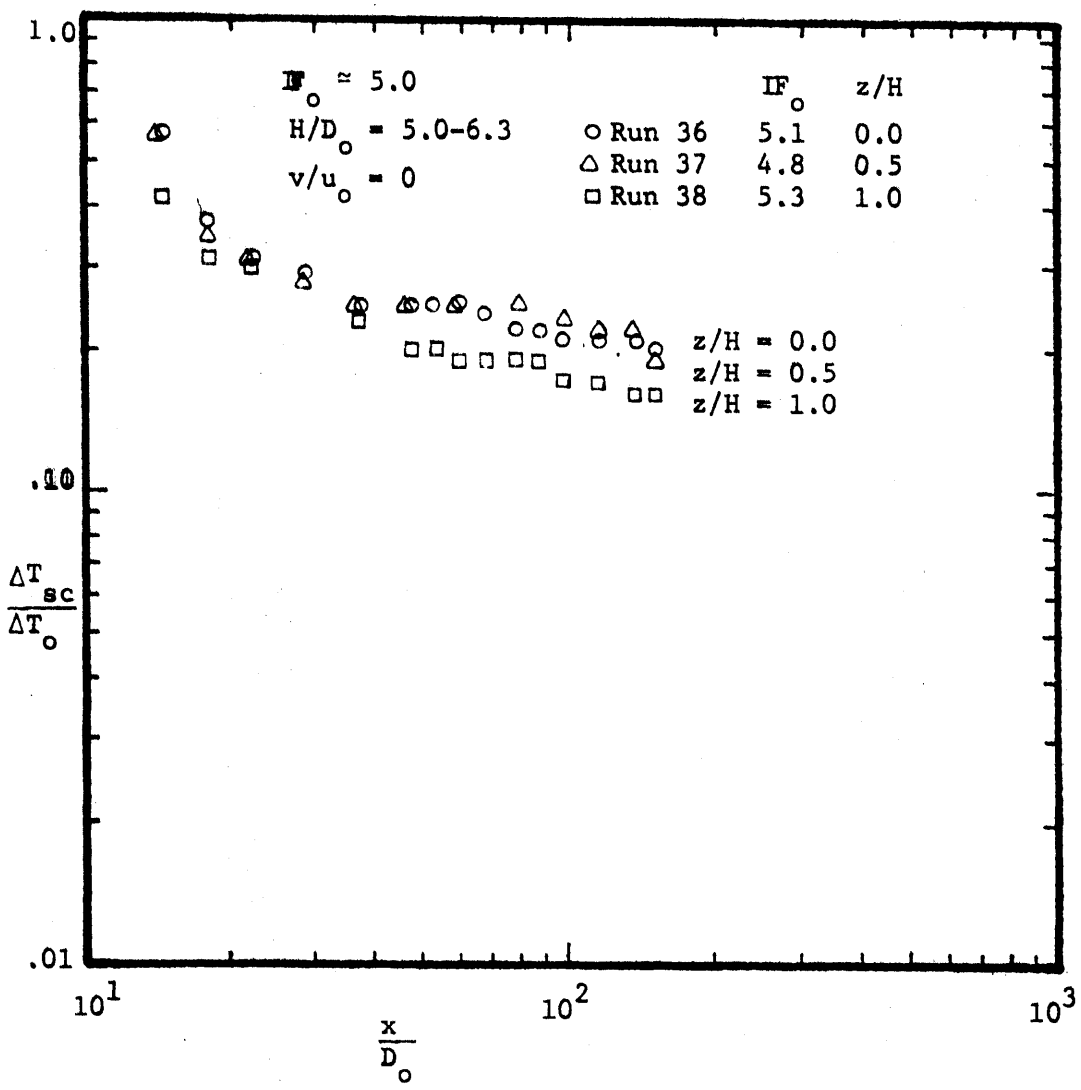

Figure 4-22: Surface Centerline Temperature Rise vs. Longitudinal Distance with Constant $IF_o \simeq 5.0$, $H/D_o = 1.9$

1) For increasing values of IF_o, the temperature dilutions increase with constant discharge submergence z/H.

2) For increasing values of relative water depth H/D_o, temperature dilutions increase with constant Froude number, IF_o.

3) For a discharge configuration (IF_o and H/D_o), increasing values of z/H significantly increase the temperature dilution in the immediate vicinity of the discharge. There is observed a positive tendency for surface dilutions to increase in the stable region. This becomes less apparent as the relative water depths decrease.

4) Maximum observed surface temperatures decrease with increasing relative discharge submergence.

Figures 4-23 to 4-28 are plots of centerline temperature rise versus longitudinal distance for near-bottom discharges, $z/H \sim 1.0$. Figures 4-23 to 4-25 illustrate the effect of relative water depth H/D_o on temperature dilution, while Figures 4-26 to 4-28 show the effect of Froude number IF_o on temperature dilution. Temperature dilution increases with increasing Froude number and increasing water depth. There is less dependence on IF_o with decreasing H/D_o.

4.2.3 Summary

In general, with decreasing relative water depth, two major phenomena interfere with jet entrainment and turbulent development:

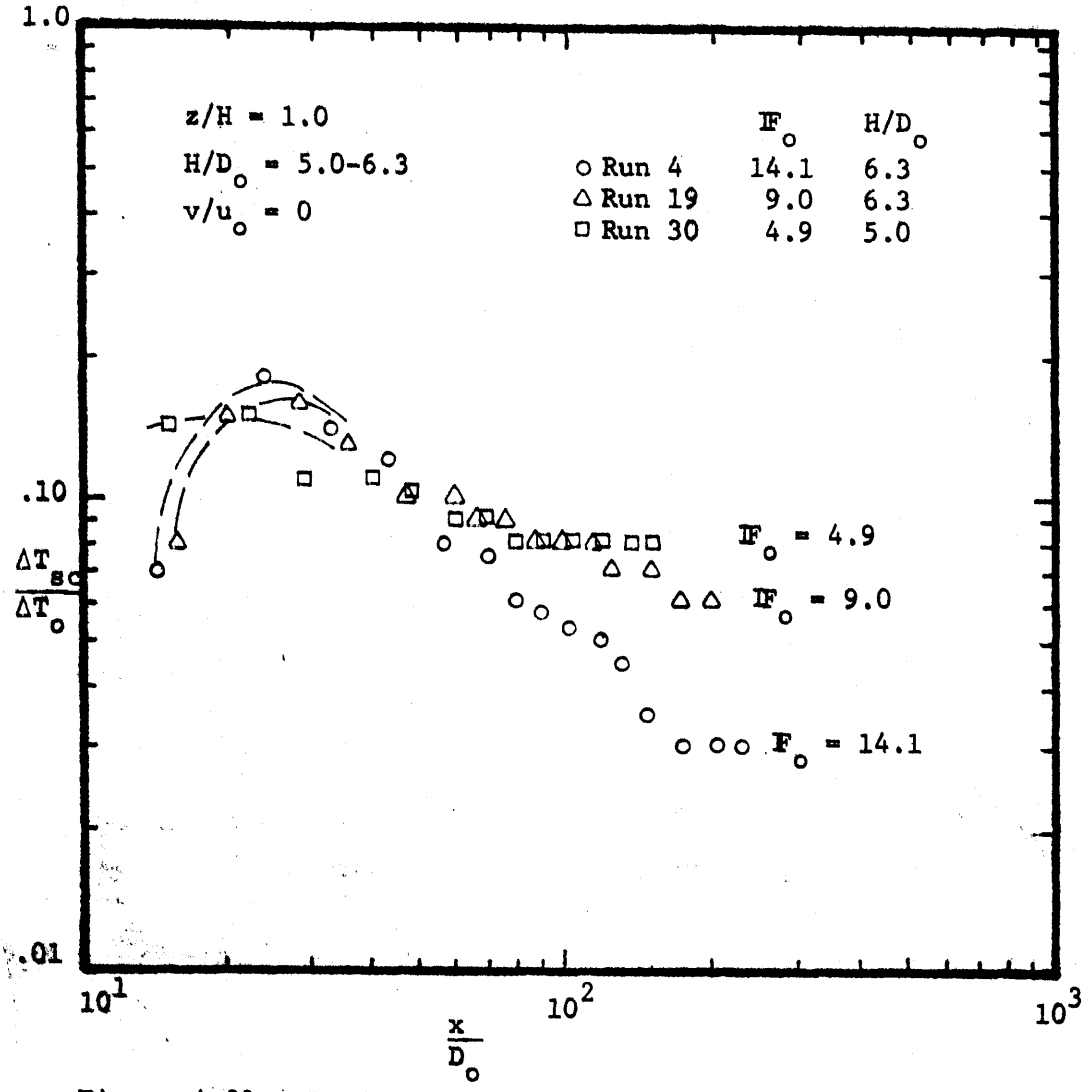

Figure 4-23: Surface Centerline Temperature Rise vs. Longitudinal Distance with z/H = 1.0, H/D$_o$ = 5.0-6.3

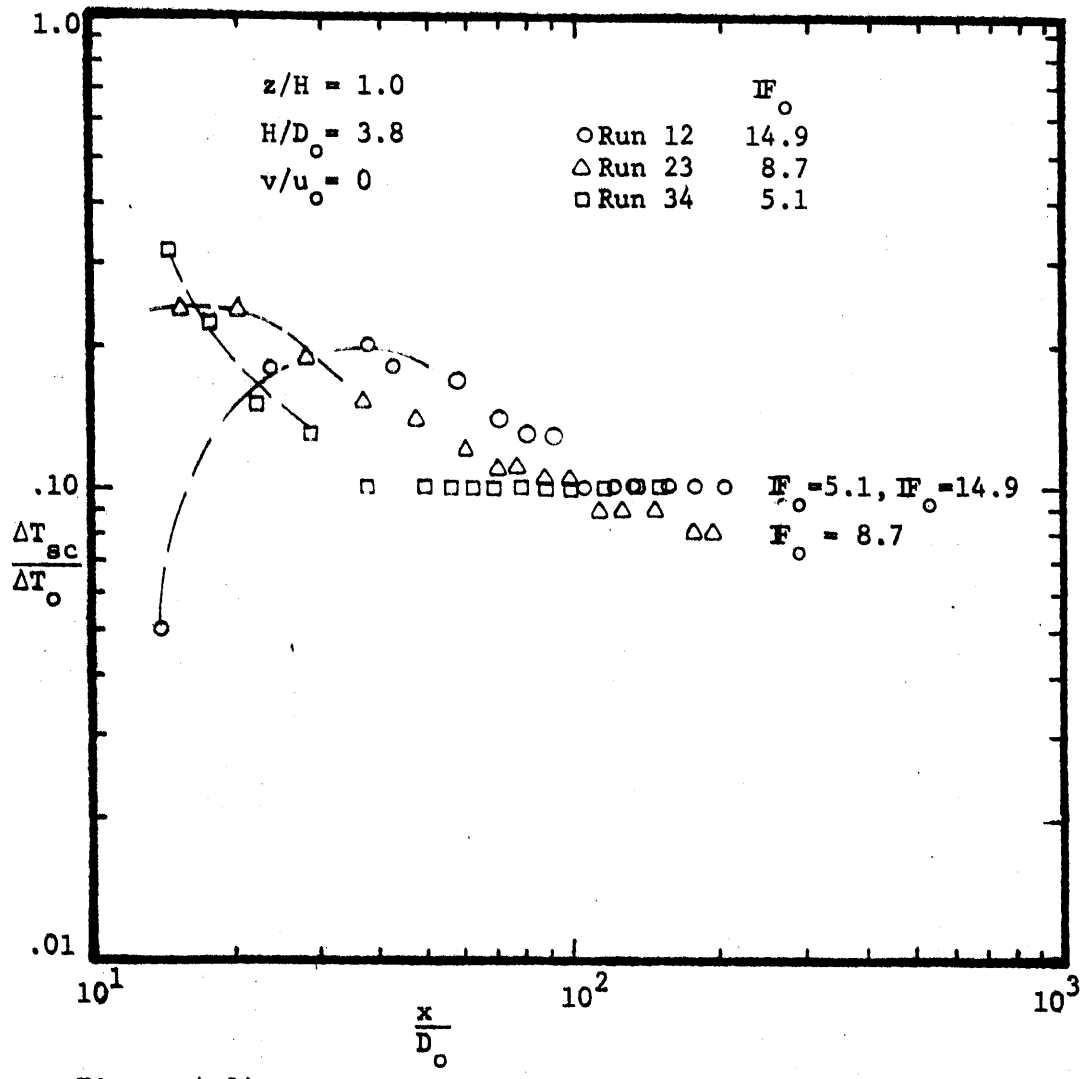

Figure 4-24: Surface Centerline Temperature Rise vs. Longitudinal Distance with z/H = 1.0, H/D$_o$ = 3.8

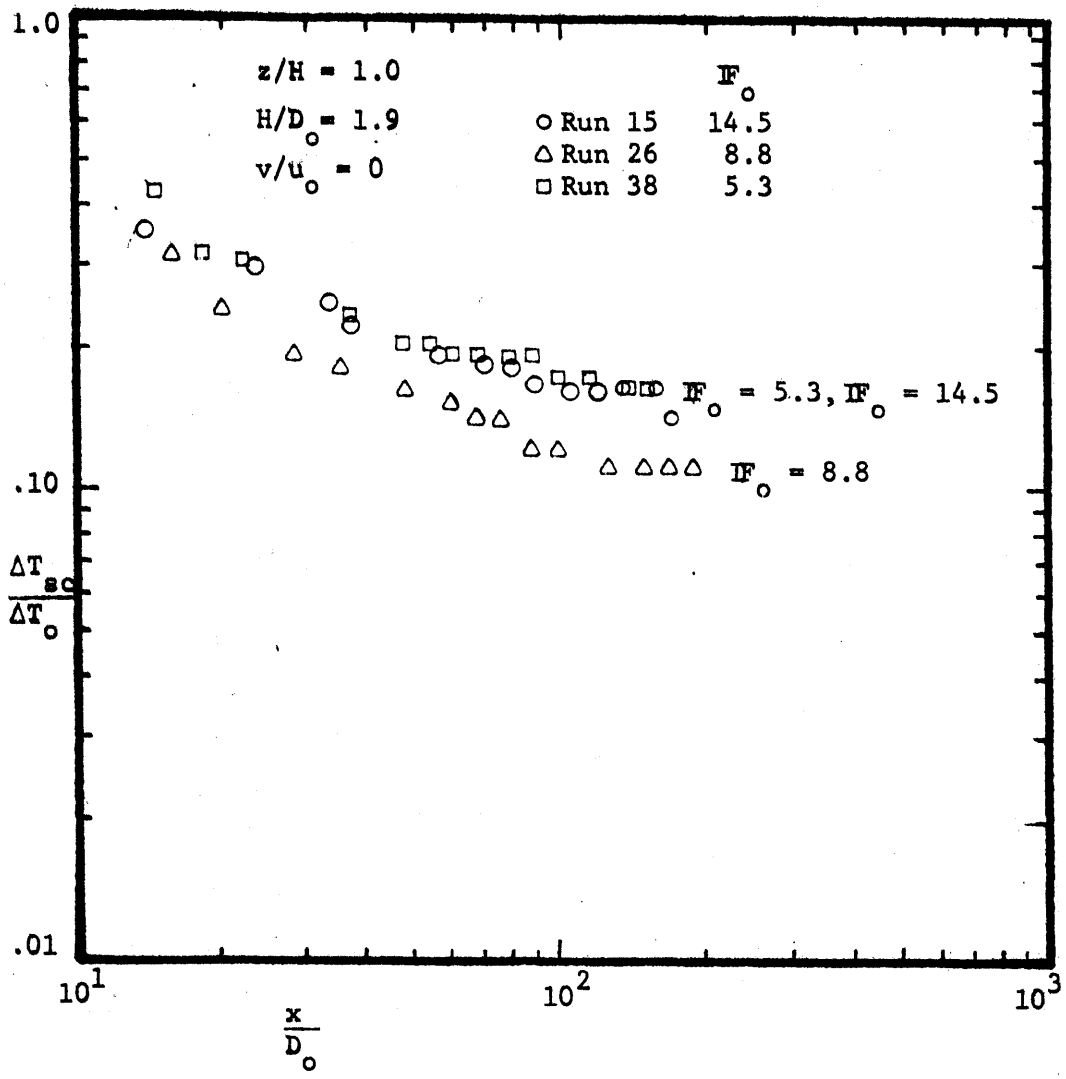

Figure 4-25: Surface Centerline Temperature Rise vs. Longitudinal Distance with z/H = 1.0, H/D_o = 1.9

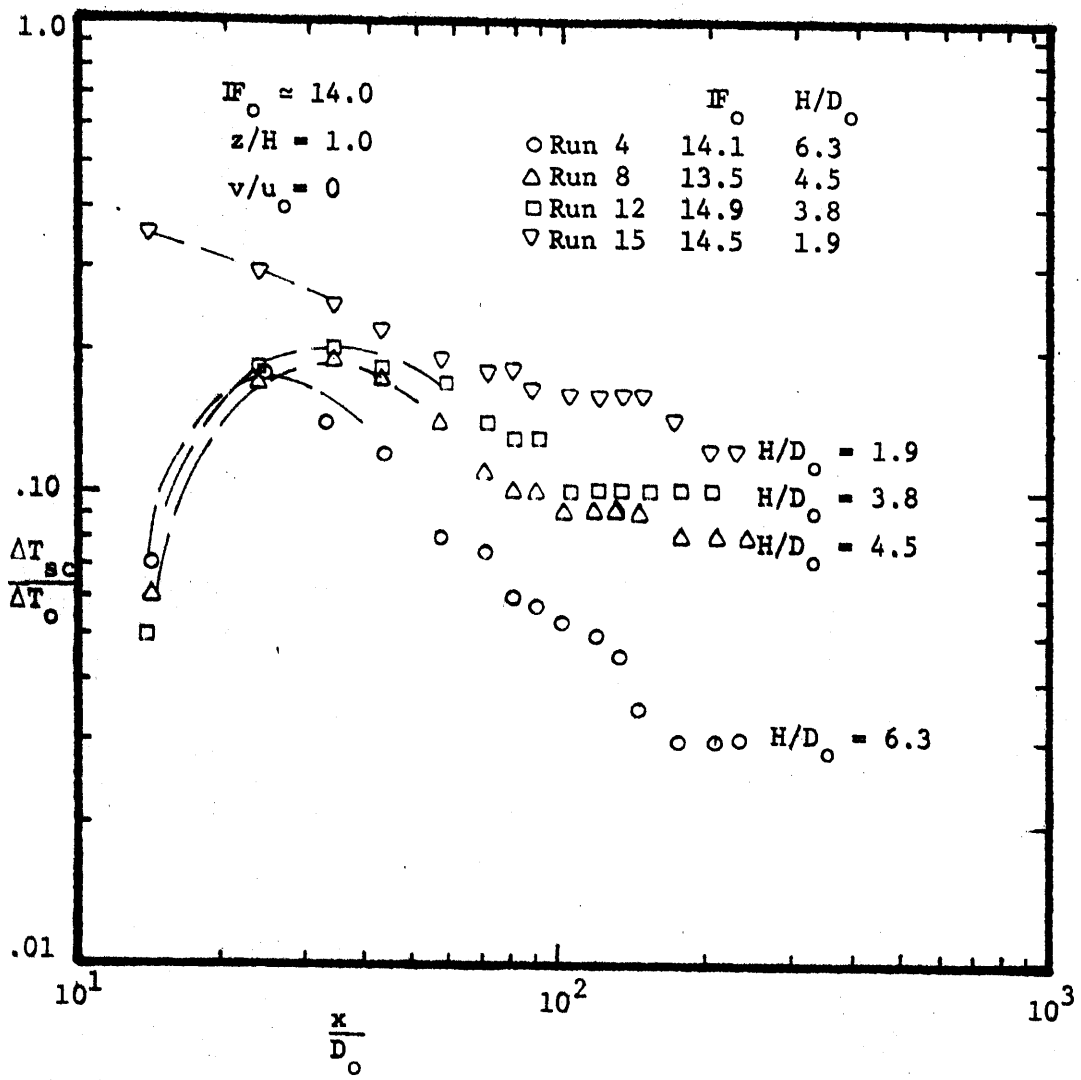

Figure 4-26: Surface Centerline Temperature Rise vs. Longitudinal Distance with z/H = 1.0, $IF_o \simeq 14.0$

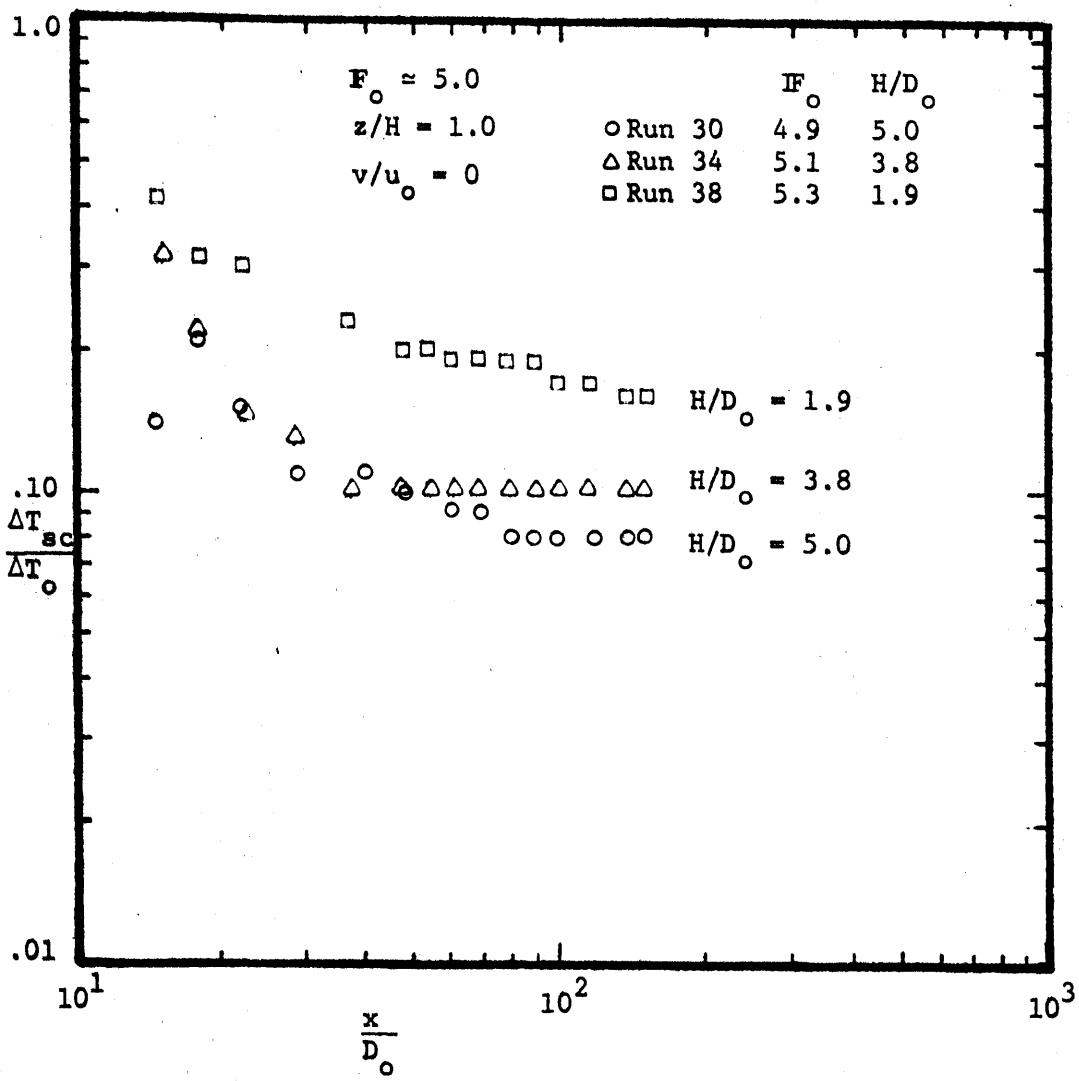

Figure 4-27: Surface Centerline Temperature Rise vs. Longitudinal Distance with $z/H = 1.0$, $F_o \simeq 5.0$

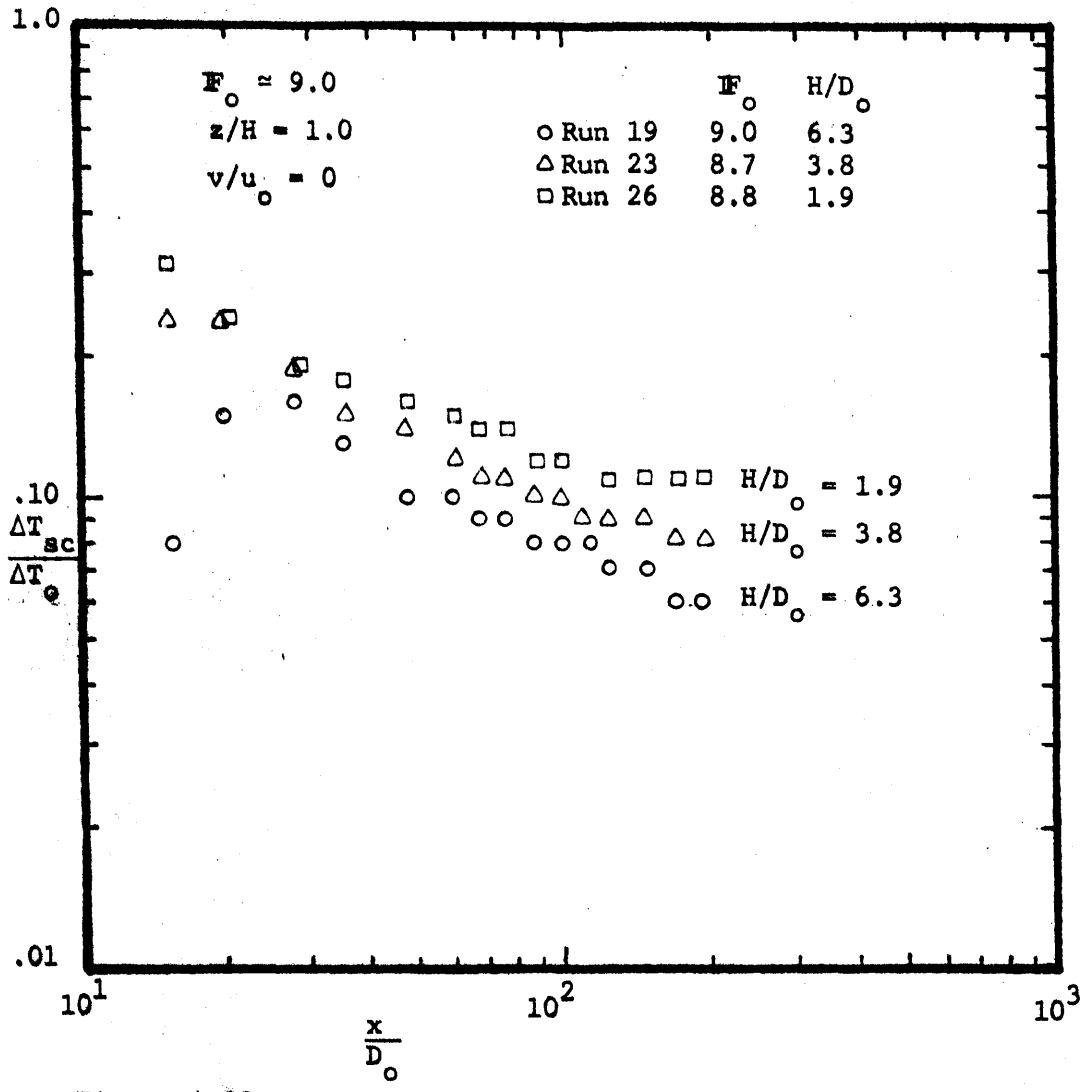

Figure 4-28: Surface Centerline Temperature Rise vs. Longitudinal Distance with z/H = 1.0, $F_o \simeq 9.0$

1) Observations using dye injection suggest that the effect of bottom friction on the velocity distribution and entrainment rate becomes more pronounced in shallow water.

2) Because of the increasing restriction on the extent of the ambient water, the entrainment of the latter by the jet will generate appreciable currents to replace the entrained water and eventually part of the heated surface layer will be re-entrained by the jet. This re-entrainment increases the temperature concentration at the surface.

4.3 Single-port Discharge with Crossflow

4.3.1 Near-Surface Discharge

The non-dimensional relative jet penetration parameter $\frac{h_{max}}{H}$ is important in characterizing the phenomena observed with ambient crossflows. All results of laboratory experiments presented were conducted at constant relative water depth, $H/D_o = 3.8$. With increasing Froude number and H/D_o constant, the water depth becomes "relatively" shallow due to increasing bottom interaction with the flow of ambient entrainment into the jet.

Figures 4-29 to 4-32 are plots of centerline temperature rise versus longitudinal distance. Figures 4-33 and 4-34 are plots of excess temperature contours versus enclosed surface area. They show the effect of Froude number and crossflow strength on temperature dilution. This is reflected in the relative jet penetration parameter $\frac{h_{max}}{H}$, since

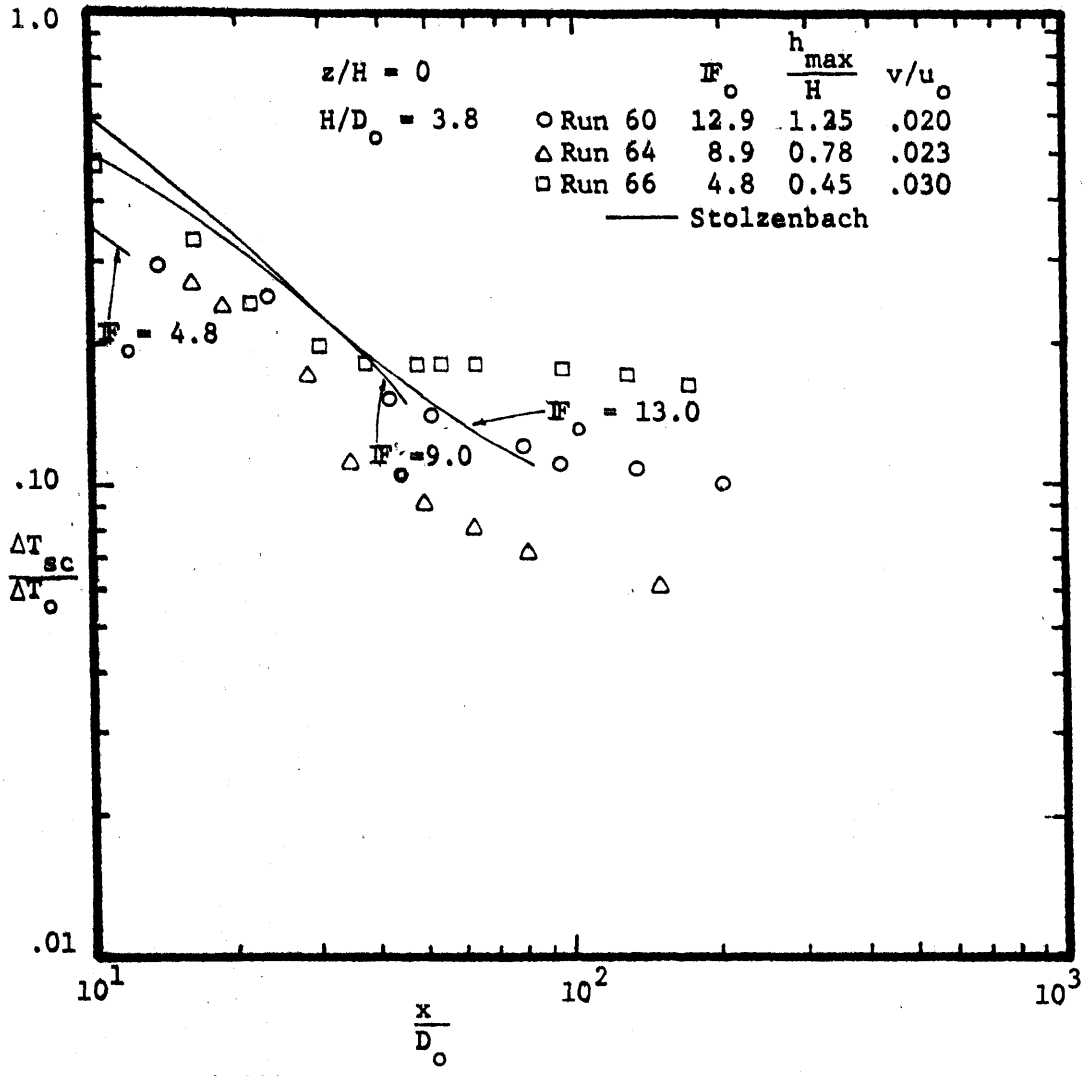

Figure 4-29: Surface Centerline Temperature Rise vs. Longitudinal Distance with near Constant $v/u_o \sim 0.060$, $H/D_o = 3.8$

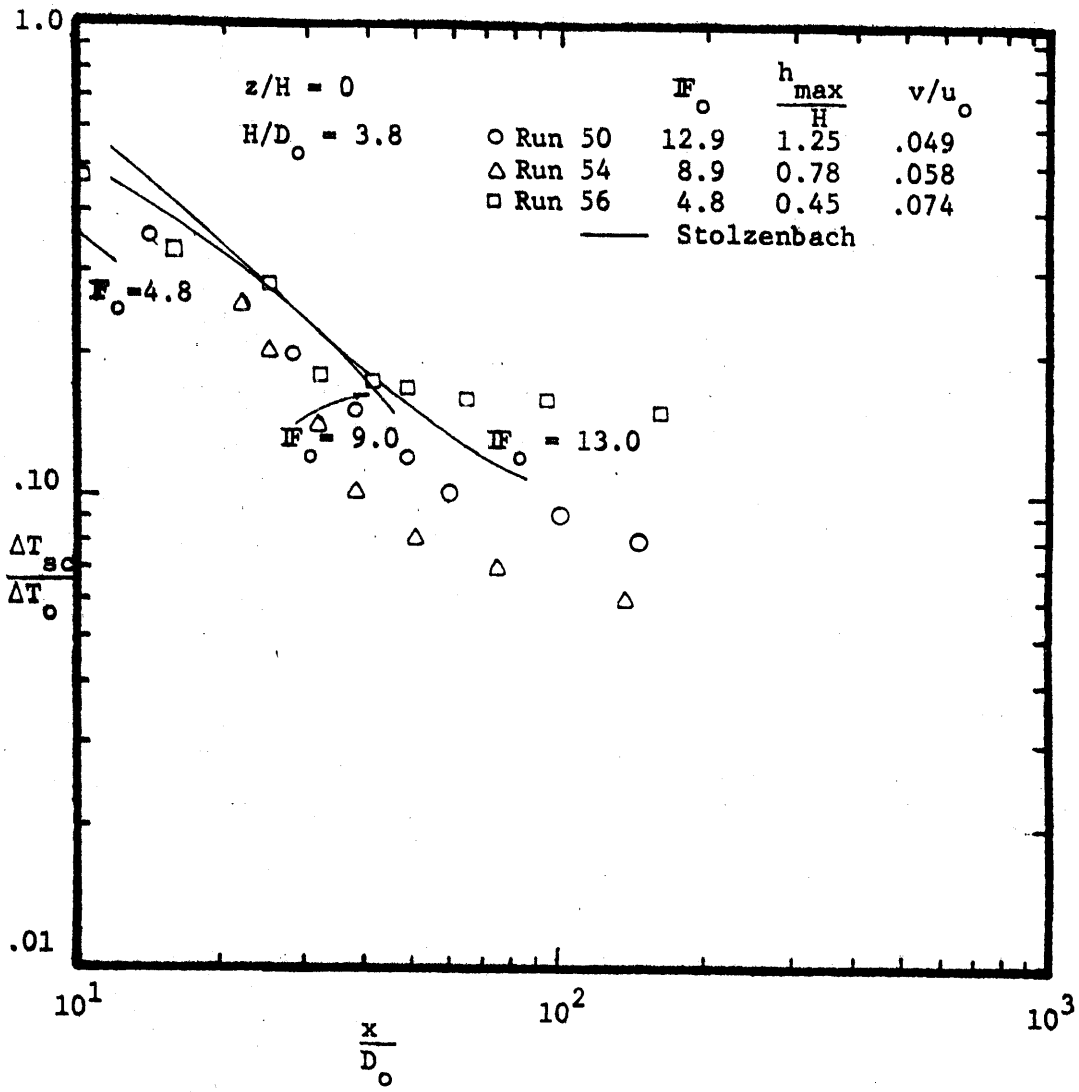

Figure 4-30: Surface Centerline Temperature Rise vs. Longitudinal Distance with Near Constant $v/u_o \sim .025$, $H/D_o = 3.8$

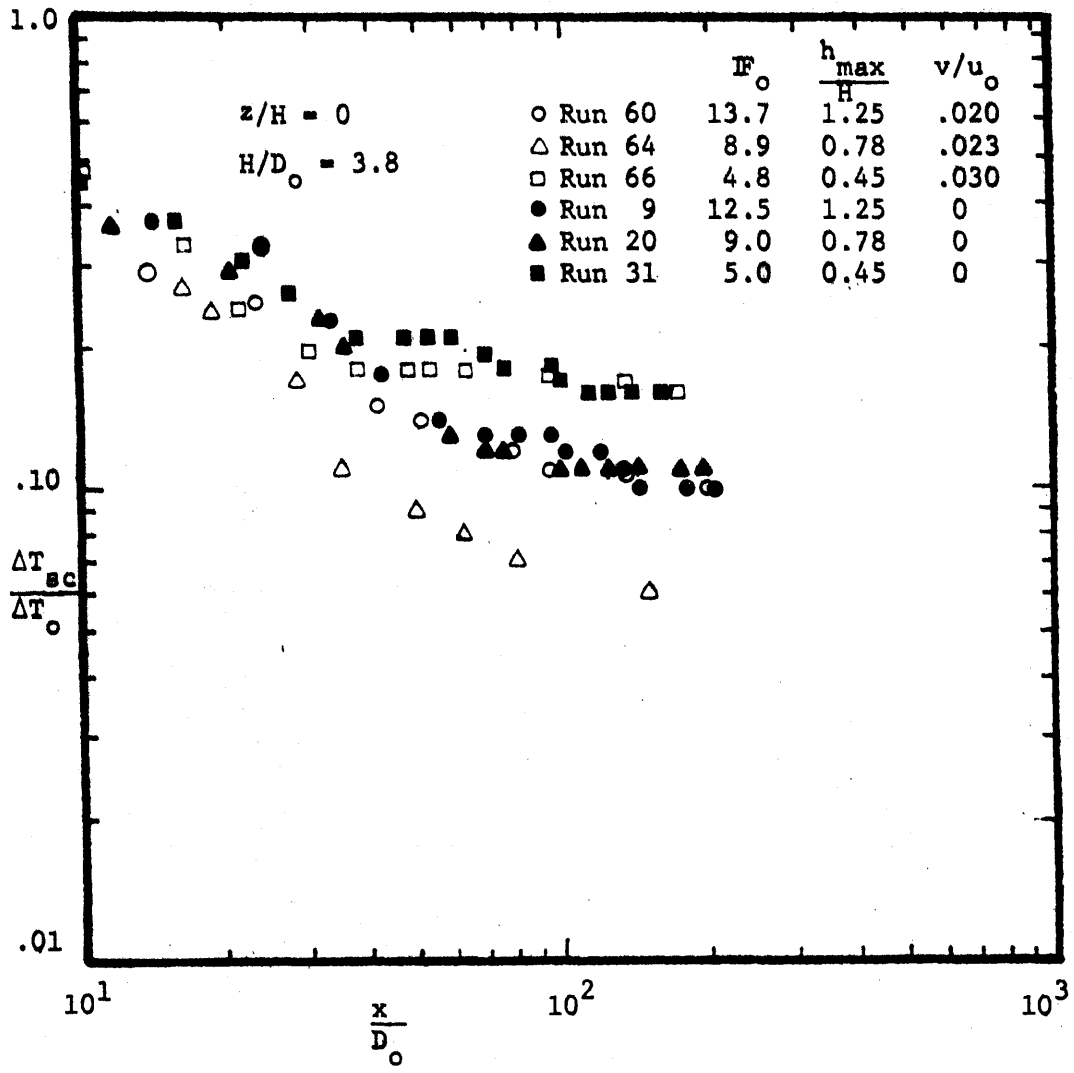

Figure 4-31: Surface Centerline Temperature Rise vs. Longitudinal Distance with Variable v/u$_o$, H/D$_o$ = 3.8

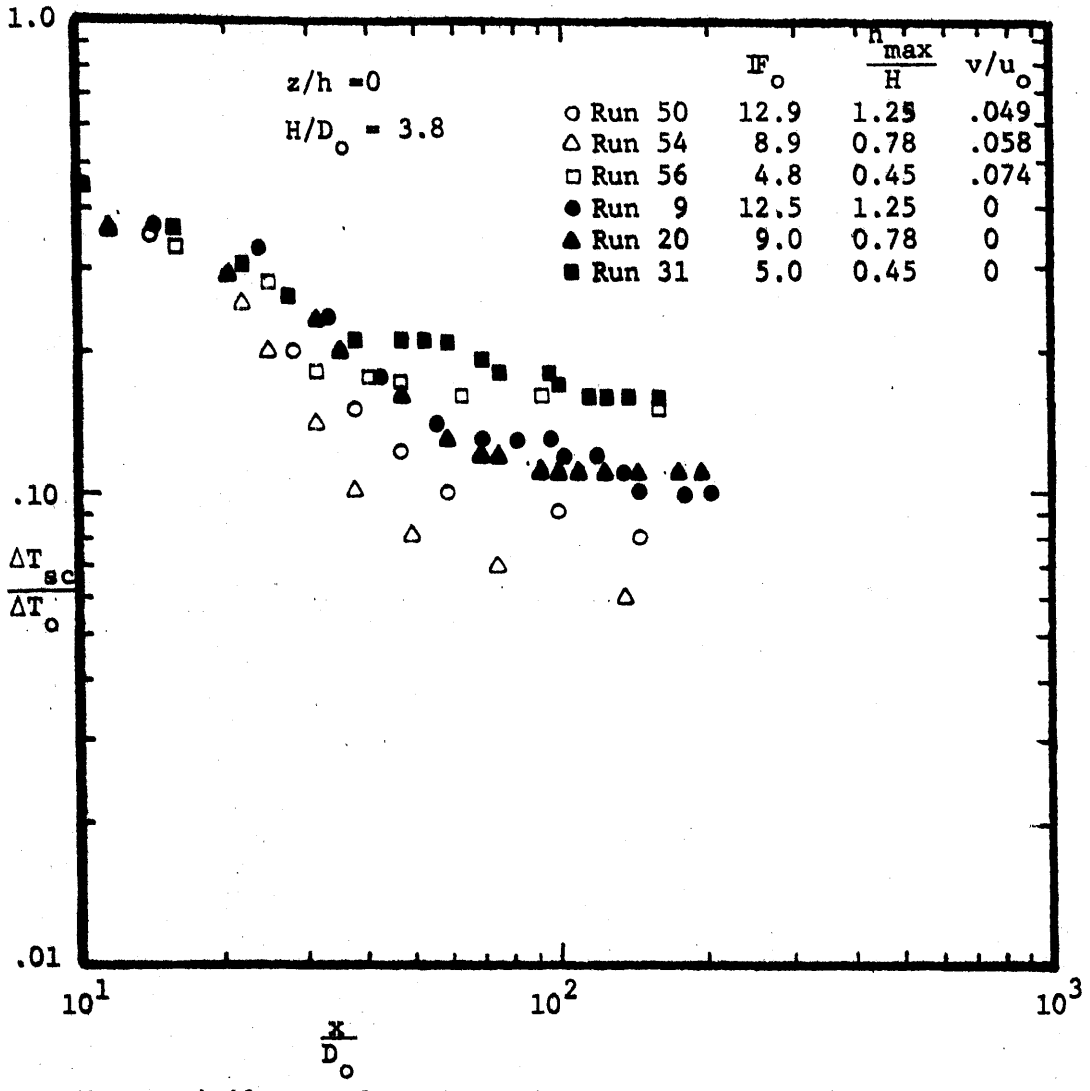

Figure 4-32: Surface Centerline Temperature Rise vs. Longitudinal Distance with v/u_o = 0 to .074, H/D_o = 3.8

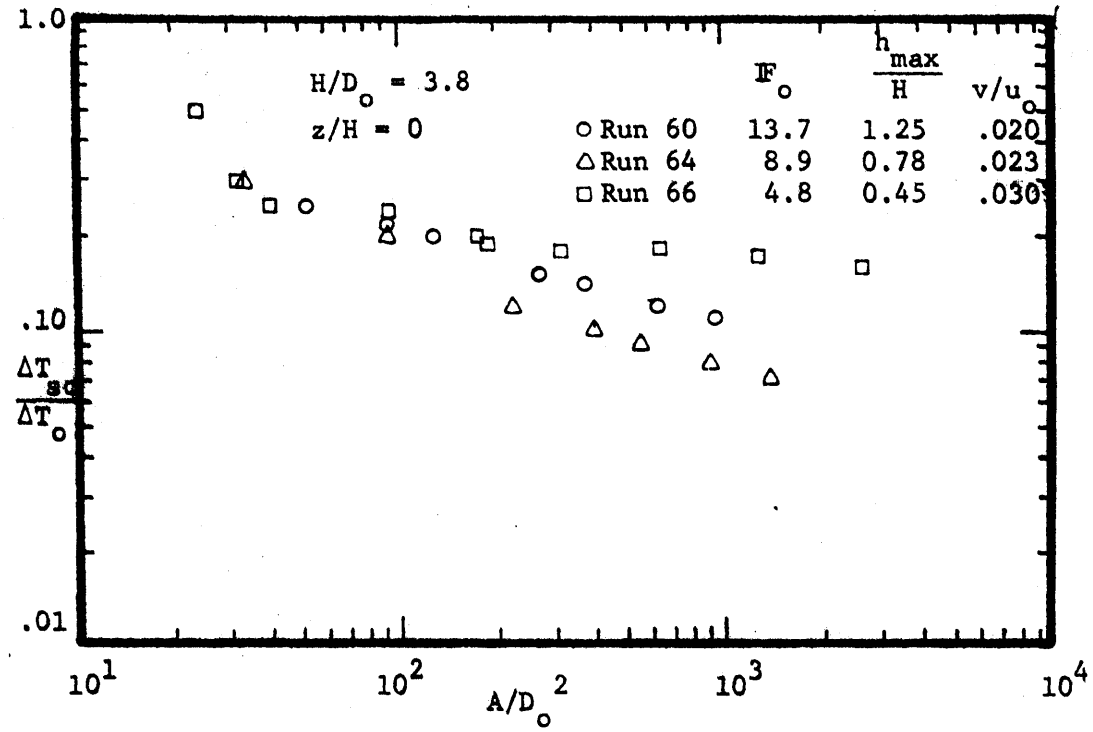

Figure 4-33: Excess Temperature Contours vs. Enclosed Surface Area with $v/u_o \sim .025$

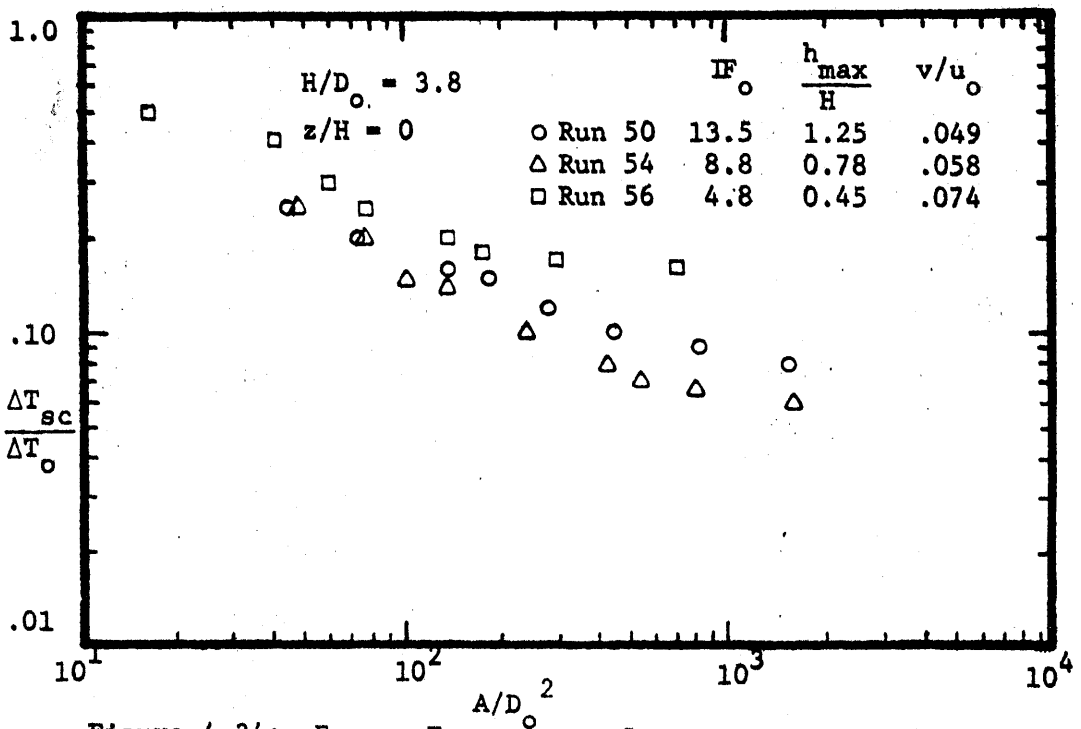

Figure 4-34: Excess Temperature Contours vs. Enclosed Surface Area with $v/u_o \sim .060$

$$\left[\frac{0.42\ A^{1/4}\ \sqrt{h_o b_o}}{H}\right] = \text{a constant for these tests} \qquad (4\text{-}10)$$

and

$$\frac{h_{max}}{H} = \mathbb{F}_o\left(\frac{0.42\ A^{1/4}\ \sqrt{h_o b_o}}{H}\right). \qquad (4\text{-}11)$$

Thus, effectively

$$\frac{h_{max}}{H} = f(\mathbb{F}_o) \qquad (4\text{-}12)$$

Figures 4-29 and 4-30 show that there is poor agreement of the crossflow configuration with Stolzenbach's prediction. In part, this is due to the relative shallow water depth at which the crossflow experiments were run.

The observed phenomena can be divided into two parts according to the magnitude of the jet penetration parameter h_{max}/H. $\frac{h_{max}}{H} = 1$ is an indication that the jet has become attached to the bottom. For $\frac{h_{max}}{H} < 1$, the following observations are noted:

1) As compared with the non-crossflow case, increased entrainment on the outer face of the jet due to a small crossflow increases dilution. See Figures 4-31 and 4-32.
2) A further increase in crossflow v/u_o induces a small but positive increase in temperature dilution.
3) Temperature dilution increases with increasing Froude number.
4) The jet deflection increases with increasing Froude number. See Figures 4-35 to 4-37.

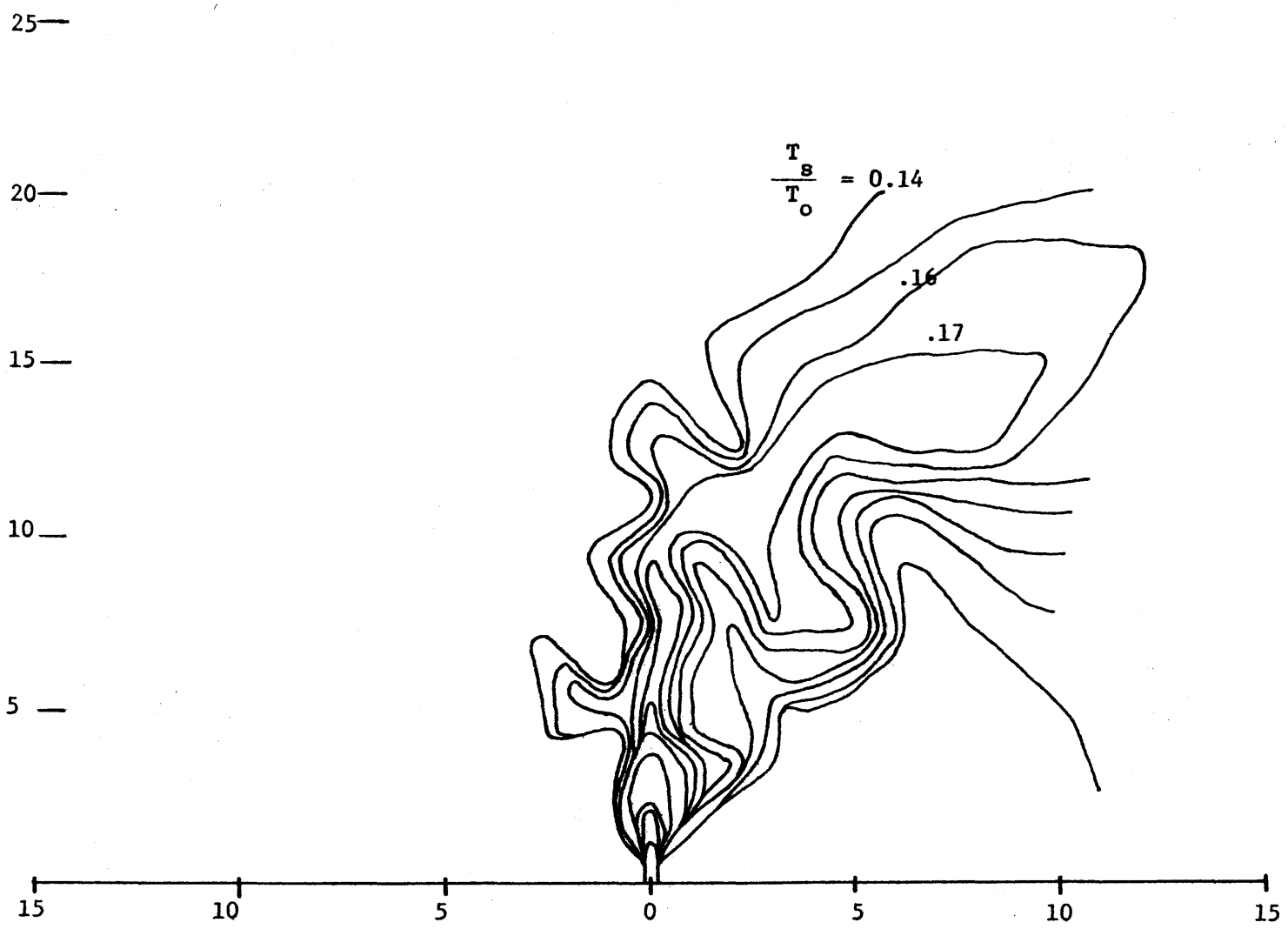

Figure 4-35: Surface Horizontal Temperature Distribution. Run No. 66, F_o = 4.8

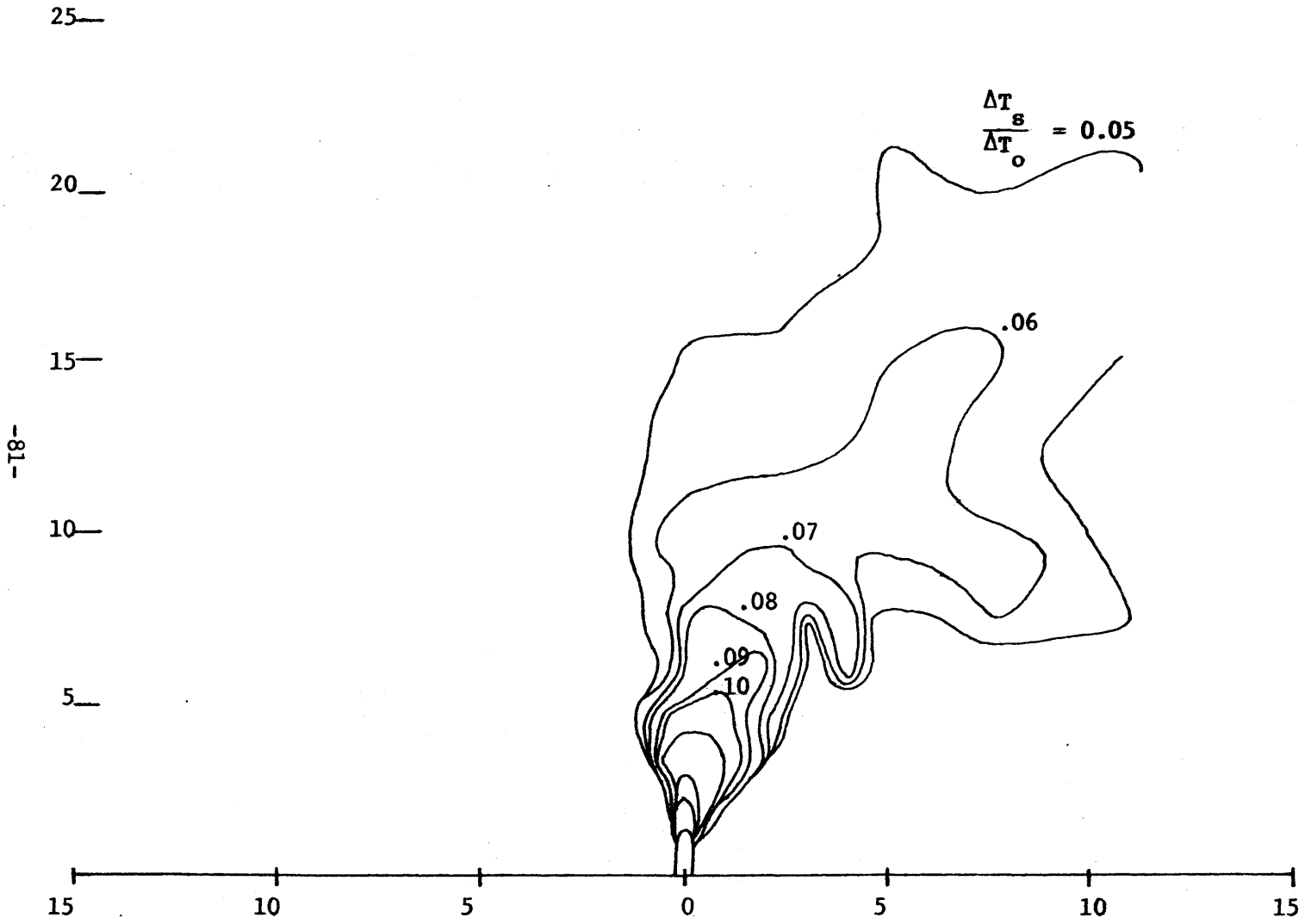

Figure 4-36: Surface Horizontal Temperature Distribution. Run No. 64, F_o = 8.9

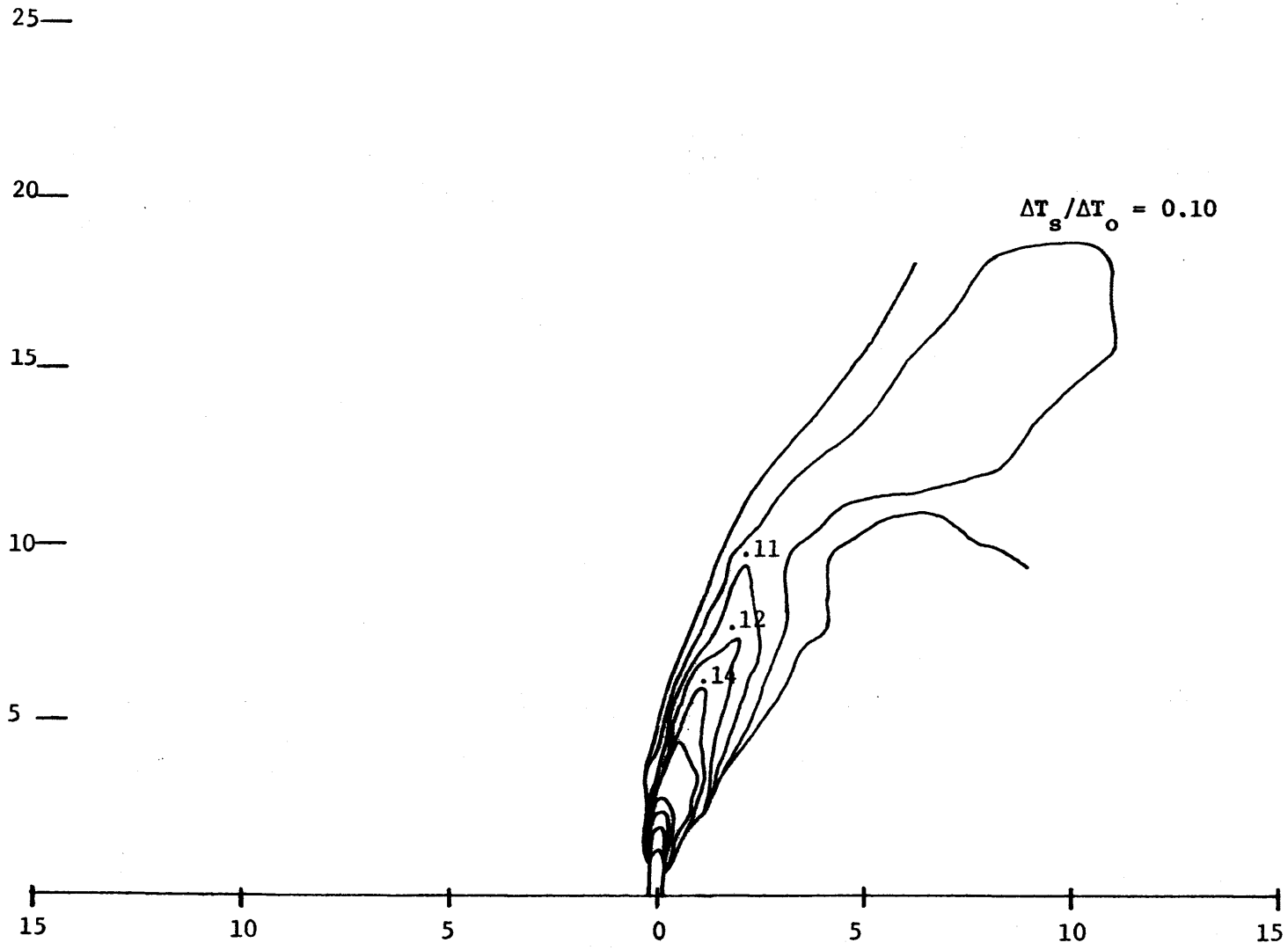

Figure 4-37: Surface Horizontal Temperature Distribution. Run No. 60, F_o = 13.0

5) Semi-steady state conditions in the hydraulic model can be achieved.

With increasing F_o, (v/u_o = constant, H/D_o = constant), the jet's vertical penetration increases, effectively causing increased blockage of the crossflow. See Figure 4-38. The result is a decrease in the volume of ambient crossflow that penetrates beneath the plume. A large re-entrainment eddy on the lee side of the jet develops and intensifies. See Figure 4-39. The results suggest that increasing the Froude number has a positive effect on temperature dilution until $\frac{h_{max}}{H} = 1$.

For $\frac{h_{max}}{H} > 1$, the jet becomes attached to the bottom. Increasing F_o increases the area of jet attachment and all of the crossflow is prevented from passing to the lee side of the plume. The temperature concentrations in the re-entrainment eddy increases until a steady state is achieved. Increasing F_o further increases the re-entrainment causing the temperature concentrations to increase.

4.3.2 Near-Bottom Discharge

The results presented were conducted at constant relative water depth, $H/D_o = 6$. Figures 4-40 and 4-41 are plots of excess temperature contours versus enclosed surface area. They illustrate the effect of Froude number and crossflow on temperature dilution. The results suggest that:

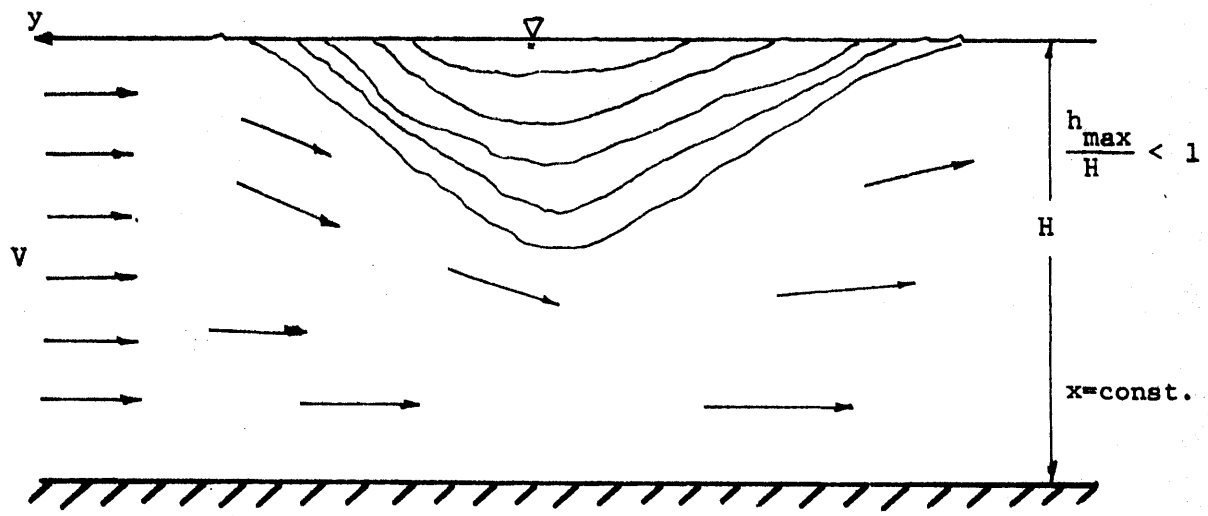

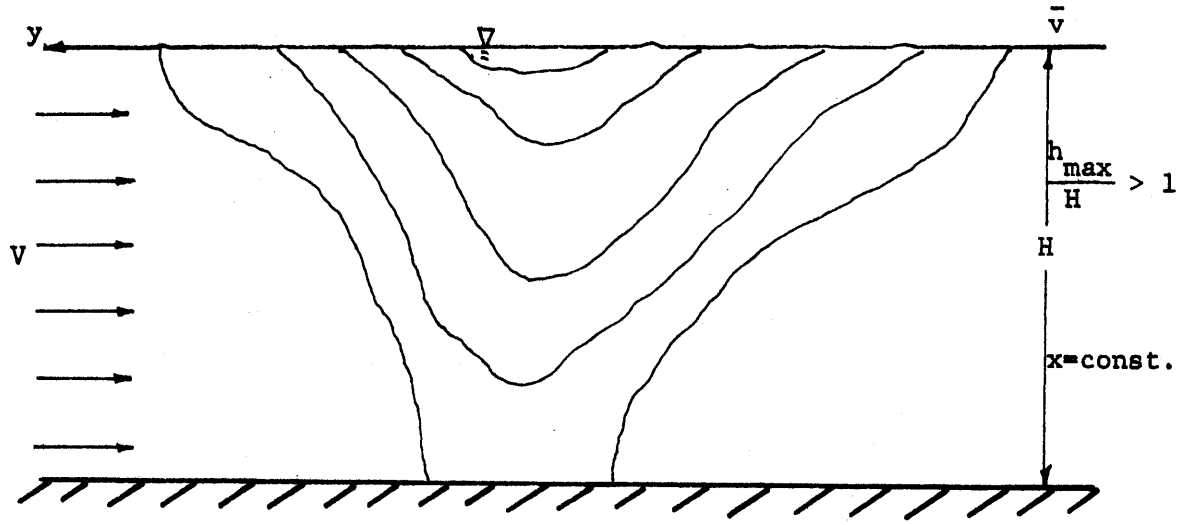

Figure 4-38: Typical Vertical Cross-section of Isotherm, x = constant, constant H/D_o and v/u_o, $z/H = 0$

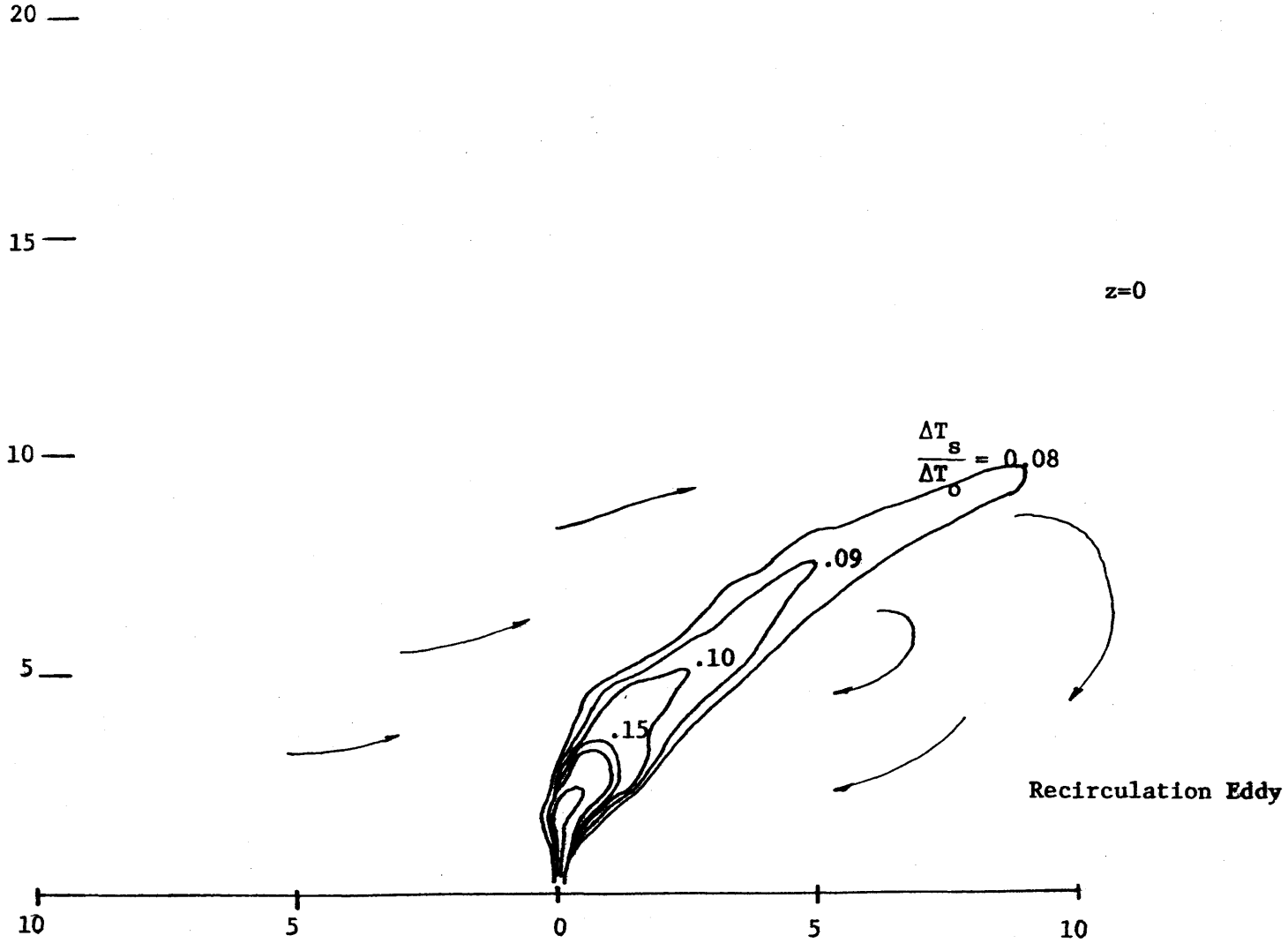

Figure 4-39: Typical Plane View of Discharge in a Crossflow, $h_{max}/H > 1$, $z/H \simeq 0$, Run No. 50

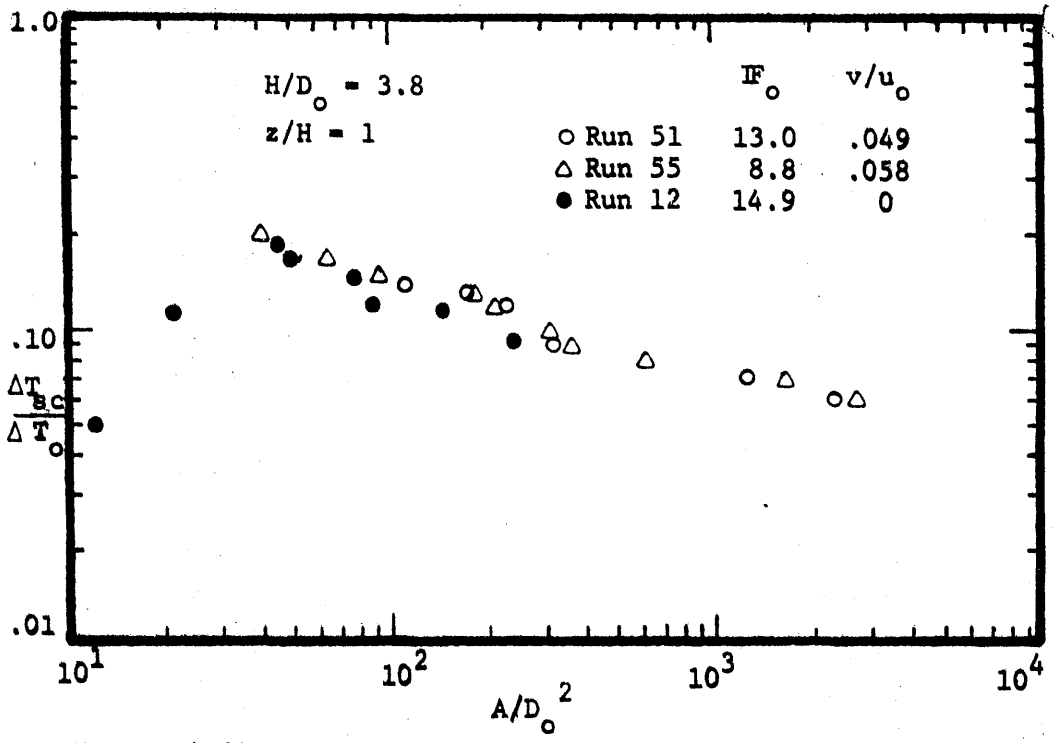

Figure 4-40: Excess Temperature Contours vs. Enclosed Surface Area with $v/u_o \sim 0.06$

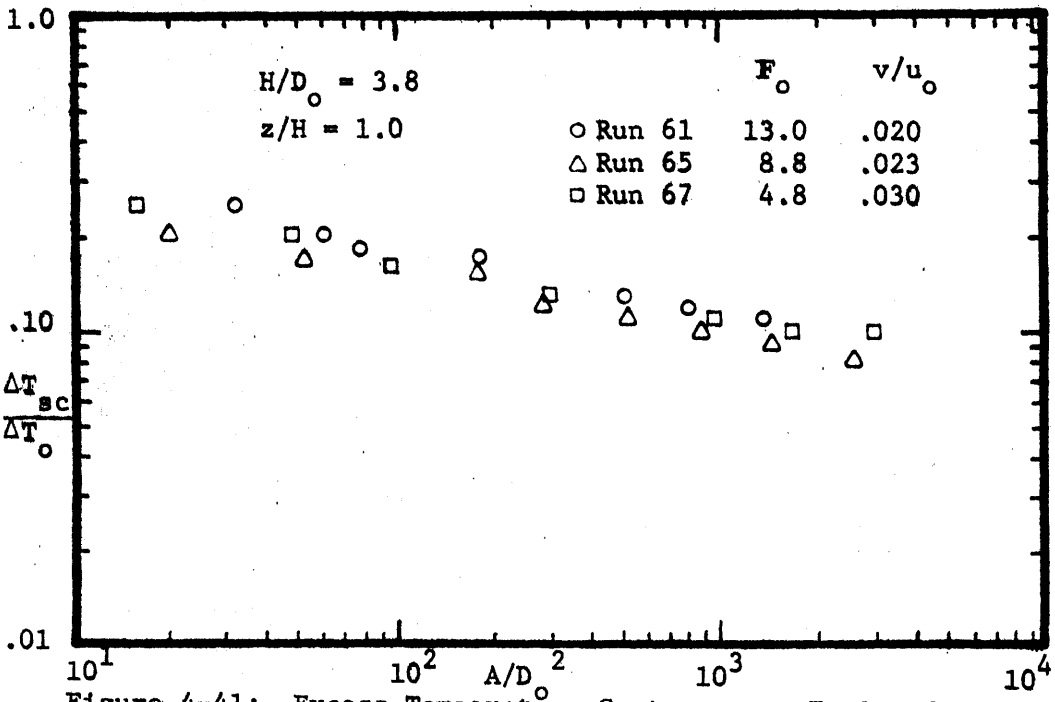

Figure 4-41: Excess Temperature Contours vs. Enclosed Surface Area with $v/u_o \sim .025$

1) Increasing the crossflow velocity increases temperature dilution.

2) Near-bottom discharges show small but positive increase in temperature dilution as compared to near-surface discharge. Compare Figures 4-33 and 4-34 with Figures 4-40 and 4-41.

3) There is less dependence of dilution on the value of IF_o as compared with the near-surface discharge. However, as IF_o is increased, the jet meanders along the bottom, increasing blockage of the crossflow and re-entrainment on the lee side.

V SUMMARY AND CONCLUSIONS

An experimental investigation of the temperature field induced by the heated effluent from a submerged single-port discharge is conducted. Primary emphasis is directed to the study of the interaction of a shallow water jet with the bottom and the free surface. The experimental program considers a discharge Q_o of heated water at temperature T_o and density ρ_o from a circular pipe of diameter D_o at the edge of a receiving body of water of large extent, with temperature T_a, density ρ_a and depth H are uniform. A uniform current v may be present in the receiving water and is parallel to the shoreline. The densimetric Froude number F_o ranges between 4.9 and 15.7, the relative water depth H/D_o ranges between 1.9 and 6.3, the relative crossflow v/u_o ranges between 0.020 and 0.074, and the relative discharge submergence Z/H ranges between near surface ($Z/H \sim 0$) and near bottom ($Z/H \sim 1$). Graphic dimensionless relationships among the pertinent parameters is presented to illustrate the jet's behavior and for use in the preliminary design of shallow water thermal outfalls.

In general, with decreasing relative water depth, two major phenomena interfere with jet entrainment and turbulent development.

1) The effect of bottom friction on the velocity distribution and entrainment rate becomes more pronounced in shallow water.

2) Because of the increasing restriction on the extent of the ambient water, the entrainment of the latter by the jet will generate appreciable currents to replace the entrained water and eventually part of the heated surface layer will be re-entrained by the jet. The re-entrainment increases the temperature concentrations at the surface.

In the absence of ambient currents the most critical parameters governing the near surface discharge behavior are the Froude number IF_o and the relative water depth H/D_o. In relatively shallow depths, the results indicate substantial deviation of temperature concentrations from those corresponding to the ideal conditions of unrestricted water depth characterizing Stolzenbach's (1971) predictive model for surface discharges. The jet penetration parameter h_{max}/H defines the discharge configuration applicable to Stolzenbach's model. For the range of parameters here in studied, it is found that if

$$\frac{H}{D_o} \geq 3.3 \ln\left(\frac{h_{max}}{.45D_o}\right)$$

the flow field is a function of the densimetric Froude number IF_o and Stolzenbach's model is applicable with respect to the assumption that the bottom does not interfere with the jet's performance. However, if

$$\frac{H}{D_o} < 3.3 \ln\left(\frac{h_{max}}{.45D_o}\right)$$

then the flow field is a function of the densimetric Froude number F_o and the relative water depth H/D_o. The theoretical results give unrealistically low temperature concentrations at low water depths with the discrepancy increasing with decreasing relative water depth. The experimental results show good agreement with Stolzenbach's et al prediction for the jet maximum penetration depth in deep water.

Varying the jet's relative submergence from near surface to near bottom significantly increases the near field temperature dilution and decreases maximum temperature concentrations. Dilutions in the stable region increase with submergence, but this becomes less apparent as relative water depths decrease.

The non-dimensional relative jet penetration parameter h_{max}/H is important in characterizing the phenomena observed with ambient crossflows. The jet's interaction with the crossflow can be divided into two parts according to whether h_{max}/H is less than or greater than one, i.e., whether the jet is, or is not, attached to the bottom. The results suggest that maximum temperature dilution is achieved with a crossflow when the discharge configuration satisfies the criteria

$$\frac{h_{max}}{H} \simeq 1.$$

The deflection of the jet plume increases with increasing Froude number. Temperature dilutions also increases with an increase in the crossflow velocity v/u_o, given that h_{max}/H remains constant. Stolzenbach's prediction with crossflows correlate

poorly with the experimental results, which is likely due to the shallow depths at which the tests were performed.

NOMENCLATURE

A	discharge channel aspect ratio, h_o/b_o
b	local width of jet, 2-D
b	horizontal surface distance from core boundary to jet boundary, 3-D
b_o	one half the width of rectangular channel
c	coefficient in the exponent of Ellison and Turner's vertical entrainment velocity function
c_n	concentration of heat in the plume in terms of density of water
D	dilution = ratio of flow in the jet to the initial flow
D_o	outfall nozzle inside diameter
F_o	densimetric Froude number of the discharge
F_o'	a characteristic Froude number = $F_o A^{1/4}$
f	a functional
f	similarity function for velocity = $(1-\zeta^{3/2})^2$
g	acceleration of gravity
g'	$\Delta\rho_o/\rho_o\ g$
H	maximum allowable penetration of the jet
h	vertical centerline distance from core boundary to jet boundary
h_{max}	maximum value of h obtained in a heated discharge
h_o	depth of discharge channel
K	experimentally determined dimensionless coefficient describing the gross effects of the turbulent mixing process
k	coefficient of heat loss
P	pressure

Q_o discharge flow

Q' rate of entrainment of the ambient water per unit length of the jet

r radial cylindrical coordinate

r vertical distance from the jet centerline to the boundary of of the core region

s longitudinal cylindrical coordinate

s horizontal distance from the jet centerline to the boundary of the core region

T mean local temperature

t similarity function for temperature = $(1-\zeta)^{3/2}$

T' temperature fluctuations

T_a ambient temperature of water

T_c jet centerline temperature

T_o temperature of water at jet exit

T_s surface temperature

T_{sc} jet centerline temperature at the surface

ΔT the local temperature rise, $T-T_a$

ΔT_c temperature rise at the centerline, T_c-T_a

ΔT_o temperature difference between the discharge and the ambient water, T_o-T_a

ΔT_s surface temperature rise, T_s-T_a

ΔT_{sc} surface centerline temperature rise

$(\Delta T)_s$ average fractional stable excess surface temperature rise in the jet

$(\Delta T_{sc})_s$ stable surface centerline temperature rise, $T_{sc}-T_a$

u,v mean velocities in s,r direction

u'v' velocity fluctuations in s,r direction

u,v,w	velocity components in the coordinate system relative to the centerline of a deflected jet
$\tilde{u},\tilde{v},\tilde{w}$	velocity components in the fixed coordinate system
$u'v'w'$	turbulent fluctuating velocity components
u_c	centerline jet velocity
u_o	discharge velocity = $Q_o/2h_ob_o$
V,v	ambient crossflow velocity
v_e	lateral velocity of the entrained flow at the jet boundary
v_s	an internal velocity
v_b	an internal velocity
w_e	vertical velocity in the jet at $z = -r$ and $0 < y < s$
w_h	internal velocity
w_r	internal velocity
x,y,z	coordinate direction relative to the centerline of a deflected jet
$\tilde{x},\tilde{y},\tilde{z}$	fixed coordinate direction
α	experimentally determined entrainment coefficient
α_y	lateral entrainment coefficient in non-buoyant jet
α_z	vertical entrainment coefficient in a non-buoyant jet
β	coefficient of thermal expansion for water
ε	spread, db/dx of the turbulent region of a non-buoyant jet
ε_o	spread, db/dx, of the turbulent region in an undeflected non-buoyant jet
ζ	either of ζ_y or ζ_z

ζ_y	dimensionless width of the turbulent region of a jet, $\lvert y\rvert - s/b$
ζ_z	dimensionless depth of the turbulent region of a jet, $z - v/h$
ϕ	lateral jet stream line from the centerline in excess of the non-buoyant value
Θ	angle between $\tilde{x}$ axis and s axis
Θ	angle between the jet centerline (x axis) and the $\tilde{y}$ axis
Θ_o	angle between the discharge channel centerline and the y axis
η	water surface elevation
ρ	mean local density of water
ρ_a	ambient density of water
ρ_c	density of the jet centerline
ρ_o	density of water at jet exit
$\Delta\rho$	difference between the ambient water density and the water density, $\rho_a - \rho$
$\Delta\rho_c$	density deficit at the centerline, $\rho_c - \rho_o$
$\Delta\rho_o$	difference between the ambient water density and the density of the heated flow at the discharge exit, $\rho_a - \rho_o$
λ	experimentally determined dimensionless coefficients describing the gross effects of the turbulent mixing process
ν	kinematic viscosity

LIST OF FIGURES

REFERENCES

1. Abraham, G., "Jet Diffusion in Stagnant Ambient Fluid", Delft Hydraulics Laboratory Publication No. 29 (1963)

2. Abramovich, G.N., The Theory of Turbulent Jets, The M.I.T. Press, M.I.T., Cambridge, Massachusetts (1963).

3. Fan, L.-N, "Turbulent Buoyant Jets into Stratified or Flowing Ambient Fluids", W.M. Keck Laboratory of Hydraulics and Water Resources, California Institute of Technology, Report No. KH-R-15, June (1967).

4. Partheniades, E., Beechley, B.C., and Jen, Y., "A Parametric Study for Surface Temperature Concentration Due to Submerged Heated Water Jets in Shallow Water", Coastal and Oceanographic Engineering Laboratory, College of Engineering, University of Florida, Technical Report No. 17, May, 1973.

5. Stolzenbach, K.D. and Harleman, D.R.F., "An Analytical and Experimental Investigation of Surface Discharges of Heated Water", Ralph M. Parsons Laboratory for Water Resources and Hydrodynamics, Department of Civil Engineering, M.I.T., Technical Report No. 135, February, 1971.

6. Stolzenbach, K.D., Adams, E.E., and Harleman, D.R.F., "A User's Manual for Three-Dimensional Heated Surface Discharge Computations", Ralph M. Parsons Laboratory for Water Resources and Hydrodynamics, Department of Civil Engineering, M.I.T., Technical Report No. 156, September, 1972.